Insert Design and Manufacturing for Foam-Core Composite Sandwich Structures

by

Alan Lares

A thesis submitted to the Faculty of Graduate and Postdoctoral Affairs in partial fulfillment of the requirements for the degree of

Master of Applied Science

in

Mechanical

Carleton University
Ottawa, Ontario

Abstract

Sandwich structures have been used in the aerospace industry for many years. The high strength to weight ratios that are possible with sandwich constructions makes them desirable for airframe applications. While sandwich structures are effective at handling distributed loads such as aerodynamic forces, they are prone to damage from concentrated loads at joints or due to impact. This is due to the relatively thin face-sheets and soft core materials typically found in sandwich structures.

Carleton University's Uninhabited Aerial Vehicle (UAV) Project Team has designed and manufactured a UAV (GeoSurv II Prototype) which features an all composite sandwich structure fuselage structure. The purpose of the aircraft is to conduct geomagnetic surveys. The GeoSurv II Prototype serves as the test bed for many areas of research in advancing UAV technologies. Those areas of research include: low cost composite materials manufacturing, geomagnetic data acquisition, obstacle detection, autonomous operations and magnetic signature control.

In this thesis work a methodology for designing and manufacturing inserts for foam-core sandwich structures was developed. The results of this research work enables a designer wishing to design a foam-core sandwich airframe structure, a means of quickly manufacturing optimized inserts for the safe introduction of discrete loads into the airframe.

The previous GeoSurv II Prototype insert designs (v.1 & v.2) were performance tested to establish a benchmark with which to compare future insert designs. Several

designs and materials were considered for the new v.3 inserts. A plug and sleeve design was selected, due to its ability to effectively transfer the required loads to the sandwich structure. The insert material was chosen to be epoxy, reinforced with chopped carbon fibre. This material was chosen for its combination of strength, low mass and also compatibility with the face-sheet material. The v.3 insert assembly is 60% lighter than the previous insert designs.

A casting process for manufacturing the v.3 inserts was developed. The developed casting process, when producing more than 13 inserts, becomes more economical than machining.

An exploratory study was conducted looking at the effects of dynamic loading on the v.3 insert performance. The results of this study highlighted areas for improving dynamic testing of foam-core sandwich structure inserts.

Correlations were developed relating design variables such as face-sheet thickness and insert diameter to a failure load for different load cases. This was done through simulations using Computer Aided Engineering (CAE) software, and experimental testing. The resulting correlations were integrated into a computer program which outputs the required insert dimensions given a set of design parameters, and load values.

Acknowledgments

I would first like to thank my thesis supervisors: Prof. Paul V. Straznicky and Prof. Jeremy Laliberté for giving me the opportunity to pursue this research work as well providing me their guidance and patience throughout the project. Without their support, this work would not have been possible.

My utmost gratitude goes out to the technical staff from the department of Mechanical and Aerospace Engineering at Carleton University. The support of Alex Proctor and Kevin Sangster in the machine shop was crucial in fabricating the various test fixtures and moulds I required for the project. I would like to give a special thanks to Steve Truttmann for his countless hours of insight and guidance in just about every aspect of this project, and especially in load frame testing.

I also thank Aaron Miller (Composites Canada) for his continuous support of the LCC projects at Carleton University.

My sincere thanks to Frank Cappelli at Baltek Inc., for the generous donation of PVC foam used for sandwich structure fabrication.

Various parts of the project were completed with the assistance of graduate students from Carleton University. I would like to thank to Ben Hamilton for his help with the 3D printer, and Brian Rutkay for his assistance during testing, both are current graduate students in the department.

I am very thankful to Laurent Loisy, an exchange student from France, who provided valuable help with the manufacturing of the bearing and bending test fixtures used throughout this project

I would also like to thank Quentin Dumery another exchange student from France for his help with the ABAQUS simulation work.

I would like to acknowledge Sander Geophysics Ltd. (SGL), NSERC Collaborative Research and Development (CRD) Grant and Carleton University for providing the financial resources for this research.

Last and certainly not least I would like to thank my friends and family for their support throughout the last couple of years.

Table of Contents

List of Tables

List of Figures

List of Figures

Chapter 1 - Introduction

This chapter begins with a general introduction to sandwich structures along with their applications in industry. The advantages of sandwich construction in the aerospace industry are presented along with the limitations. The GeoSurv II Unmanned Aerial Vehicle (UAV) project will be discussed along with the UAV Prototype, which is the test bed for this research. Finally this chapter will set up the research goals and the contributions to the field of low cost composites (LCC) manufacturing with its focus on UAV design.

1.1 - Composite Sandwich Structures

The requirement to make structures lighter and stronger has been an ongoing focus in nearly all facets of aerospace, mechanical and civil engineering. Sandwich structures were born out of this necessity. They are comprised of two thin sheets with strong in-plane material properties, which are stabilized with a lower density, lightweight medium between them. The result of this combination is a structure capable of withstanding not only high tensile loads, but also compressive, bending and torsional loads [1], [2].

The principle of sandwich construction is common in nature. The bones in human and animal skeletons can be used as examples of a foam-like core, sandwich construction. Tree branches can also be used to exemplify such construction due to having a stiff exterior with a soft-core. These natural structures are subjected to complex and repetitive load cases. The bones in the human leg can sustain bending, torsion, shear,

impact, or any combination thereof. As in the aerospace industry, nature poses a requirement for material optimization; hollow bird bones are an excellent example of minimal use of material with maximum strength [2].

Composite structures today are being used in more structures, as their advantages are becoming more understood. Different companies have investigated several concepts in the past few years in developing a full composite sandwich fuselage. The German government aerospace research organization - "Deutsches Zentrum fuer Luft und Raumfahrt" (DLR) has proposed a sandwich structure design for a fuselage, where the outer skin is only intended as an aerodynamic fairing [1], [2].

The Royal Swedish Navy has been using fibreglass composite sandwich construction for over 20 years on all of their ship hulls. They were able to show that a properly designed and manufactured composite sandwich hull could match or exceed the capabilities of a steel one. One of their newest ships, the *Visby*, is a stealth boat, which employs a carbon-epoxy sandwich design. The initiative of The Royal Swedish Navy has spurred many of the other Scandinavian countries to adopt similar practices. Also, Australia's Navy uses high performance foam sandwich composites for its inshore mine hunters [1]. There are countless more examples of sandwich applications across many different disciplines.

Vinson. J (2005) presents a good example of the relative strength of a monocoque or monolithic (thin walled, reinforced) structure versus a sandwich structure. Consider the two structures in Figure 1-1. The sandwich face-sheets have a thickness of t_f and the core depth is h_c; similarly, the monolithic plate has a thickness of $2t_f$. Clearly, the

monolithic plate has essentially the same weight as the two face sheets of the same material. If the ratio of the face sheet thickness to core depth (t_f/h_c) equals to 1/20, the flexural stiffness of the sandwich structure is 300 times that of the monolithic plate. The result is that sandwich structures experience much lower deflections when subjected to a lateral load. They have a higher overall buckling load and higher flexural natural vibration frequencies when compared to monolithic plates, with a minimal increase in weight [1].

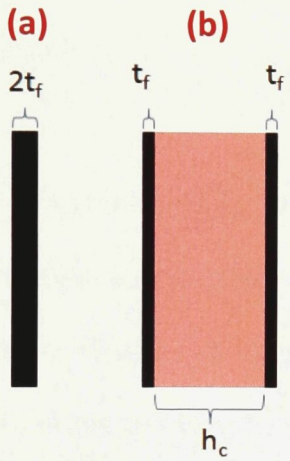

Figure 1-1 - (a) Monolithic plate with thickness $2t_f$. (b) Sandwich structure with face-sheet thicknesses of t_f and a core depth of h_c [1].

To continue this thought experiment, consider the same two structures, and a bending moment per unit width *M*, that is applied to the two structures. The resulting stress at the face-sheet of the sandwich structure is 1/30 of the stress of the monolithic structure. Clearly, even if the sandwich structure is twice or even three times the weight of the monolithic structure, which does not normally happen, it is still very desirable to use since the face stresses are reduced by a factor of 30 and the flexural rigidity is increased 300 times [1] [5].

While the weight savings benefits of sandwich structures are apparent, they also possess excellent thermal insulation characteristics, depending on the type of core materials used [5].

While sandwich structure cores can be made of nearly any type of material and design, they can generally be classified into four categories, as listed below. Figure 1-2 illustrates the different core types:

a. Honeycomb core
b. Foam or solid core
c. Truss (corrugated) core
d. Web core

Honeycomb cores represent the vast majority of sandwich structures used today in aviation. The two most common types of honeycomb cores are the hexagonally shaped cell-structured (Hexcel) core and the square cell (egg-crate) core. Web core sandwich structures are best represented by a group of I-beams attached together at the flanges, and are often seen in navy ship hulls. Truss core structures are predominantly being used in the construction of modular, lightweight bridges.

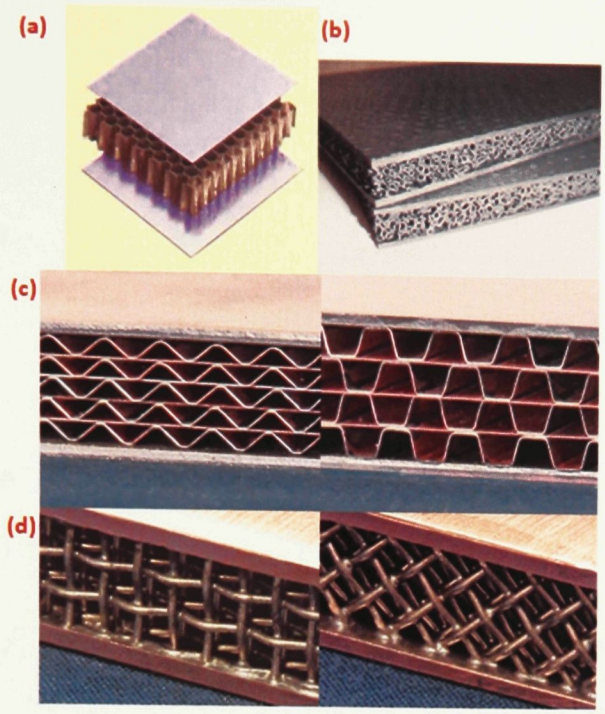

Figure 1-2 - Honeycomb core (a), foam/solid core (b), Truss core (c) and web core (d) [6], [7], [8].

Foam or solid cores are relatively inexpensive and can be comprised of balsa wood, or an endless array of plastic/foam materials with varying material properties. A popular choice for foam core sandwich structures is polyvinylchloride (PVC) foams [1].

Despite the advantages that sandwich structures bring, there are also several drawbacks that must be considered depending on the intended applications. There is a risk of local buckling when subjected to discrete, in-plane compressive or shear loads due to the thin face-sheets which predominantly carry the load. In addition to local buckling, core shear instability and face wrinkling are also problematic. Fire resistance can also be an issue depending on the type of core that is used in the construction (balsa, plywood etc.) [1], [5].

Since the introduction of composites into airframes more than 30 years ago, lightning strikes have been a significant problem. Federal Aviation Administration (FAA)

certified composite aircraft are typically struck by lightning once or twice per year, unlike their metal counterparts; composite airframes are either non-conductive (i.e. fibreglass) or very low conductivity (carbon fibre) and thus do not have the ability to dissipate the electrical current to the rest of the airframe when struck. Currents up to 200,000A will choose the path of least resistance. In the case of an unprotected composite airframe, the consequences can be catastrophic. Since the current is not properly dissipated, metal control cables can be vaporized, control hinges welded, fuel vapours ignited, etc. Traditionally, conductive paths have been introduced into composite structures by embedding copper or aluminum mesh/strands in the composite laminate or by bonding aluminum foil to the outside structure. These added layers of conductive material solve the issue of lightning strikes, however, they add weight and can decrease the overall performance of the laminate [9].

Non-Destructive Inspection (NDI) techniques such as ultrasonic, x-ray, eddy-current etc. are valuable as they can effectively detect defects and cracks in airframes without causing damage to the structure being inspected. In an effort to continue increasing the safety of aircraft and meet the demands of aviation safety regulations, there are many research and development (R&D) projects with the aim of integrating Structural Health Monitoring (SHM) systems into airframes. SHM systems are a form of real-time inspection tool, which in some cases can be embedded directly into the airframe. It continuously monitors the airframe and can detect when damage appears. However, the SHM of composite airframes is very difficult. The fracture mechanics and crack propagation of composite airframes is complex and not well understood. This, coupled with the ineffectiveness of current SHM systems to detect damage in such

structures, makes the safety and certification of composite commercial aircraft a significant problem [10]. With the amount of composite materials increasing in new aircraft designs, health monitoring will continue to be an issue in the foreseeable future.

Although suited for handling distributed loads, sandwich structures are in structural applications exposed to discrete loads at joints and interfaces with other structural components. Due to the relatively soft core of sandwich structures, it is important to embed hard points or inserts to locally reinforce areas that are subjected to local or discrete loads. Properly designed insert systems can safely transfer these loads to the surrounding airframe. It is important to classify these load cases and their associated values in order to properly design insert systems.

There are 3 basic discrete load cases for sandwich structures that are relevant to insert design; out-of-plane shear or pull-out caused by a transverse loads, in-plane shear, and bending (either with or without shear). These three loading conditions are shown in Figure 1-3.

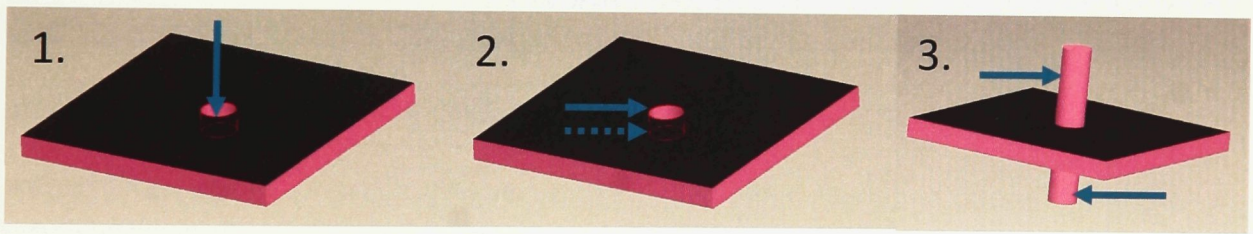

Figure 1-3 - Common load cases: (1) Out-of-plane load (2) In-plane shear (3) Bending (with or without shear).

Sandwich structures are not well suited for supporting concentrated out-of-plane loads. When subjected to pull-out loads, the core is susceptible to local crushing this is because the core is no longer locally supporting the face-sheet and the skin is then more vulnerable to damage. This loading condition should be avoided when designing

airframes and will thus not be considered for the purposes of this research. The two loading conditions that will be considered in this research will be in-plane shear and bending with shear.

This section covered the strengths and weaknesses of composite sandwich structures, why they are desirable in airframes and some of the design challenges associated with using them. The following section presents the state of the research in the area of low cost composite manufacturing at Carleton University and also introduces the test platform for the UAV research; the GeoSurv II Prototype.

1.2 - Overview of the UAV Research and the GeoSurv II Prototype

The GeoSurv II project is a multi-year, multi-disciplinary project. Successive teams of fourth year undergraduate students have been developing a UAV that will be capable of autonomous operation and able to conduct airborne geophysical surveys. Sander Geophysics Ltd., which has partnered with Carleton University, currently conducts such surveys with a manned aircraft fleet. The advantages of using UAV for such surveys include the higher resolution of geomagnetic data due to lower flight altitude of the UAV, increased safety of the operators (i.e. no pilots) and lower capital and operating costs.

The GeoSurv II Prototype under development features an almost exclusively carbon-epoxy airframe to reduce its magnetic signature. A low magnetic signature is desirable, as the interference from ferromagnetic components will affect the geomagnetic sensors (magnetometers) mounted on the UAV wing tips. The GeoSurv II Prototype is in its 7th year of development and is currently being readied for first flight. Figure 1-4

shows the as-built GeoSurv II prototype, and Table 1-1 lists physical and design properties.

Figure 1-4- Image of the assembled GeoSurv II Prototype (February 2010) [11].

Table 1-1 - GeoSurv II Specifications.

GeoSurv II Feature	Value
Wing Span	16 ft
Length	14ft
Height	3ft
Engine Power	30 hp
Cruise Speed	60/100kts
Weight	200lb

Undergraduate students on the GeoSurv II project are tasked with the design and manufacturing of a full-scale prototype. At the graduate level there is ongoing research focused on the development of critical UAV technologies. This research is divided into the following five areas:

- Low Cost Composites (LCC),

- Geomagnetic Data Acquisition (GDA),
- Obstacle Detection (OD),
- Autonomous operations (AO)
- Magnetic Signature Control (MSC)

The LCC research focuses on the development of all aspects of the design and manufacturing of complex composite components. Figure 1-5 illustrates the overall research methodology for the LCC research team for the past 5 years.

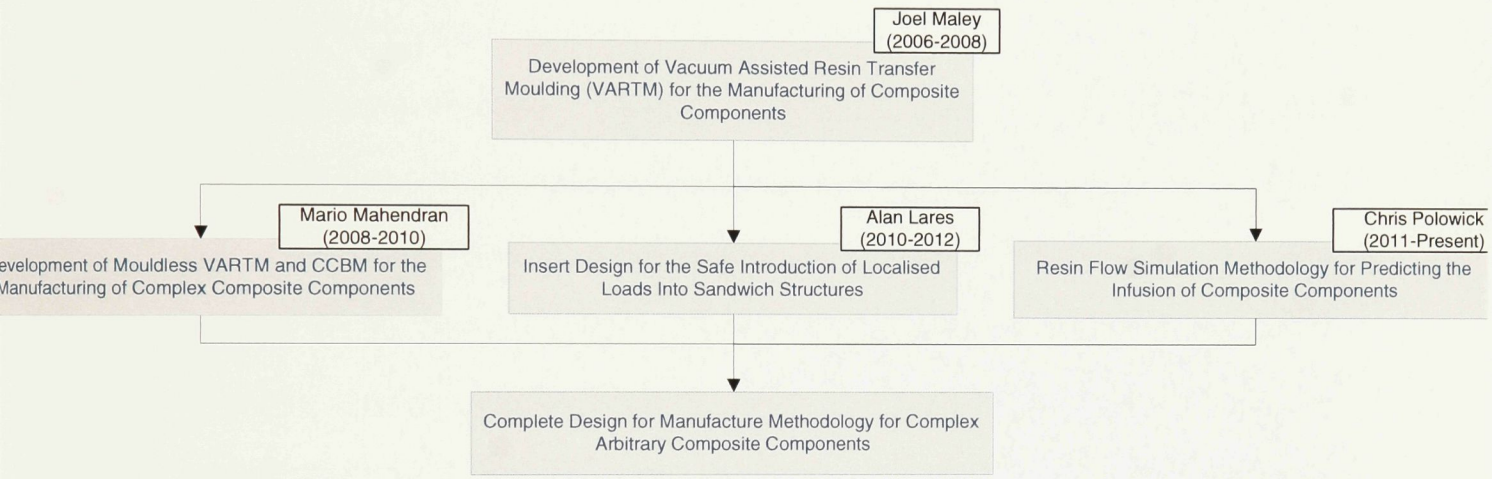

Figure 1-5 - LCC research methodology.

As was already mentioned, the goal of this research team is to develop a complete methodology for manufacturing aerospace grade composite components of arbitrary shape at low cost. The first step towards this goal was to select a suitable manufacturing process for creating composite components.

J. Maley, in 2006-08, identified Vacuum Assisted Resin Transfer Moulding (VARTM) as a suitable process for manufacturing small batches of composite components [12]. J. Maley further identified the possibility of infusing complex sandwich components through a "mouldless" process and used the GeoSurv II fuselage as his test platform. The results showed a potential but also a need for refinement in part quality, tolerances and repeatability.

In 2008-10 M. Mahendran further developed the mouldless manufacturing procedure that J. Maley had started [11]. Closed Cavity Bag Moulding (CCBM) was developed which employed a re-usable, form fitted vacuum bag with embedded resin channels. CCBM promised to speed up production times for batches of parts, increase part tolerances and finish. To test the performance of the new CCBM process, a second fuselage for the GeoSurv II was designed using Design for Manufacturing (DFM) principles, optimised with the aid of Computer Aided Engineering (CAE) software and, infused using CCBM. The results showed a significant improvement in tolerances, finish, and repeatability over the traditional method. In addition to these improvements, the weight of the new fuselage showed a decrease of approximately 30% as compared to its predecessor, due to the redesign and improved infusion process.

J. Maley had investigated using Liquid Injection Moulding Simulation (LIMS) software to predict where the inlet and outlet infusion lines should be positioned on the part to ensure efficient and complete resin infusion of the component. M. Mahendran employed the results of J. Maley's work to help with the placement of the inlet and outlet lines for the CCBM infusion of the second GeoSurv II fuselage. As the components become larger and more complex it is apparent that a method for predicting where the

infusion lines should be placed needs to be developed. C. Polowick is currently investigating this area further. The need for insert design will be discussed in the following section along with the thesis objectives, organization and contributions.

1.3 - Thesis Objectives and Organization

This thesis aims at developing a methodology for designing inserts for arbitrary foam-core sandwich structures, with the goal of safely introducing discrete loads into the surrounding structure. The result of this work will give a designer wishing to design a sandwich airframe structure, a means of quickly specifying and manufacturing optimized inserts.

This work begins with an investigation into the current methods for insert design and different insert design concepts used in composite sandwich structures today. The previous insert designs used in the GeoSurv II Prototype were investigated and tested to obtain baseline data to be improved upon. Based on the study of current insert designs, the deficiencies in the previous designs, and the identified design criteria, new inserts were developed. A material selection and manufacturing development study was also carried out. Once the design was finalized it was optimised for the GeoSurv II fuselage and tested against the previous insert designs. The effects of vibration on the load carrying capabilities of the new inserts was also studied. ABAQUS finite element simulations were conducted to develop correlations between failure loads and key design variables such as face-sheet thickness, core-height, insert diameter etc. These correlations were verified empirically with coupon testing. This thesis is organized into the following chapters:

- Chapter 2: Insert Design and Development
  Literature review on the current insert designs and design methods along with an overview of the previous insert designs of the GeoSurv II Prototype. The overall thesis organization for developing a new insert system is also presented.

- Chapter 3: Previous Insert Design Benchmark Testing
  The previous two insert designs that were used in the GeoSurv II prototype are performance tested in order to generate baseline data to compare with subsequent insert designs to.

- Chapter 4: New Insert Design
  The new insert design is finalized along with the manufacturing process and materials that are best suited for the new design. This was accomplished through a material selection study and testing. The design is optimized for the GeoSurv II and tested against the previous designs to validate its performance.

- Chapter 5: The Effects of Vibration on the v.3 Insert Joint Strength
  The effects of vibration caused by the GeoSurv II engine are explored. Residual strength tests are performed in bearing and bending to assess the impact of the vibrations on the new insert design.

- Chapter 6: Methodology Development for Sizing Inserts
  ABAQUS FEA simulations are performed to develop correlations between maximum load values and different insert and sandwich structure design parameters. The simulations are validated though coupon testing.

- Chapter 7: Conclusions & Future work
  The conclusions of this research work are discussed along with the recommendations for future work.

To reach the goal of developing a new insert design, and to develop a methodology for designing optimized inserts for arbitrary foam-core sandwich structures, a thesis 'roadmap' was developed and is presented in Figure 1-6. Its purpose is to organise the research to present a clear path to meeting the final objectives.

Although SI units are generally used in research, the aerospace industry still uses the imperial system of units, which will be used in this thesis work.

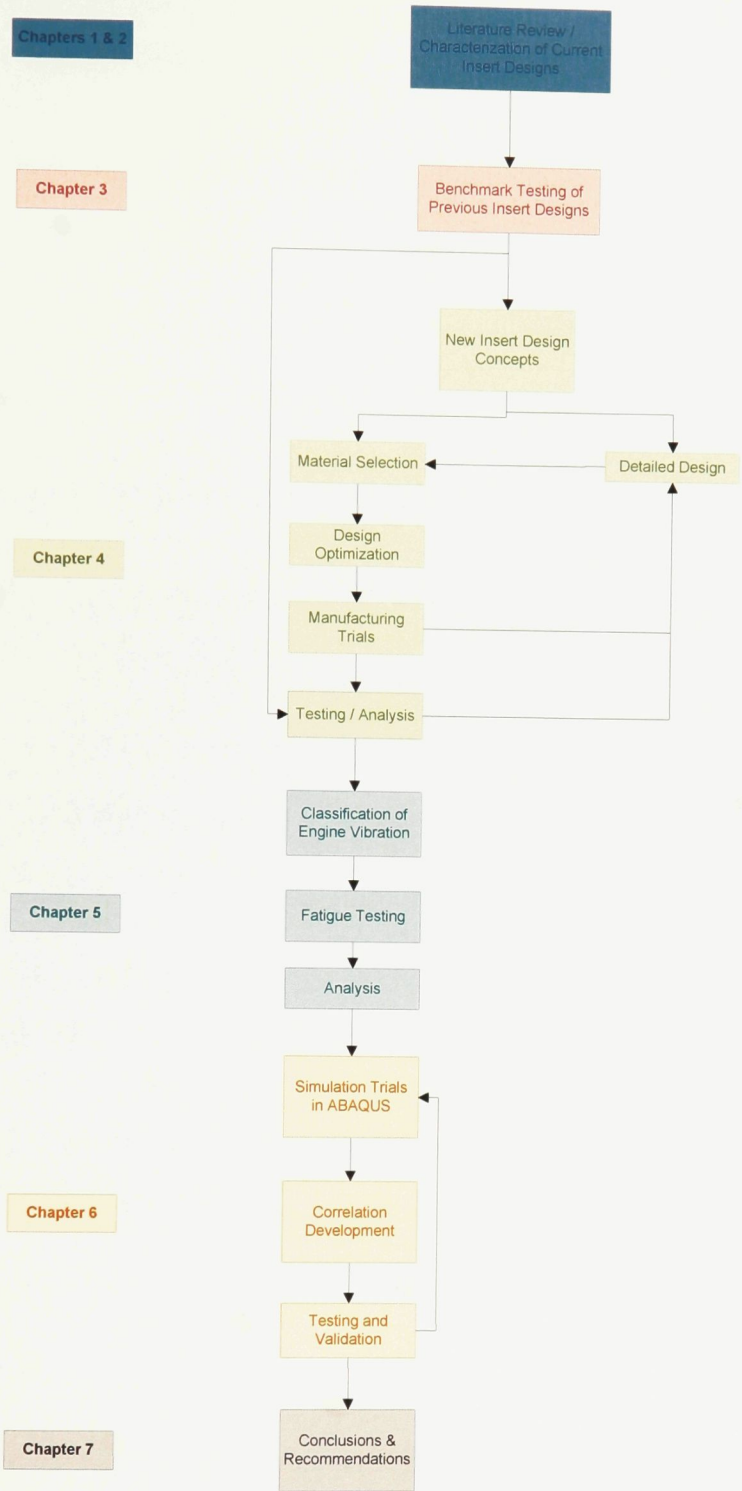

Figure 1-6 - Thesis organization.

Chapter 2 - Insert Design and Development

This chapter begins with a review of the current literature on insert systems, analysis and design methods. An overview of the previous insert designs on the GeoSurv II fuselage is presented and the methodology for the design of the new insert system is described in detail.

2.1 - Review of Current Insert Systems and Design/Analysis Methods

As mentioned in the previous section, an insert is a component that is embedded into the core of a sandwich panel at an attachment point, to locally reinforce the area. Typical materials used are plywood, wood, PVC foam or metal; essentially any stiffer and stronger material than the surrounding core [13]. Despite the fact that core inserts have been used extensively in industry for a long time, little has been published in the field of insert design and manufacturing [14]. A list of relevant research in the field of sandwich structure inserts is presented next.

Song *et al.* [15] performed an experimental study on the pullout and shear failure loads of composite sandwich insert joints. The specimens were fabricated using a Nomex honeycomb core with carbon-epoxy composite face-sheets. The results of this research will be presented in section 2.1.1.

Bianchi *et al.* [14] performed pullout tests on hot and cold bonded inserts, and also developed an analytical model for predicting the pullout strengths of each. The test coupons were all aluminum honeycomb core sandwich structures. The results showed that hot bonded inserts (i.e. inserts integrated into the sandwich panel before panel

curing) had higher pullout and shear strengths over cold bonded inserts installed post panel manufacturing.

Raghu *et al.* [16] investigated the variability of the insert pullout strength of all aluminum honeycomb sandwich panels as well as of Rohacell closed-cell foam core sandwich panels with fibreglass face sheets. Through-thickness, fully potted and partially potted (blind) inserts were examined experimentally. The test results were compared to Finite Element Analysis (FEA) predictions for the failure loads. The results showed that the variability of the pullout strength of the inserts in foam core was lower than for the inserts embedded in the honeycomb sandwich panels.

Burchardt [17] considered the fatigue characteristics of a four-point bend test on a sandwich panel containing an insert using numerical fatigue calculations as well as employing the finite element method (FEM). The numerical models were based on the experimental tests performed by Kristensen and Mortensen [18]. The sandwich structure modelled in the simulations was comprised of cross-linked PVC foam core material and glass/polyester composite lamina faces. The results showed that the stiffness of the insert material had almost no influence on the fatigue crack propagation.

The European Space Agency (ESA) has published an Insert Design Handbook (IDH) [19], which helps designers choose a specific size insert for a given applied load. The IDH is, however, limited to the pullout load case and to honeycomb sandwich panels. Despite this limitation, it does provide some helpful design guidelines that can be applied to foam-core sandwich structures. These guidelines will be discussed in Chapter 4: New Insert Design.

It can be seen from the literature survey that honeycomb sandwich panels dominate the field of sandwich structure insert design. Very few studies have been found on PVC foam core, carbon-epoxy face sheet sandwich panels. Nevertheless, many of the findings in the above studies will be useful in the improved design of carbon-epoxy skinned, foam core sandwich panel inserts. The study conducted by Song et al. [15] was identified as being of particular use for the design of new insert systems for UAV.

2.1.1 Parameters Affecting the Insert Joint Strength of Composite Sandwich Structures Under In-plane Shear Loading

Song *et al.* [15] conducted a study to investigate the effects of certain parameters such as the core height, core density, face sheet thickness and insert clearance on the failure loads of sandwich structure inserts. The two load cases investigated were pullout and shear; however, for the purpose of this review, only the shear case will be considered. The work by Song *et al.* was conducted with SI units. To keep consistent with their work it shall be presented as such in this section.

The sandwich panels were comprised of a Nomex honeycomb core and a carbon-epoxy composite face sheet. Figure 2-1 shows the schematic for the shear test and the test set-up in the universal material-testing machine (Instron 5582). Figure 2-2 shows the schematic of the cross-section of the sandwich structure insert joint.

Eight different types of specimens were tested. The parameters that were varied were the core height, core density and the face sheet thickness for each of the two load cases. Each specimen type included 5 specimens for a total of 40. Table 2-1 shows the details of the test specimens.

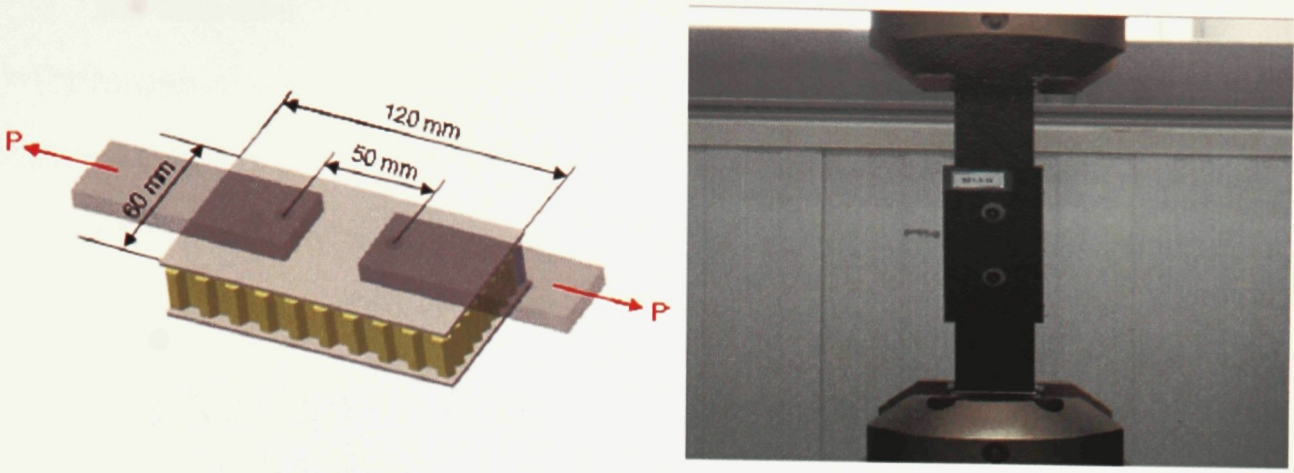

Figure 2-1 - Schematic of shear test (left) and image of experimental test setup (right) [15].

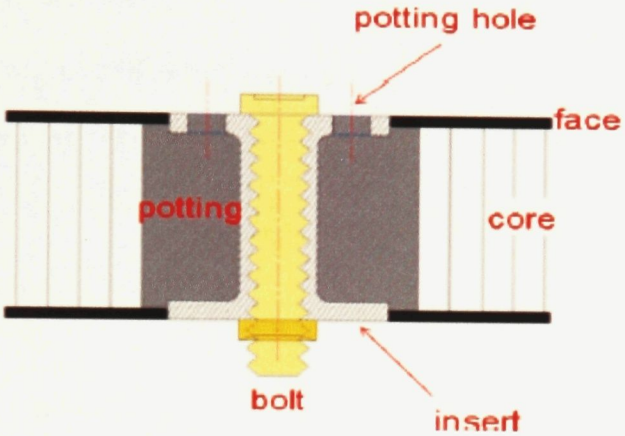

Figure 2-2 - Schematic of the sandwich structure joint cross-section [15].

Table 2-1 - Shear specimen details [15].

ID	Face	Core				
		Designation	Height (mm)		Density	
			(mm)	(in)	lb/ft^3	kg/m^3
S01	[45/0]s	PN2-3,0-1/8	17.78	0.70	3	48
S02	[45/0]s	PN2-3,0-1/8	22.86	0.90	3	48
S03	[45/0]s	PN2-3,0-1/8	27.94	1.10	3	48
S04	[45/0]s	PN2-5,0-1/8	17.78	0.70	5	80.1
S05	[45/0]s	PN2-8,0-1/8	17.78	0.70	8	128.1
S06	[45/0/45]s	PN2-3,0-1/8	17.78	0.70	3	48
S07	[45/0]s	PN2-3,0-1/8	17.78	0.70	3	48
S08	[45/0]s	PN2-3,0-1/8	17.78	0.70	3	48

The face-sheet was a pre-impregnated, plain weave, carbon-epoxy fabric (WSN3k) supplied by SK Chemical. The film adhesive FM73 by Cytec [15] was used for bonding the face sheets to the Nomex core in a co-curing step. All specimens were fabricated in an autoclave by co-curing. The manufacturing process for the specimens is shown in Figure 2-3.

The sandwich panels were cut into 120x120mm (4.72x4.72in) and 60x120mm (2.36x4.72in) sections. The holes were milled using a 15mm drill, and the insert was made from Al 2024-T4 and into NAS 1834 (Wall Panel Inserts). The fastener used during the loading operations was a M5SCM wrench bolt. The insert potting material was Hysol EA9394 made by Henkel.

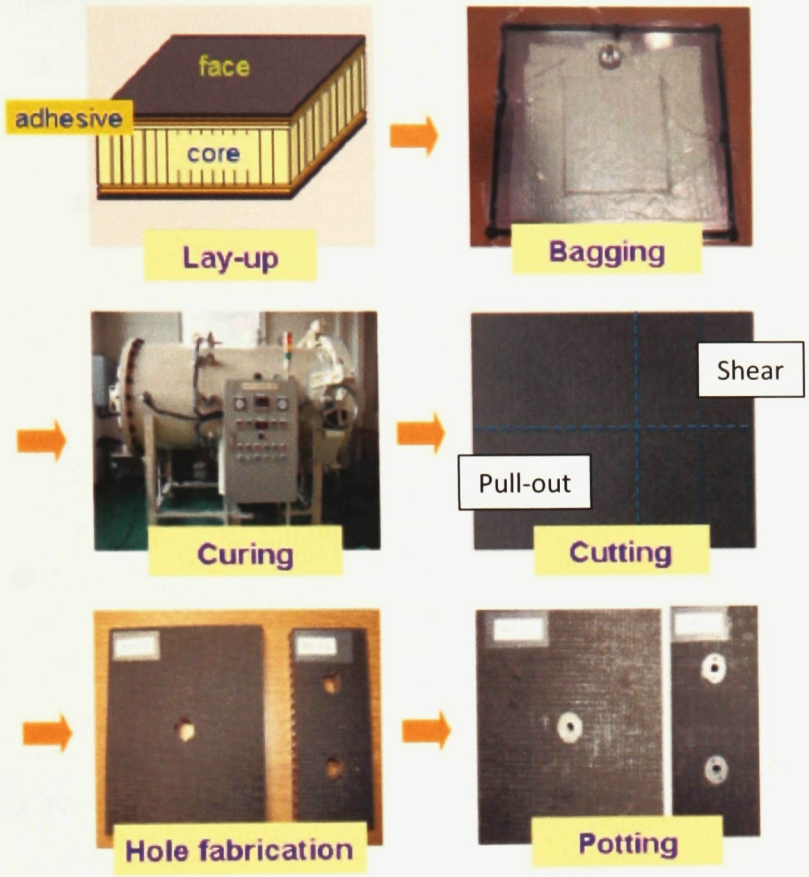

Figure 2-3 - Manufacturing process cycle for specimen construction [15].

The failure load was defined as the first drop in the load-displacement curve, which corresponds to the end of the linear-elastic region. A typical load displacement curve can be seen in Figure 2-4.

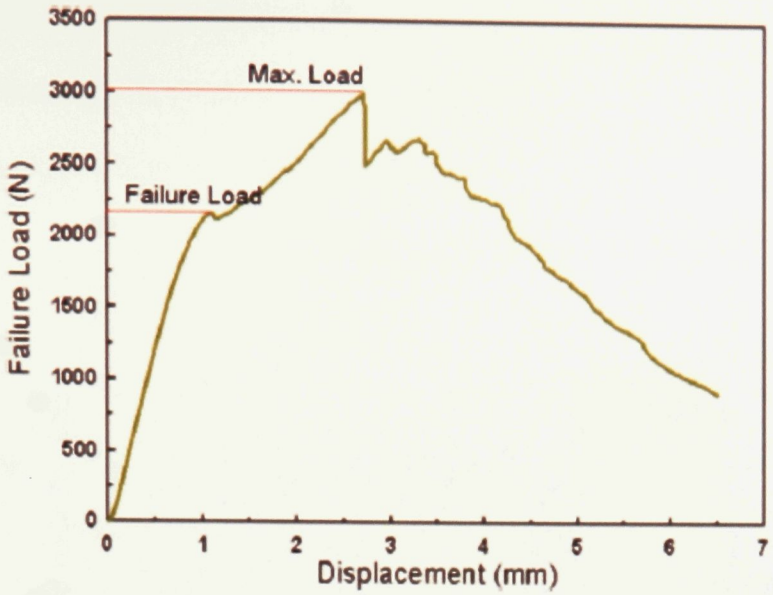

Figure 2-4 - Typical Force vs. Displacement Curve [15].

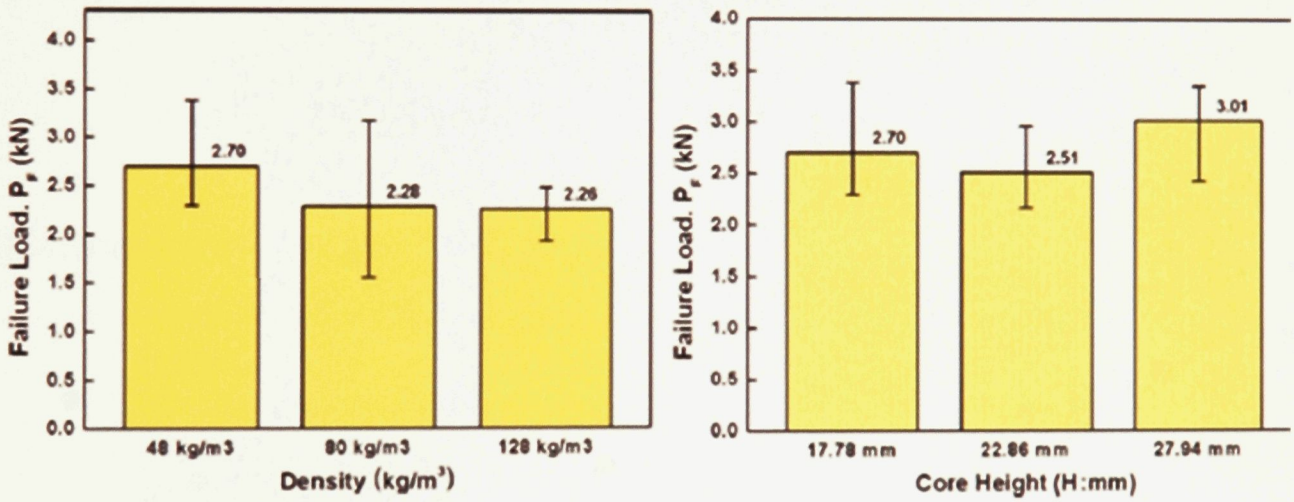

Figure 2-5 - Effects of core height on the shear failure load (right), Effects of core density on the shear failure load (left) [15].

Figure 2-5 shows the failure loads associated with varying core height and density. The results show no significant increase in the failure load as a result of increasing the thickness of the core. Similar to the results of varying core height, the failure loads do not increase when the core density increases. Figure 2-6 shows the failure

loads associated with increasing face thickness. The results show that there is a near linear proportionality between the face thickness and failure load. The results clearly show that, as expected, the failure loads are dominated by the face thickness.

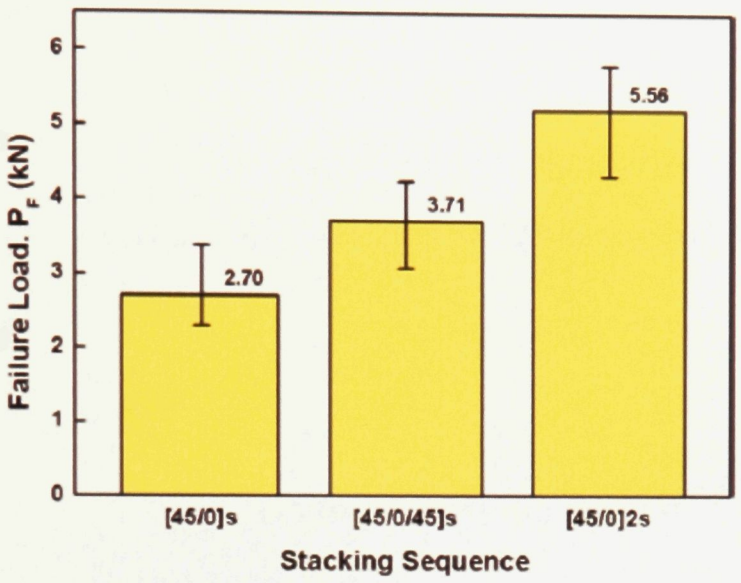

Figure 2-6 - Effects of face thickness on the shear failure load [15].

The following conclusions were made from this research work:

- Density of the core has a negligible effect on the bearing strength of sandwich structures.
- The core height has a negligible effect on the bearing strength of the sandwich structure.
- The face-sheet thickness is linearly proportional to the bearing strength of the sandwich structure.

2.1.2 - Current Insert Designs and Guidelines

Aerospace structures are typically comprised of several components joined together by bonding, welding or by mechanical fastening. Joints are one of the most

common failure points in aircraft, and special attention to all aspects of the joint design must be made to ensure a safe airframe design [20].

The following subsection describes the HI-LOK, HUCK-COMP/TITE, and composite fasteners that are used for joining composite panels. Although there are many more fastener types used in the aerospace industry, these three were selected due to their adaptability for sandwich structure applications. The plug and sleeve nature of these systems is attractive for sandwich panels, and the reasons are discussed in detail in Chapter 4: New Insert Design.

HI-LOK Metallic Fastener

The Hi-Lok metallic fastener was the primary fastener used for composite joints in the early 1970s, still used in limited applications today [21]. Figure 2-7 illustrates the plug and sleeve nature of the design. These fasteners were traditionally used for metallic structures and therefore no attention was paid to clamp-up forces, which could locally crush the composite laminate. A variation on the Hi-Lok fastener is the Eddie bolt 2 which can be seen in Figure 2-8. It is similar in design; however, it uses the 'Eddie Lobes' for torquing instead of the collar wrenching device in the case of the HI-LOK. When the predetermined torque is reached, the lobes deform into the pin thread flutes and the system is locked in place.

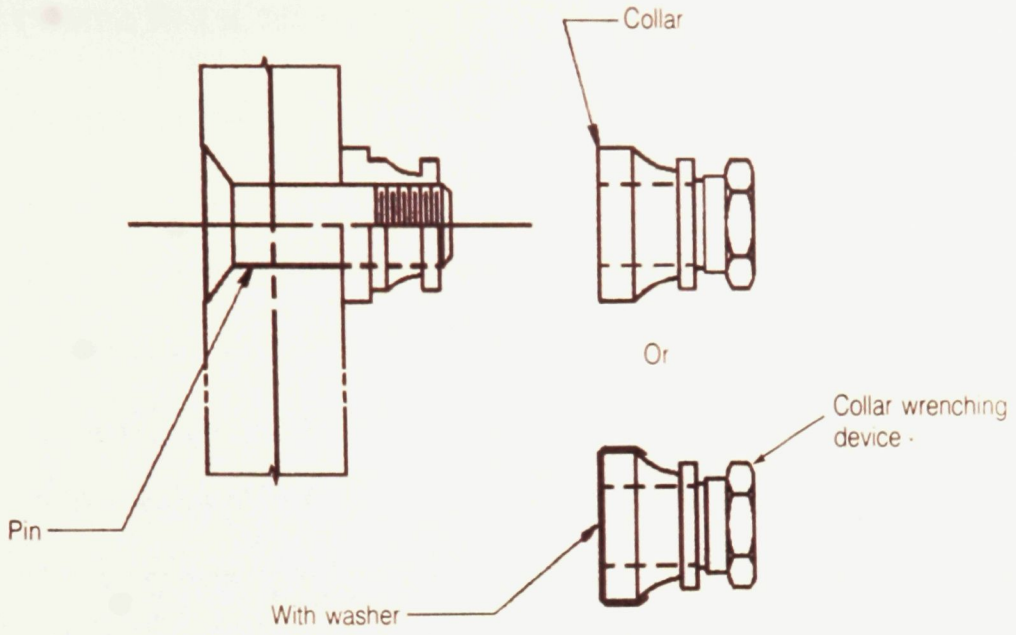

Figure 2-7 - HI-LOK Metallic Fastener [21].

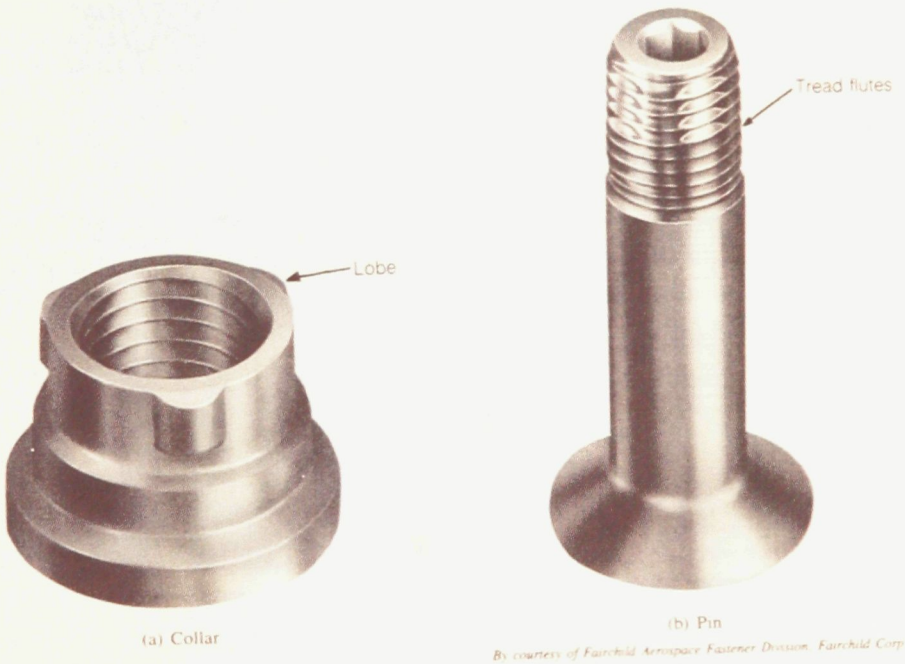

Figure 2-8 - Eddie bolt 2 metallic fastener [21].

HUCK-COMP& HUCK-TITE Titanium Fasteners

The HUCK-COMP and HUCK-TITE fasteners in Figure 2-9 are specifically designed for monolithic composite structures. They are an all titanium lockbolt system, with Ti-6Al-4V for the pin and commercially pure titanium for the collar. HUCK-TITE fasteners are designed for a slight interference fit of approximately 0.001 to 0.006 inches, improving the structural strength and fit of the joint without damaging the laminate. A sleeve on the pin of the HUCK-TITE fastener causes the interference. After the collar is installed, the remaining pin that is protruding is snapped off at the breakaway point [21].

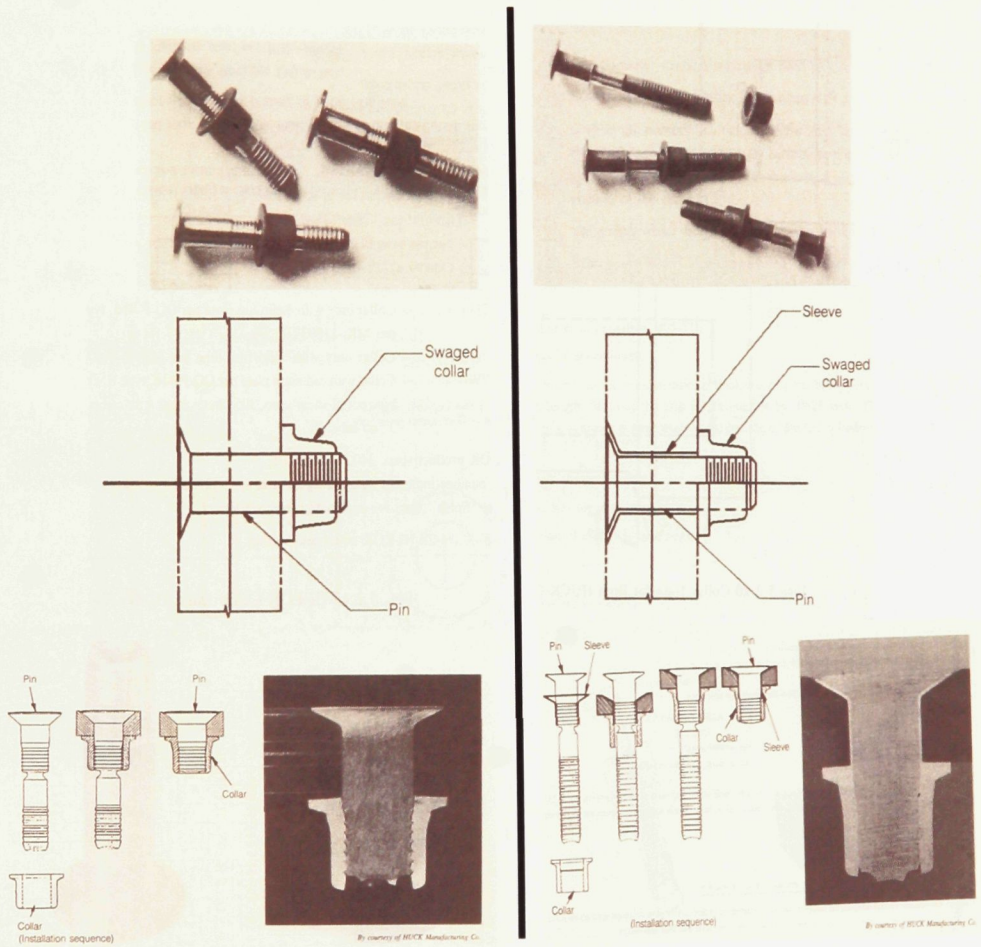

Figure 2-9 - HUCK-COMP (Left) HUCK-TIGHT (right) fasteners [21].

Composite Fasteners (Non-metallic)

Composite fasteners offer many qualities that make them an ideal solution for the joining of components. Fibre selection combined with a suitable resin to provide the adequate strength necessary to handle the applied loads [21]. Advantages of using composite over metallic fasteners for this research include:

- Reduced weight
- Low magnetic noise
- Eliminates dissimilar material corrosion

Generally, two types of composite fasteners are used:

A. Thermoset:

- Plug and sleeve design
- Machined or cast/moulded to final shape

Figure 2-10 illustrates the typical moulding and installation sequence for a thermoset composite fastener.

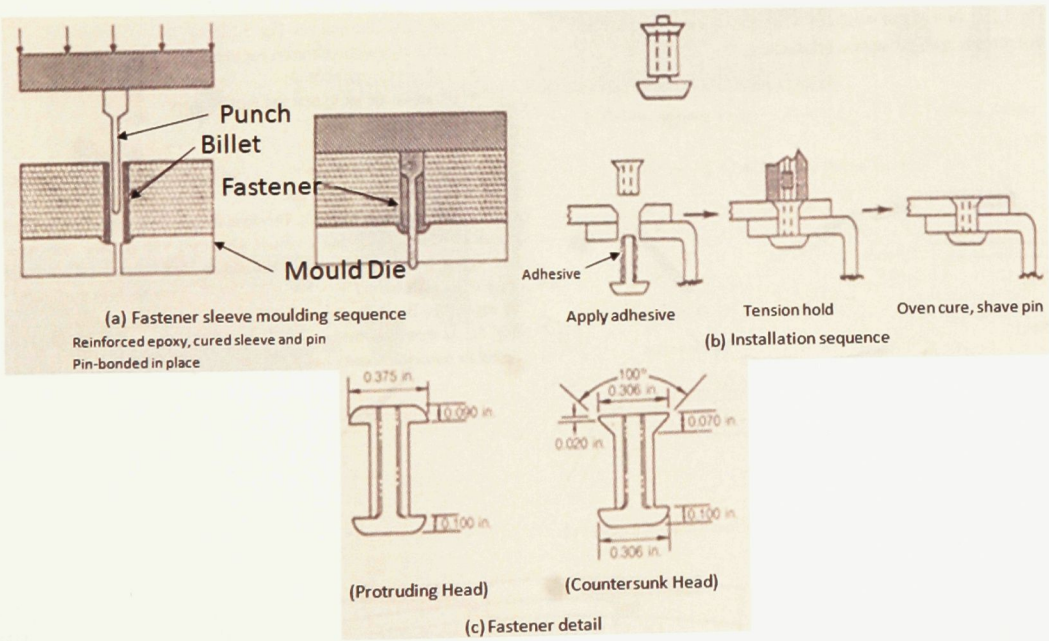

Figure 2-10 - (a) Fastener sleeve moulding sequence, (b) Installation sequence, (c) fastener detail [21].

B. Thermoplastic:

- Rivet style fastener
- Ultrasonic die set to heat and form to shape

Figure 2-11 shows the procedure for the installation of a thermoplastic composite fastener with the use of an ultrasonic die [21]. Figure 2-12 shows a few examples of composite material fasteners.

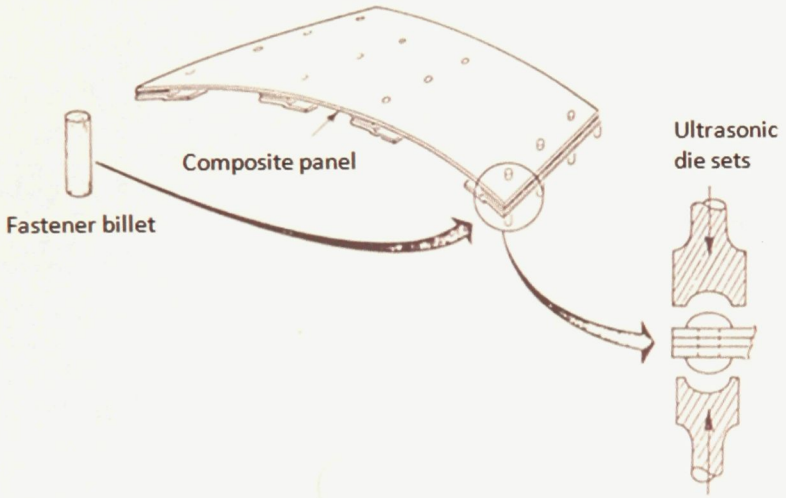

Figure 2-11 - Ultrasonic Thermoplastic fastener [21].

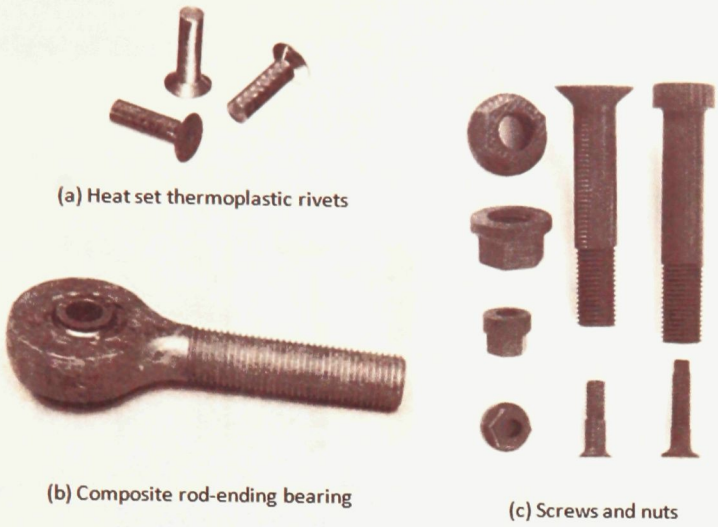

Figure 2-12 - Composite Material fasteners [21].

The findings of Song *et al.*, who set out to determine which parameters of a honeycomb sandwich panel affect its joint strength when subjected to shear loading, can be applied to foam-core sandwich panels. The results of their work showed that the load carrying capacity is linearly proportional to the face-sheet thickness of the sandwich panel. It was also shown that the core height and core density have a negligible effect on the bearing strength of the joint.

HI-LOK, HUCK-COMP/TITE and composite fasteners were studied in this literature review because they have attractive design features for foam-core, composite sandwich structures. The plug and sleeve nature of these designs reinforces the free-edges of the hole made in the laminate by compressing the plies together. The flanges of the inserts also allow for bending loads to be spread over a greater area of the face-sheet, decreasing the load concentration of the joint.

The following section describes the previous two insert designs that have been implemented in the GeoSurv II fuselage.

2.2 - Overview of the Previous GeoSurv II Insert Designs

In this section, the two previous insert designs used in the GeoSurv II fuselage are presented, along with advantages, disadvantages and the areas that require improvement. A more detailed comparison between the different insert designs is presented in Chapter 4: New Insert Design.

Two fuselages were manufactured for the GeoSurv II prototype. Version 1 (v.1) was manufactured using Vacuum Assisted Resin Transfer Moulding (VARTM) in March of 2008 by Mario Mahendran and Joel Maley [11], [12]. The infusion setup and the final part are shown in Figure 2-13.

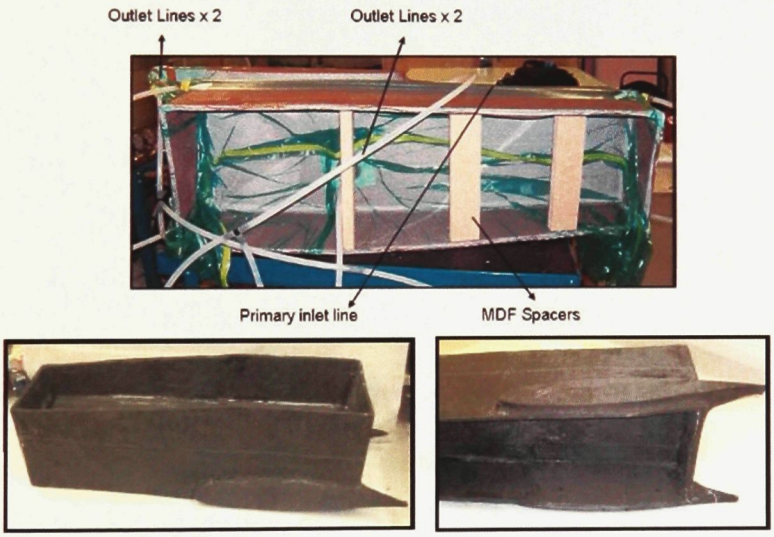

Figure 2-13 - Fuselage v.1 infusion setup and post cured part [12].

The insert system for v.1 features 1-in diameter Polyoxymethylene (Delrin) inserts that are bonded into drilled holes after the fuselage is manufactured.

Figure 2-14 describes the manufacturing steps for the installation of the v.1 insert system. Figure 2-15 shows the v.1 insert integrated into a test coupon used for bending trials. Figure 2-16 shows a cross section of a typical v.1 insert joint, the load paths in bearing and bending are illustrated.

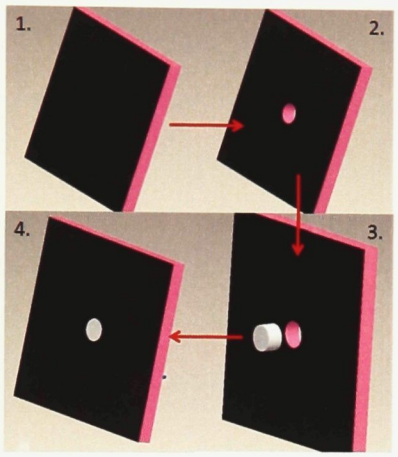

Figure 2-14 - Procedure for the installation of v.1 inserts.

The manufacturing steps are as follows:

1. The sandwich structure is manufactured and cured.
2. Two pilot holes; 1/4 inch then 1/2 inch in diameter are drilled through the sandwich panel, after which the pilot hole is expanded to 1-in with a handheld Dremel tool. A 1-in diameter template is placed over the face-sheet to aid in expanding the hole to the desired diameter.
3. The Delrin insert is machined to the desired thickness to match the panel width and is bonded into place with SC-780 room temperature cure epoxy.
4. The panel is then allowed to cure for 24 hrs at room temperature and then the fastener clearance hole is drilled in the centre of the insert.

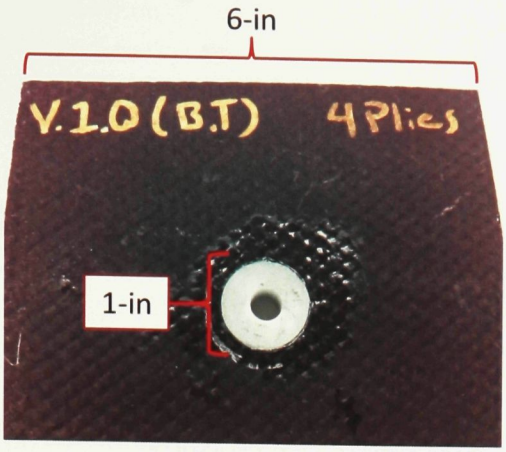

Figure 2-15 - Test specimen with a v.1 insert installed.

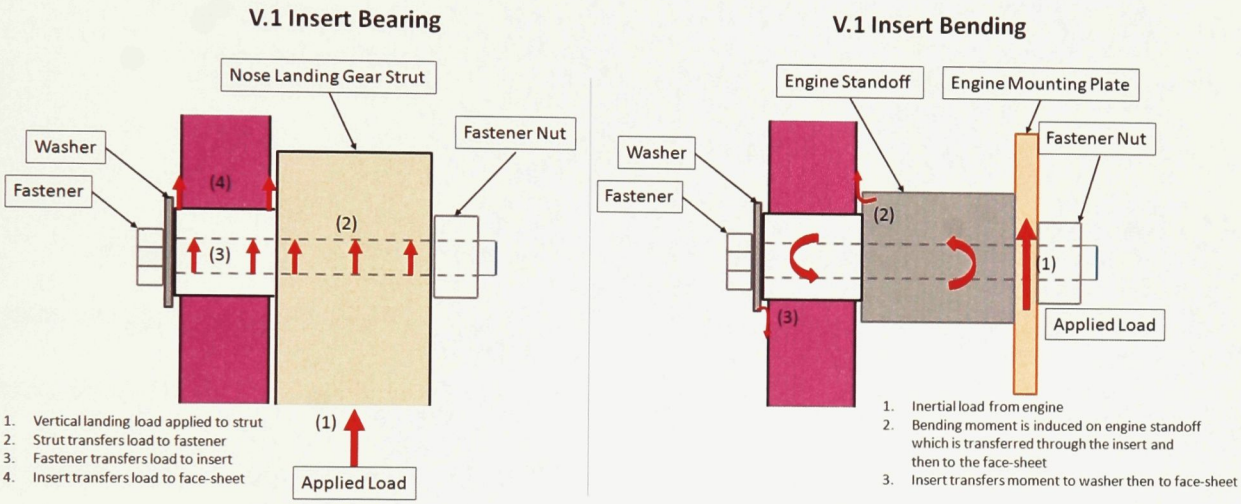

Figure 2-16 - Cross-section view of the v.1 insert assembly, illustrating the load paths under bearing and bending loads.

Some attractive features of the v.1 insert system include:

- **Inspection:** It is easy to identify damage or defects in the insert and surrounding sandwich panel.
- **Manufacturing:** The complexity of the insert itself is very low resulting in rapid, repeatable and inexpensive manufacturing.

Disadvantages include:

- **Bonding:** There are known bonding issues between epoxy and Delrin; the insert does not adhere well to the foam or the carbon face-sheet, despite surface preparation (sanding, cleaning etc.).
- **Repair:** No established method or procedure for repairing/replacing surrounding sandwich structure in the case of local failure.
- **Repeatability:** The method for cutting out the hole for the insert is imprecise and can lead to damage of the laminate around the edge of the hole. This is also an impractical manufacturing step for mass production or automation of any kind, as the quality of the hole depends largely on the skill of the operator. It is difficult to keep the insert in the proper position during curing as the insert or the uncured adhesive tends to move due to gravity. After the adhesive has cured it is sometimes possible to see areas where the adhesive has 'pooled' and an uneven bond line was created.
- **Additional hardware:** In order to cope with the bending loads, large metallic washers are installed on either side of inserts which adds weight to the overall insert system (this will be described in more detail in Chapter 3: Previous Insert Benchmark Testing).

Version 2 (v.2) of the fuselage was redesigned and manufactured in August of 2010 by Mario Mahendran [11]. Infusion method was changed to Closed Cavity Bag Moulding (CCBM) which features a reusable vacuum bag; this process will be discussed in more detail in the specimen manufacturing section of Chapter 3: Previous Insert Benchmarking Tests. The final infusion setup and the cured component are shown in Figure 2-17 [11].

Figure 2-17 - Fuselage v.2 infusion setup and final cured component [11].

The insert system for the v.2 fuselage features a 1-in diameter fibreglass 'puck' that is bonded into the foam core using West System 205 epoxy before the face-sheets are laid-up and infused. The result is an insert embedded in the sandwich panel. Figure 2-18 illustrates the procedure for installing the v.2 insert system. Figure 2-19 shows a test specimen with a v.2 insert installed. Figure 2-20 shows the cross-section of a typical v.2 insert joint, the load paths under bearing and bending are illustrated.

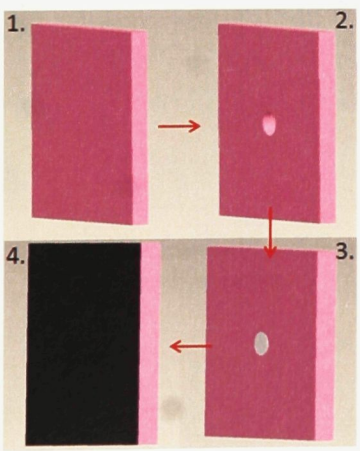

Figure 2-18 - Procedure for the installation of v.2 inserts.

The installation steps are as follows:

1. The foam core is manufactured to the desired shape.
2. A 1-in diameter hole is drilled into the foam where the insert is to be located.
3. The fibreglass insert is bonded into place and allowed to cure.
4. The core is laid-up and infused; once the panel is cured, a bolt clearance hole is drilled.

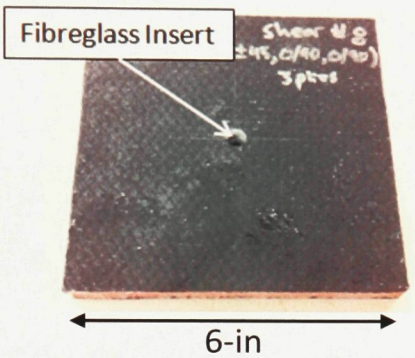

Figure 2-19 - Test specimen with a v.2 insert installed.

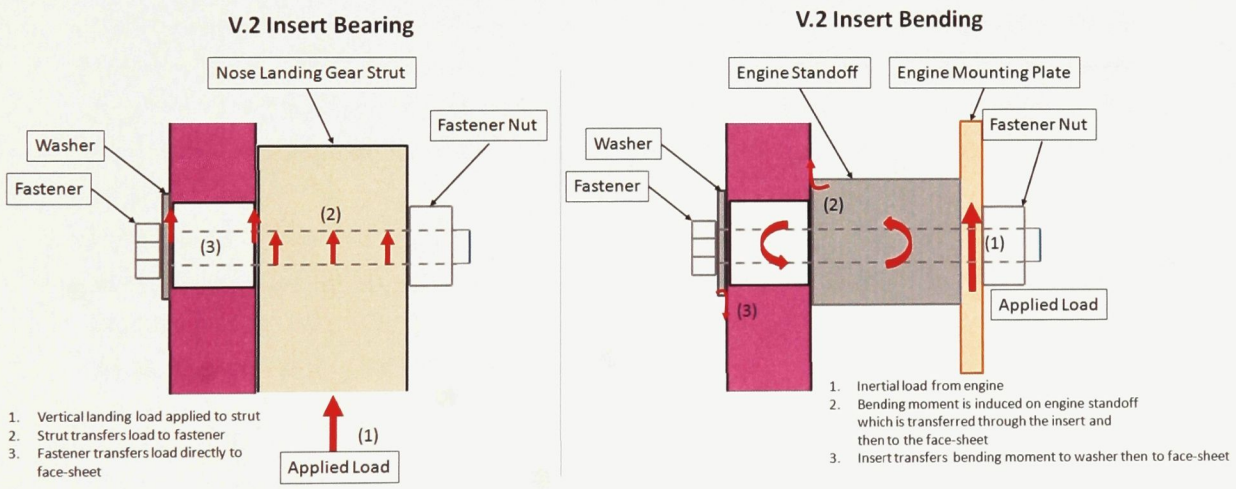

Figure 2-20 - Cross-section view of the v.2 insert assembly, illustrating the load paths under bearing and bending loads.

Advantages of the v.2 insert design include:

- **Bonding:** The fibreglass insert ensures good adhesion with both the foam core and the carbon-epoxy skin.
- **Manufacturing:** Large holes in the cured face-sheet are not necessary which helps speed up installation time and lower manufacturing difficulty.
- **Repeatability:** the hole in the foam-core and the fibreglass insert itself are pre-machined before infusion; this process ensures a good fit for every insert. It is much simpler to machine the hole precisely in the foam core than it is to cut a hole through the cured face-sheet as in v.1. Through the manufacturing process described in Figure 2-18 it is easy to place the insert in the desired location since the two face-sheets keep the insert in the proper position during the infusion and curing of the panel.

Disadvantages include:

- **Inspection:** Since the insert is covered by the face-sheet it is difficult to inspect any damage that may be present in the sandwich structure. If the insert has disbonded from the face-sheets and from the core, the load-carrying capability of the joint decreases.
- **Repair:** If a joint is damaged, there is no procedure developed for repairing or replacing the insert and the surrounding structure. Further development would be required to ensure that failures between the sandwich and insert body are avoided.
- **Wear and Tear:** In the absence of an additional bushing being installed, with repeated assemblies, the bolt or pin can cause the face-sheet to delaminate, which will decrease the bearing load carrying capacity of the joint. Additional hardware could be installed to limit the contact of the pin with the face-sheet such as the previously mentioned bushing; however, this adds weight and complexity to the design.
- **Additional Hardware:** Same as v.1.
- **Bolt Clearance Hole:** The insert is embedded in the sandwich structure before infusion, when the part is fully cured, it is difficult to locate the center of the insert to drill the bolt clearance hole.

Neither of the previous insert systems did consider the effects of fatigue loading in their design and development. The GeoSurv II airframe and fuselage experience vibration due to the engine mounted on the rear bulkhead. The effects of this vibration on

the load carrying capacity of inserts are investigated as part of this research and the study is presented in Chapter 5: The Effects of Vibration on the Insert Joint Strength.

As can be seen from this overview of the previous insert designs, there are several areas to be improved upon such as:

- **Repeatability:** Both of the insert designs presented have problems with manufacturing repeatability. In the case of v.1 inserts, the method for cutting the hole to install the insert is imprecise. For v.2 inserts, it is difficult to locate the centre of the hole in order to drill the bolt clearance hole.
- **Inspection:** v.2 inserts are embedded in the sandwich structure and therefore damage to the insert cannot be easily spotted.
- **Additional Hardware:** Both designs have the need for large washers on either side of the insert to spread the bending load across the face-sheets of the sandwich structure. This function could be incorporated into the design of the insert and the use of large steel washers could be limited or eliminated.

The next chapter will assess the performance of the previous insert designs in order to establish a baseline with which to compare future insert designs.

Chapter 3 - Previous Insert Design Benchmark Testing

In order to design an improved insert system, it is necessary to assess the performance of the previous insert designs. This chapter provides baseline data for comparison with future designs.

3.1 - Summary of Expected Loads for the GeoSurv II Prototype

This section outlines the locations on the GeoSurv II airframe that experience discrete loading and provides the critical load cases and values at each of those locations. The Prototype has four major locations where localized loads are introduced into the fuselage, as shown in Figure 3-1:

1. **Wing-to-fuselage interface** – lift, drag and moment loads, by the carry-through spar and shear bolts
2. **Main landing gear** – landing loads, by attachment bracket fastened to inner fuselage structure
3. **Nose landing gear** – landing loads, by shear bolts
4. **Engine mount** – thrust and engine inertia, by engine stand-off mounts

The main load cases for each of the major joints above are bearing or a combination of bearing and bending. In the case of the nose landing gear there is a small element of pull-out. This pull-out force is negligible in comparison with the other load cases and will not be considered further.

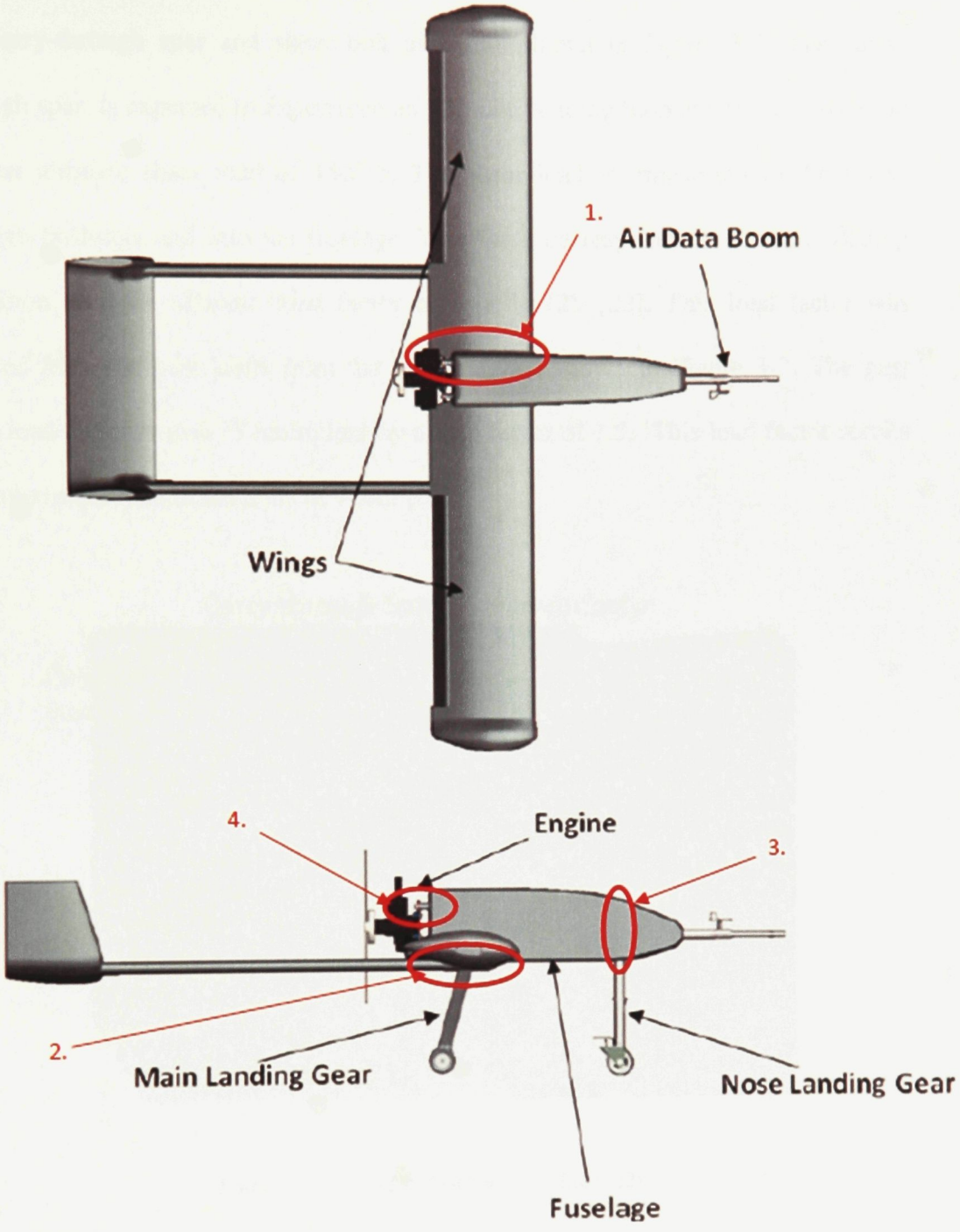

Figure 3-1 - Discrete load points on the GeoSurv II Prototype [22].

The wing loads due to aerodynamic forces are introduced into the fuselage via the carry-through spar and shear bolt assembly shown in Figure 3-2. The carry-through spar, is expected to experience an ultimate bending moment of 4.82×10^4 lb-in and an ultimate shear load of 1500lb. The shear load is transferred to the carry-through bushings and into the fuselage. This force corresponds to ultimate loading condition with an ultimate load factor of n = 10.125 [22]. This load factor was derived from the gust loads from the V-N diagram shown in Figure 3-3. The gust limit load factor is n=6.75 multiplied by a load factor of 1.5. This load factor results in a maximum load in the bolts of 720lb [22].

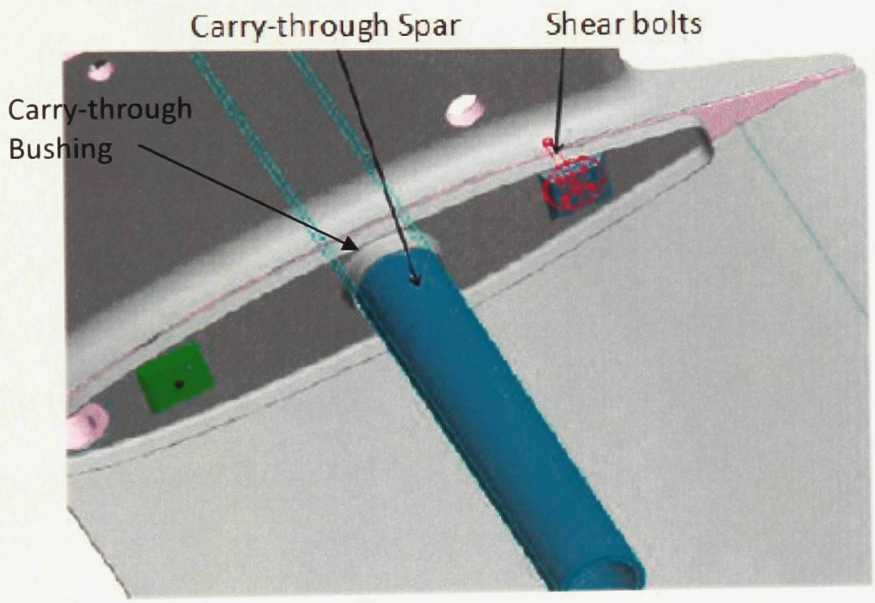

Figure 3-2 - Wing to fuselage interface [22].

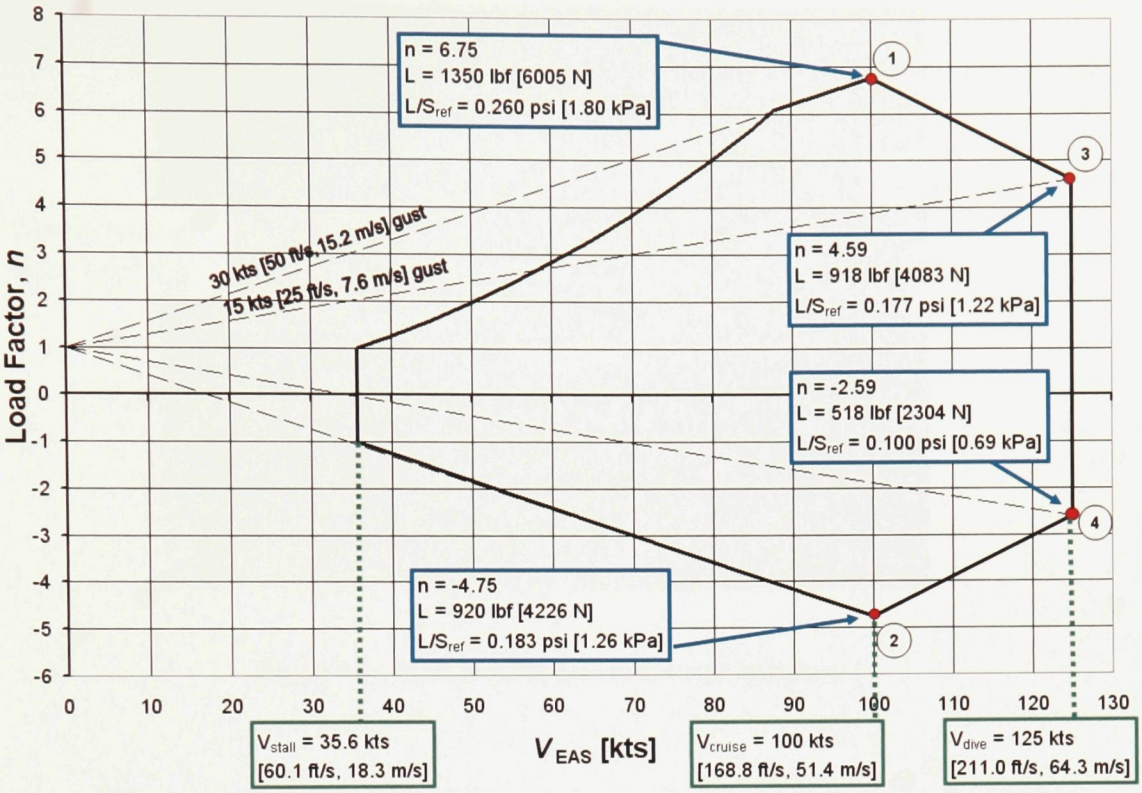

Figure 3-3- 200lb GeoSurv II V-N Diagram Details [20].

The main landing gear vertical and forward landing forces were determined to be 255lb, and 170lb respectively [22]. These loads are introduced to the fuselage via the main landing gear attachment bracket, which is bolted to the lower, inner fuselage structure. This assembly can be seen in Figure 3-4.

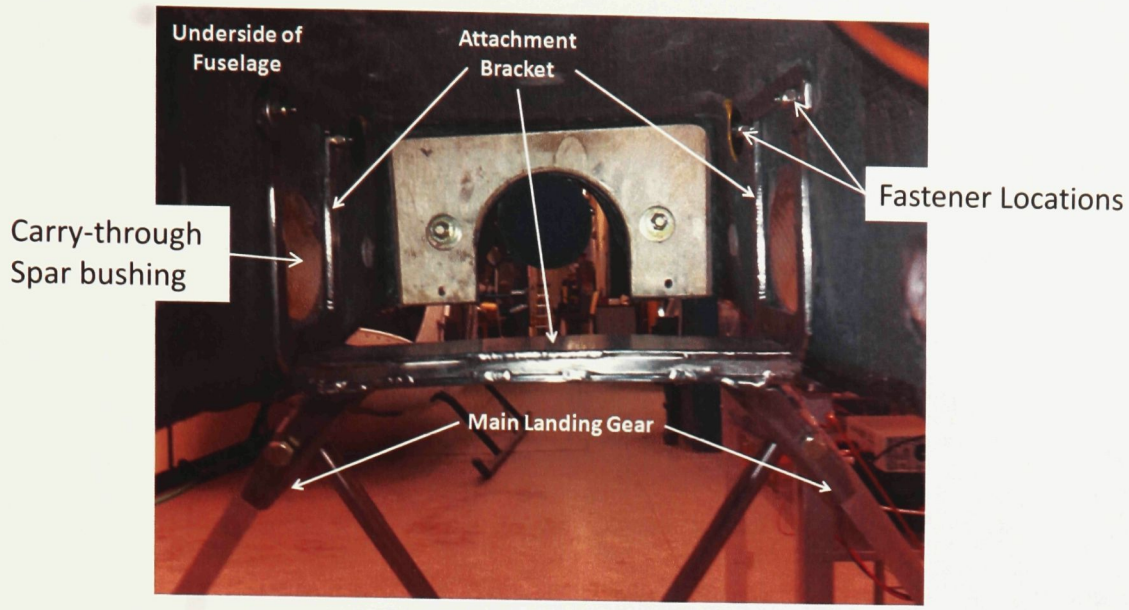

Figure 3-4 - Main landing gear to fuselage interface.

The nose gear loading conditions and magnitudes are outlined in the Carleton UAV standards document, derived from FAR 23 regulations, including [23]:

23.499: Supplementary conditions to nose wheel:

I.	Vertical load:	90lb
II.	Drag Load:	54lb
III.	Forward Load:	27lb
IV.	Side Load:	48lb

Figure 3-5 shows the layout of the nose landing gear to fuselage interface. The nose gear is attached by three shear bolts, one at the top of the nose landing gear main strut through the top cap, and two through the attachment bracket. The nose landing gear was designed and tested by Alan Lares in 2009-2010 [23].

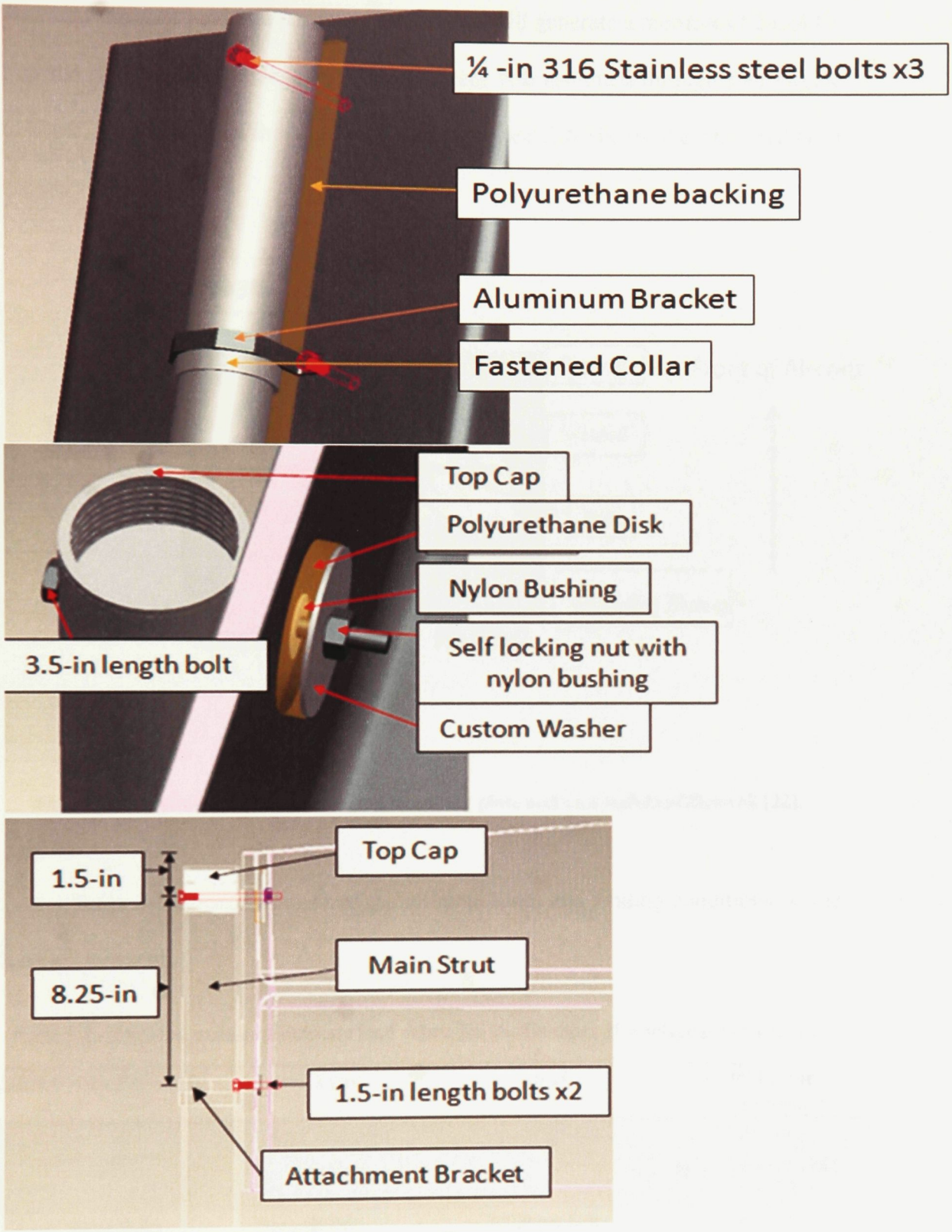

Figure 3-5 - Nose landing gear to fuselage interface [23].

At ultimate loading conditions, the engine will generate a moment of 24.24 lb-ft on the rear bulkhead assembly. This moment is transmitted through four engine stand-off bolts and into the sandwich panel. Figure 3-6 shows the rear bulkhead assembly.

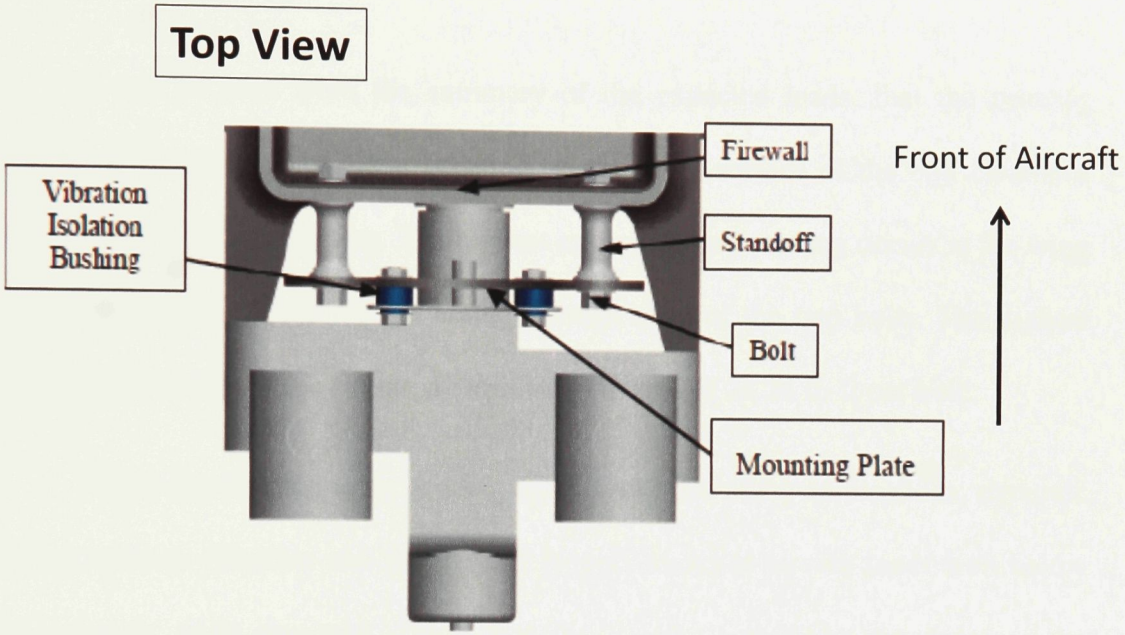

Figure 3-6 - Connection between engine mounting plate and rear bulkhead/firewall [22].

Table 3-1 below summarizes the ultimate loads and loading conditions on the fuselage structure.

Table 3-1 - The load cases and ultimate load values for the GeoSurv II fuselage prototype [22].

Interface with Fuselage	Load Type	Load	Load factor used in design
Wing: Carry-through spar/bushing	Bending moment	4.82×10^4 lb-in	n = 10.125
	Shear force	1500 lb	n = 10.125
Wing: Shear Bolts	Shear Force	720lb per bolt	n = 10.125
Main Landing Gear	Vertical Load	250 lb	n=3
	Forward Load	170 lb	n=3

Nose Landing Gear	Vertical Load	90 lb	n = 2.25
	Drag Load	54 lb	n = 2.25
	Forward Load	27 lb	n = 2.25
	Side Load	48 lb	n = 2.25
Engine Mounting Plate	Engine Weight	202 lb	
	Engine Thrust	210 lb	
	Engine Torque	24.24 lb-ft	

It can be seen from the summary of the expected loads, that the primary loading cases are in-plane shear (bearing on the inner surface of the bolt clearance hole) and out of plane bending. The highest expected shear loading occurs at the wing to fuselage interface with 720 lb acting through each of the two bolts. The highest bending load occurs at the engine mount with a torque of 24.24 lb-ft per bolt.

While considering static loading is adequate for some applications, dynamic loading such as vibration and fatigue can initiate cracks at service loads well below the materials' yield strengths. These dynamic loading conditions can decrease the service life of the component [17]. Dynamic loading and its effects on the load carrying capability of sandwich structure inserts will be investigated in Chapter 5: The Effects of Vibration on the v.3 Insert Joint Strength.

3.2 - Bearing Tests: v.1 and v.2 Inserts

The following subsections will outline the bearing test setup, results and discussion for the v.1 and v.2 insert designs. The bearing & bending tests for the v.2 inserts were performed in the summer of 2010 by Mario Mahendran. The testing for the v.1 inserts were performed during the time-frame of this research project.

3.2.1 - Bearing Test Experimental Setup

The sandwich structure coupons used for testing were made to represent the fuselage structure of the GeoSurv II Prototype. The core consists of PVC foam with a density of 6.2 lb/ft^3. The core height for the v.1 inserts was chosen to be 0.5 in, to simplify manufacturing. The v.2 insert coupons used 0.85 in core height for the sandwich panel to mimic the bulkhead of the GeoSurv II Fuselage. The use of two different core heights is justified because the primary parameter affecting bearing strength in foam-core sandwich panels is the face-sheet thickness [15]. All of the panels are 6x6 in, in size. Figure 3-7 shows a typical test coupon.

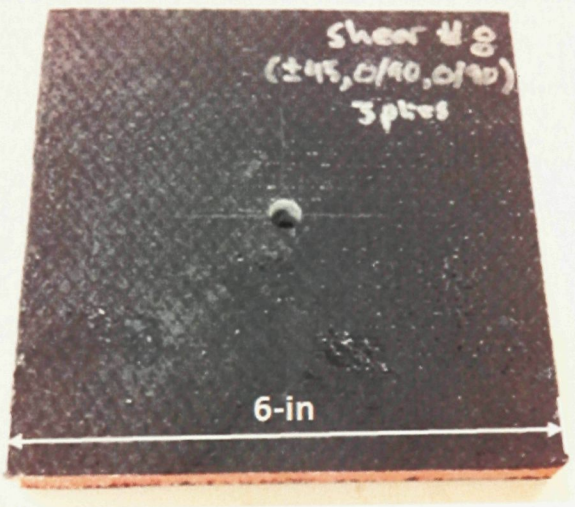

Figure 3-7 - Typical sandwich coupon.

All specimens were infused by CCBM. The full CCBM bag and coupon manufacturing procedures are outlined in Appendices A & B respectively.

Two different ply counts were tested for each of the two designs; a 2 and 4-ply face-sheet. The two different ply counts represent different areas of the fuselage. The wing to fuselage interface has 4 plies per skin, whereas the front bulkhead has 2 plies.

Quasi-isotropic layup patterns are close to the optimum for providing maximum fastener strength [21]. For this reason and in order to simplify later analyses, quasi-isotropic laminates will be predominantly used in this research.

A total of 15 specimens between the two designs were tested. The following naming convention was used to label the different specimens in this research:

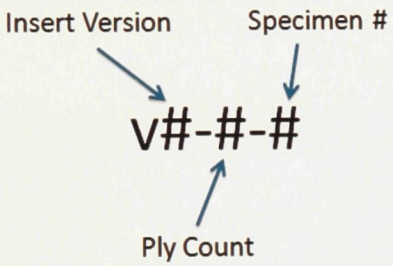

Figure 3-8 shows the loading scenario for the bearing tests. The specimens were tested using a Material Test System (MTS) load frame 22 kip capacity, Model 647.10A-01, Serial #: 1305166. The test specimen and load frame are shown in Figure 3-9. All of the coupons were tested at the same displacement rate of 0.1875——, and the data was sampled at a rate of 10 Hz. The following section discusses the results from testing.

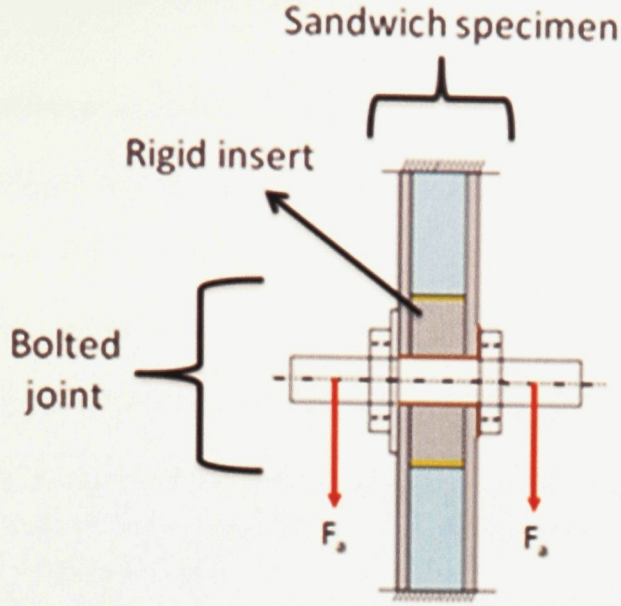

Figure 3-8 - Bearing test load case [11].

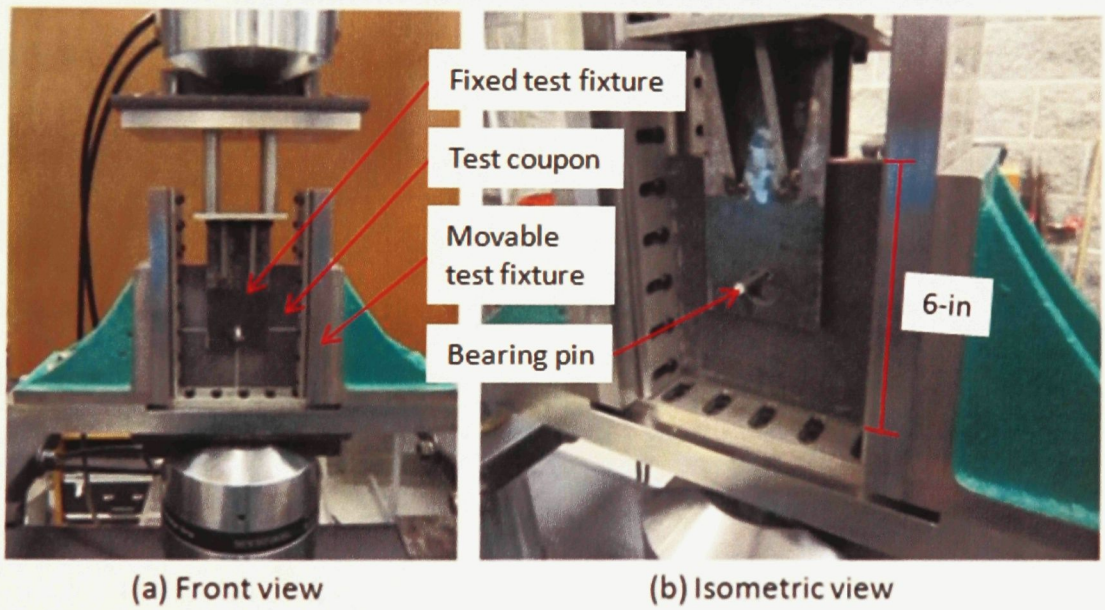

Figure 3-9 - Bearing test coupon in the load frame [11].

3.2.2 – Bearing Test Results and Discussion

As was mentioned in section 3.1 the highest bearing load on the GeoSurv II fuselage is at the wing to fuselage interface. The shear load at this joint under ultimate loading conditions is 720 lb. Ideally, the 4-ply sandwich structure joint should consistently fail when subjected to this load. With this design goal, the performance parameters that were be used to benchmark the two insert designs were:

- **Failure load:** 720 lb, determined using the force versus displacement graph described in section 2.1.1. The graphs were generated from the load frame test results.
- **Stiffness:** The force vs. displacement trace should be smooth (should not have spikes, indicative of cracking, disbonding, misalignment etc. during loading). The performance should also be consistent between trials (low scatter) and linear (negligible plastic deformation).

Table 3-2 shows the test matrix and resulting stiffness values and the measured maximum load values.

The failure load results for the 4-ply and 2-ply specimens are shown in Figure 3-10 and Figure 3-11 respectively. It can be seen that v.1 inserts have a higher average failure load than v.2. Comparing Figure 2-15 (v.1 insert) and Figure 2-19 (v.2 insert), it can be seen that the stress concentration on the face-sheet during bearing loading is higher in the v.2 insert design. This is due to the smaller radius hole in the face-sheet as compared to the v.1 insert design.

Table 3-2 - Test matrix for the v.1 and v.2 insert bearing tests.

Specimen #	Sandwich Layup	Insert Material	Stiffness (lb/in)	Max Load (lb)	Weight of Insert Including Washers (lb)
v.1-2-1	(+-45,0/90)	Delrin	30446	1512	0.10
v.1-2-2			36377	1554	0.10

v.1-2-3			30337	880	0.10
v.1-2-4			31387	1447	0.10
v.1-4-1	(+-45,0/90,0/90,+-45)		39902	1521	0.10
v.1-4-2			31391	1247	0.10
v.1-4-3			32749	1344	0.10
v.1-4-4			35724	1591	0.10
v.2-2-1	(+-45,0/90)	Fibreglass	44139	969	0.11
v.2-2-2			24889	848	0.11
v.2-2-3			38002	858	0.11
v.2-2-4			33642	929	0.11
v.2-4-1	(+-45,0/90,0/90,+-45)		29139	1264	0.11
v.2-4-2			35075	1196	0.11
v.2-4-3			32209	867	0.11

During the testing of the v.1, 4-ply specimens it was seen that the force versus displacement curve became non-linear at approximately 1400-1500 lb. Upon removal of the steel loading pin it was apparent that the non-linear trend in the graph was due to the pin plastically deforming under the load. Since the loading conditions and data after the onset of non-linearity are not representative of the joint stiffness and strength, the tests were manually terminated at approximately 1500 lb, prior to the insert failure. Since the tests were stopped at approximately the same load value, the scatter in first load drop values for the 4-ply, v.1 inserts is very low. It is therefore not possible to say with certainty which of the two insert designs is more consistent based on the 4-ply tests.

Unlike the 4-ply tests, the 2-ply specimens were loaded until failure was observed. There was no plastic deformation since the specimens failed below 1400 lb. Since all of the specimens were loaded to failure it is possible to compare the consistency of the two designs. The results indicate that v.2 inserts have less variability in terms of failure loads.

It is important to note that for both designs, the average failure loads were significantly higher than the required ultimate load value of 720 lb, which implies that both v.1 and v.2 inserts are overdesigned. There is, therefore, room for optimization of weight. There was significant variability in failure loads for both insert designs; this is an area that requires improvement.

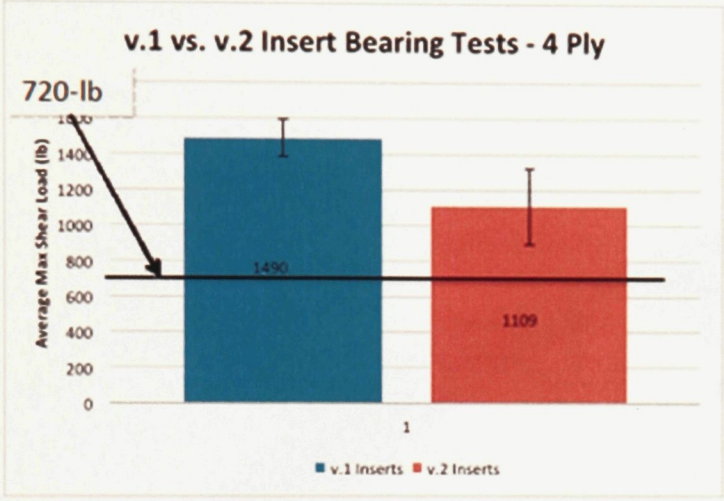

Figure 3-10- Average of the failure loads for the 4-ply v.1 and v.2 insert bearing tests.

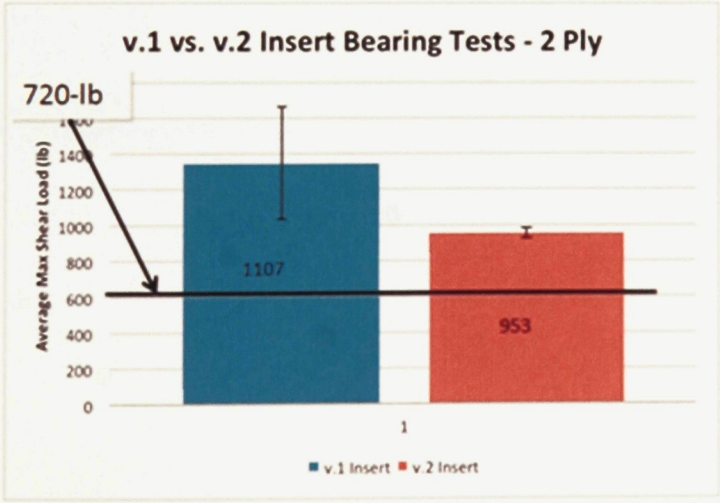

Figure 3-11 - Average failure loads for the 2-ply v.1 and v.2 insert bearing tests.

Figure 3-12 and Figure 3-13 show the average of the stiffness values for the 4-ply and 2-ply bearing tests. Both figures compare the v.1 and v.2 insert designs. The data for each individual test specimen was normalized to ensure that when the forces were averaged, they corresponded to the same displacement. This was done by shifting the zero displacement points. The hatched bands represent scatter, one standard deviation about the mean.

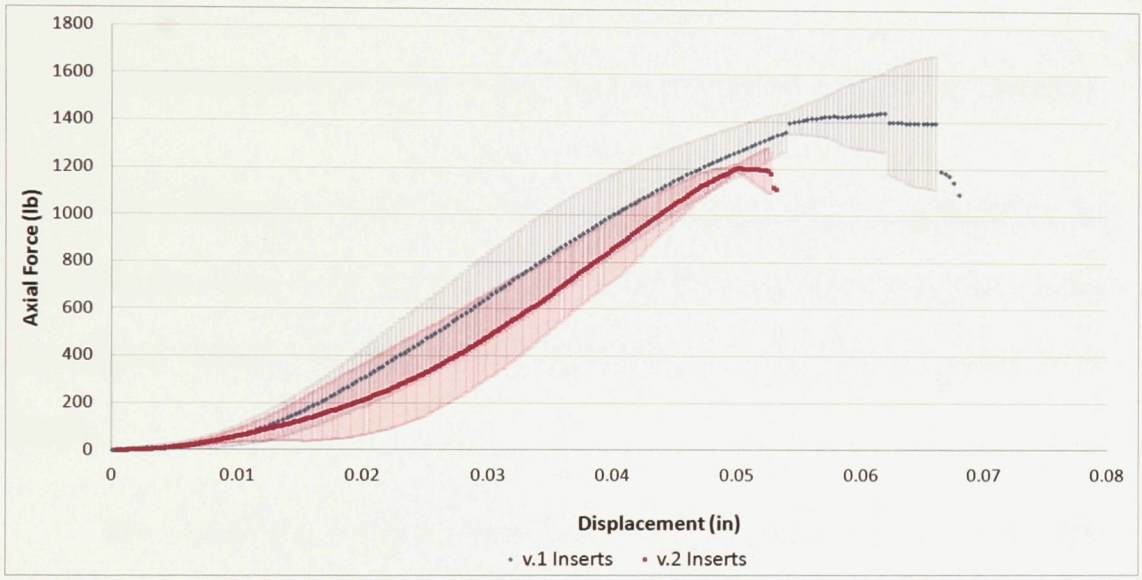

Figure 3-12 - Comparison of the stiffnesses between v.1 and v.2 inserts 4-ply sandwich specimens.

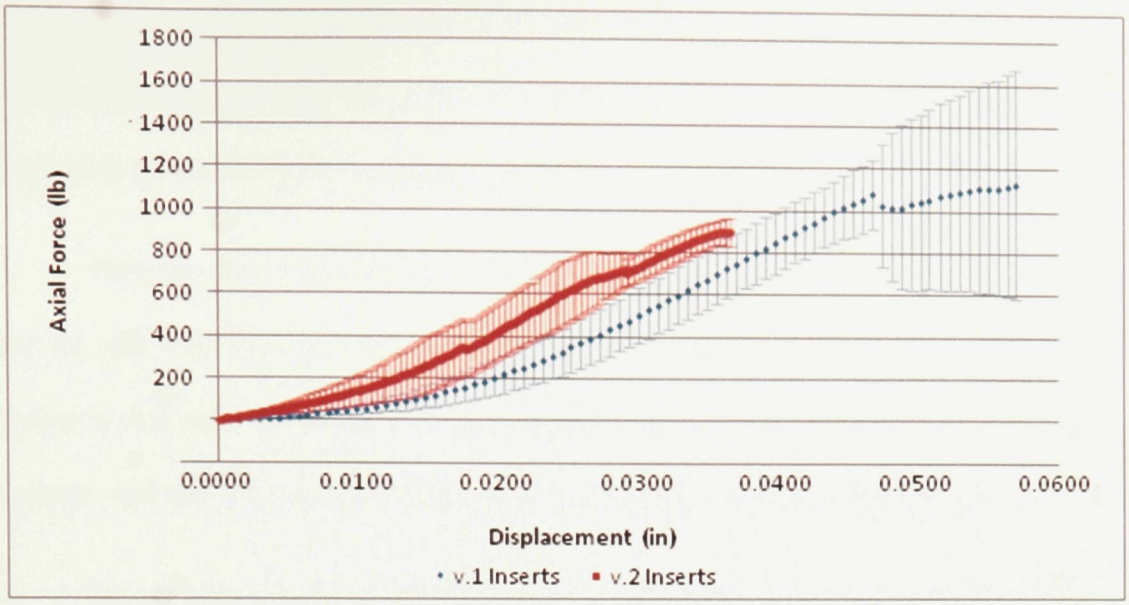

Figure 3-13 - Comparison of the stiffness's between v.1 and v.2 inserts 2-ply sandwich specimens.

The stiffnesses of both the v.1 and v.2 insert designs were very similar as can be seen by the slopes in the two graphs. It is difficult to conclude which insert design has a higher stiffness; however, the data does provide a basis for comparing future designs.

The sample rate for data acquisition for all specimen tests was 10Hz. The specimens v.2-4-2, v.2-4-3, and v.1-2-4, were inadvertently sampled at a lower frequency yielding fewer data points than the other specimens. Despite this test error, the results are adequate (the data points are not too sparse). The effect of using these samples with fewer data points when calculating the average stiffnesses can be seen in Figure 3-12 and Figure 3-13. In Figure 3-13 for example, it can be seen that the v.1 stiffness curve has fewer points than v.2. This is because when averaging the results for all 4 specimens, it is only possible to use the data points that correspond to the same displacement values between each specimen. In other words, the axial

displacement values between specimens must match. Since specimen v.1-2-4 has fewer sample points that the others, the density of the data points for the overall average is governed by the sample rate of that specimen test.

Near the first load drop on the graphs of both Figure 3-12 and Figure 3-13, it can be seen that there are discontinuities and the error bars become irregular. The reason is that each specimen fails at a slightly different load value, and therefore the average, and the standard deviation associated with the sample, change abruptly.

It was determined that the strength to weight ratio of the v.1 inserts was higher than that of the v.2 design in bearing. The lower weight combined with the fact that the joint has a lower stress concentration than the v.2 design, would lead to a higher strength to weight ratio.

In summary, this section analyzed the results of the bearing tests performed on the v.1 and v.2 inserts, for both a 2 and 4-ply sandwich structure. It was determined that the v.1 inserts have a higher overall strength and a higher strength to weight ratio. The v.1 inserts also displayed higher variability due to the poor bonding between the insert and sandwich structure. The v.2 inserts have less variability in the measured failure loads as observed in the 2-ply tests. The variability in the stiffness between the two designs is relatively similar. It is concluded that both designs have areas that can be improved upon, specifically in the areas of strength and variability. Both designs are considered overdesigned in bearing.

3.3 - Bending Tests: v.1 and v.2 Inserts

The following section presents the bending tests performed for both the v.1 and v.2 insert designs.

3.3.1 – Bending Test Experimental Setup

It was decided that there were too many operational errors during the testing of the v.2, 3-ply specimens such as: misalignments, coupon manufacturing mistakes and inadequate sample rates. These tests were performed in the summer of 2010. Further discussion on this subject can be found in section 7.2.3 of M. Mahendran's thesis [11]. For these reasons the bending specimens that will be used for this research will be the 4-ply specimens.

The only notable difference in the manufacturing of the bending test coupons as compared to the bearing tests is in the clearance hole, which measures 3/8-in in diameter.

Table 3-3 shows the test matrix for the bending tests. A total of 8 specimens were tested between v.1 and v.2 inserts. The layup was chosen to represent the rear bulkhead of the GeoSurv II fuselage.

Table 3-3 - Test matrix for the v.1 and v.2 insert bearing tests.

Insert Bending Tests					
Version 1			**Version 2**		
Specimen #	**Ply Orientation**	**Number of Plies**	**Specimen #**	**Ply Orientation**	**Number of Plies**
1	(+-45,0/90)	4	1	(+-45,0/90)	4
2	(+-45,0/90)	4	2	(+-45,0/90)	4
3	(+-45,0/90)	4	3	(+-45,0/90)	4
4	(+-45,0/90)	4	4	(+-45,0/90)	4

Figure 3-14 shows the loading scenario of the bending test, and Figure 3-15 shows a typical coupon in the load-frame. The same MTS load frame was used for both the bearing and bending tests.

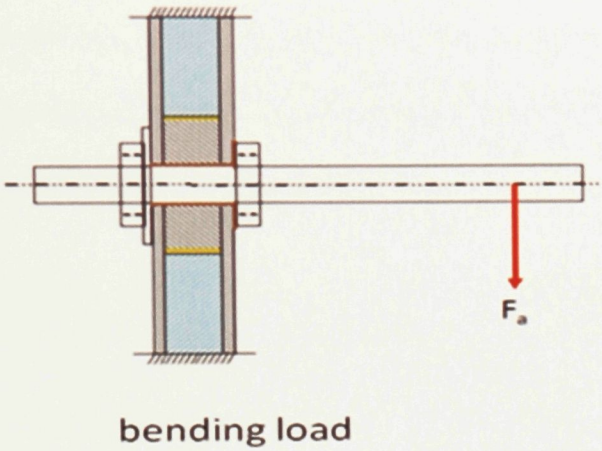

Figure 3-14 - Bearing test load case [11].

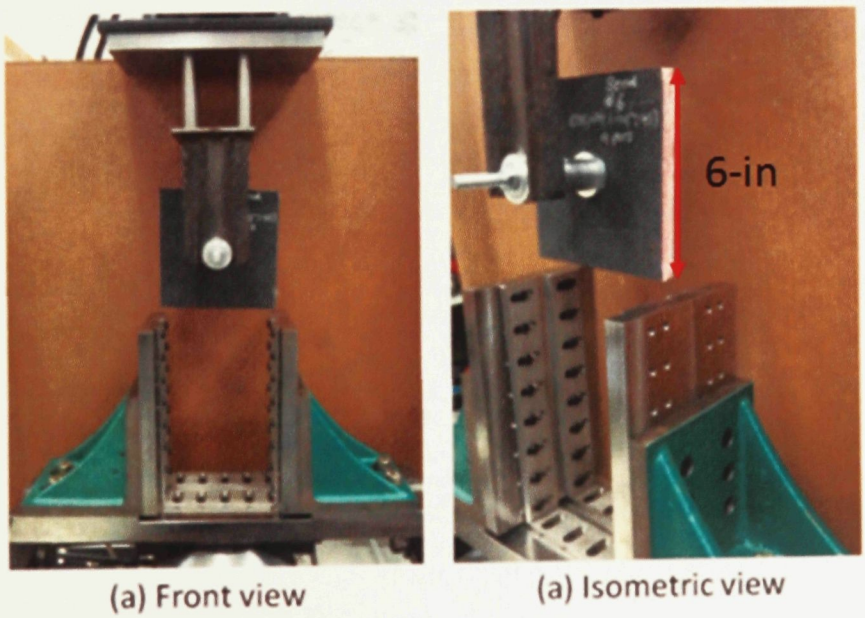

Figure 3-15 - Bending test coupon in the load frame [11].

3.2.2– Bending Test Results and Discussion

As was mentioned in the previous sections, the highest bending moment that the fuselage will experience is 24 ft-lb. The engine standoff mounts measure 0.20 ft, which results in an ultimate applied load (F_a, see Figure 3-14) of 121 lb. If the joint is designed properly, it should fail at a loaf F_a of 121 lb. Keeping this design guideline in mind, the following parameters will be used to compare and establish a benchmark for the performance of the v.1 and v.2 designs in bending:

- **Failure load:** Target: 121 lb, determined using the force vs. displacement plots as described in Chapter 2, section 2.1.1. The graphs will be generated from the testing in the load frame.
- **Stiffness:** From the force vs. displacement graph, the stiffness should be smooth (should not have load spikes, indicative of pre-failure, cracking, disbonding, misalignment etc.). It should also be consistent between trials (low scatter) and linear (negligible plastic deformation). The graph is a representation of performance.

The tests were manually terminated at approximately 600 lb, well beyond the ultimate loading conditions. This was done because in the previous (discarded) 3-ply tests [11], the pin, and test fixture were plastically deforming at a measured load of approximately 1200 lb. Figure 3-16 shows an example of such a case. In order to prevent damage to the test apparatus, the 4-ply tests were terminated at 600 lb.

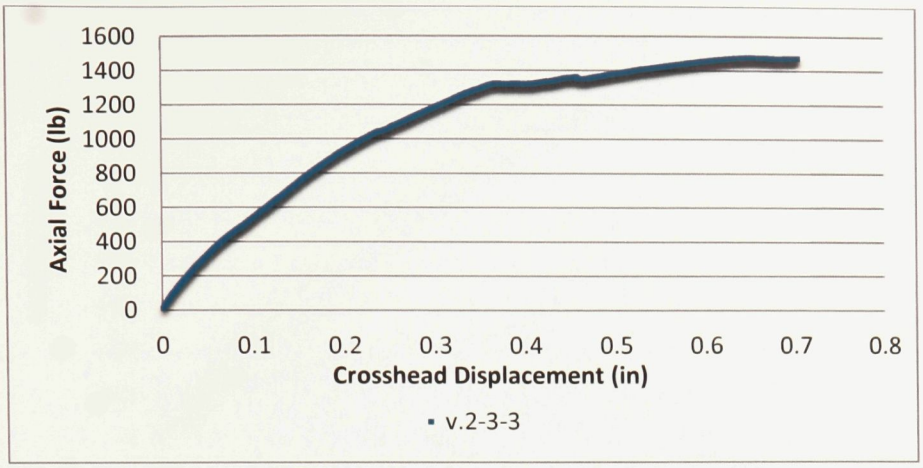

Figure 3-16 - An example of the force versus displacement curve of the v.2, 3-ply specimen tests [11].

Figure 3-17 shows the results of the v.1 inserts. There are some features in these results that bear discussion.

From the graph it can be seen that between approximately 100-300 lb an initial failure is observed. This failure can be explained with the help of Figure 3-18, which shows the cross-section of a v.1 specimen in the test fixture. A gap between the washer and the face-sheet on the bottom side of the joint can be seen. This gap is caused by the Delrin insert not being flush with the face-sheet on both sides of the sandwich structure; it slightly protrudes at either side. The reason is the different manufacturing methods: the Delrin insert was precision machined using a lathe while the sandwich panel was manufactured using CCBM, which produces a part with less dimensional accuracy.

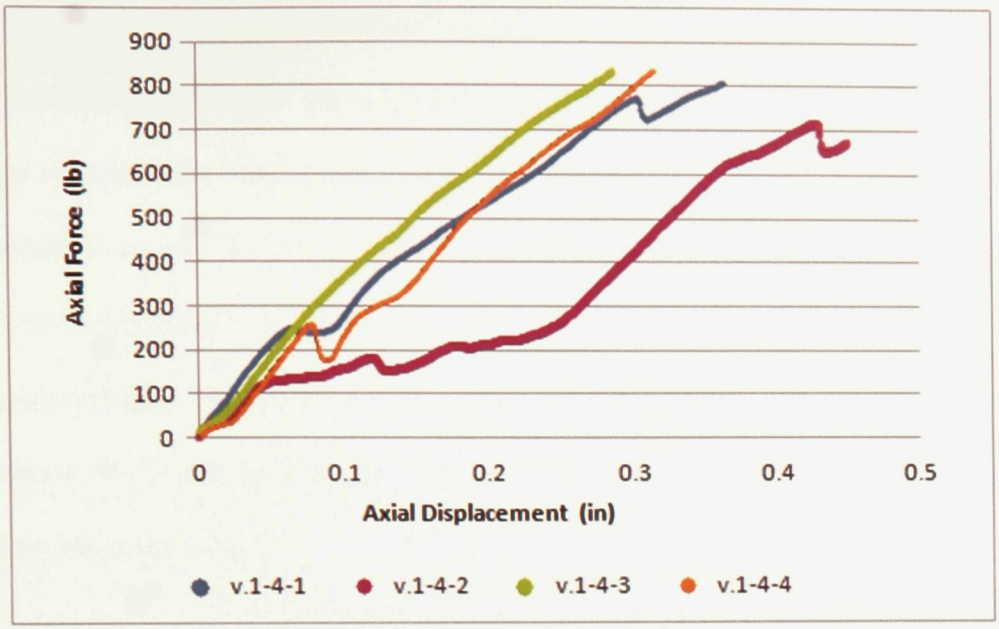

Figure 3-17 - Test results for the v.1, 4-ply bending tests.

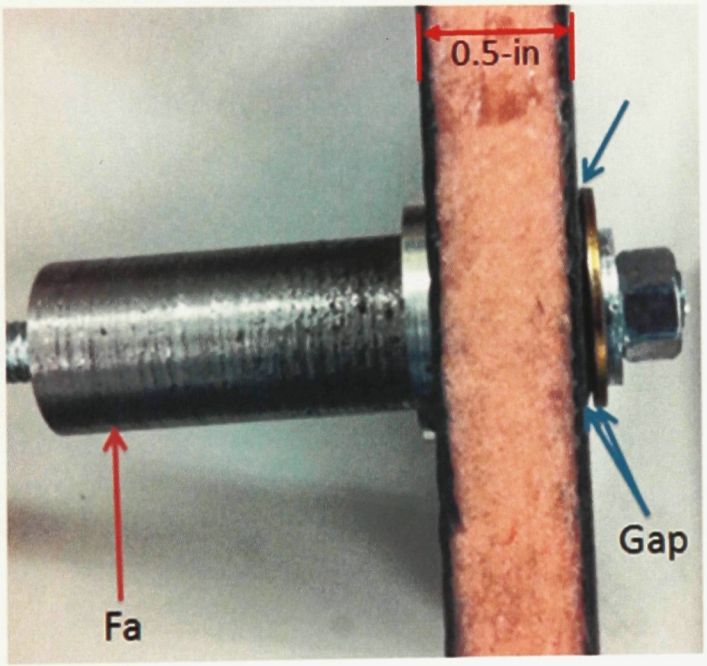

Figure 3-18 - Cross-sectional view of a bending specimen.

When the load is applied, it is transferred directly into the insert since the washer is not flush with the face-sheet. The insert is thus forced to rotate within the

sandwich structure. The failures seen in Figure 3-17 (v.2-4-1, v.2-4-2, v.2-4-4) are the inserts disbonding within the sandwich structure. After the insert disbonds, it no longer transfers any load to the surrounding structure and simply 'floats' within the sandwich structure. As the assembly rotates and the washer regains contact on the face-sheet, the measured load increases once more. Cracking was heard during testing at approximately 100-250 lb, which supports this hypothesis. Furthermore, when the specimen was removed from the apparatus after testing, the insert could be easily pushed out of the panel.

Specimen v.1-4-2 had a larger protrusion of the insert on both sides of the panel thus, the joint had further to rotate before the washer made contact with the face-sheet than the other specimens. That is the reason why the curve flattens out at a load of 150lbf for a longer period.

Figure 3-19 shows the combined force-displacement curves for both v.1 and v.2 inserts. It can be seen that the v.2 inserts are on average stiffer than the v.1 inserts. The reason is that the v.2 design allows for a flush contact of the washer with the face-sheet. This ensures that the bending load is transferred directly and more uniformly to the sandwich structure. In the case of the v.1 insert design, the load passes through the insert and then to the sandwich structure, only after the insert disbonds.

The breaks or 'discontinuities' in the graph are again a result of individual specimens failing and as a result shifting the overall average of the stiffness curve.

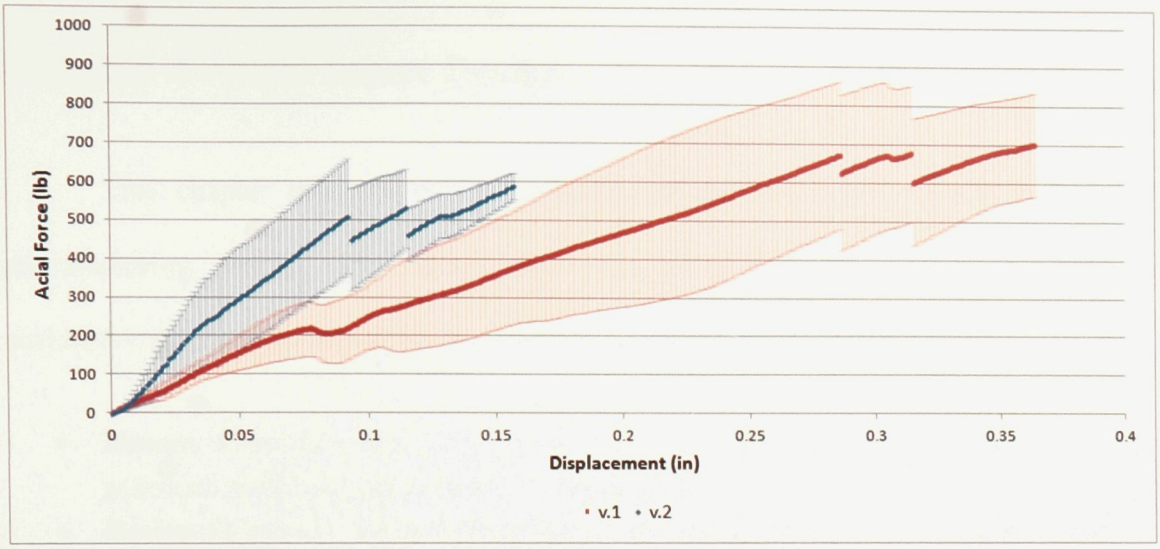

Figure 3-19 - Force versus displacement curves for the 4-ply insert bending load tests, v.1 and v.2 inserts.

The purpose of this chapter was to explain the previous insert designs, and establish a comparison basis for the new insert design. It is clear from the performance tests of both the v.1 and v.2 insert designs that there is room for improvement. Areas that should be addressed in an improved design include:

- A more optimized design; to handle 700 lb in bearing and 120 lb in bending, v.1 and v.2 inserts were overdesigned.
- Less scatter between specimens.
- More linearity in the stiffness, less discontinuities and spikes suggesting premature failures and disbonds during testing.

The next chapter presents the design process of an improved insert system, which takes into account the strengths and weaknesses of the previous two designs as well as other designs that are commonly used in industry.

Chapter 4 – New Insert Design

This chapter presents the development of the new insert system design and manufacturing process. The methodology used to develop the new insert system is outlined in Figure 1-6. The following topics are covered in this chapter:

- **Design Criteria:** The requirements for the new design are established; any potential designs must conform to these criteria.
- **Design Synthesis:** The best conceptual designs are identified for further study.
- **Manufacturing Process Selection:** Potential materials and manufacturing methods are investigated.
- **Material Performance Testing:** The candidate materials are tested and their performance assessed.

These topics will establish the design, manufacturing process and the materials used for the v.3 inserts.

4.1 – Design Criteria

The purpose of designing a new insert system is to improve upon the limitations of the current designs. The following criteria and guidelines are proposed for the v.3 design:

- **Strength:** Static and dynamic strength are optimized for the specific load case/ magnitudes (optimization of the v.3 insert design will be discussed in Chapter 6). The dynamic loading will be addressed in Chapter 5. The joint fails at ultimate loading condition.
- **Weight:** The insert system should be as light as possible.
- **Magnetic Signature:** The magnetic interference caused by the insert must be minimal.
- **Manufacturability:** The inserts are easily and rapidly produced.

- **Ease of Integration/ Assembly:** The inserts are easily installed into the structure, with little preparation and installations steps. This ensures structural consistency and repeatability between joints.
- **Cost:** Materials, processing and manufacturing should be cost effective. The candidate materials and processes should be investigated to choose the most cost effective manufacturing solution.
- **Repair and Maintenance:** The insert system should easily replaced or repaired in the event that it becomes damaged.

The aforementioned design criteria were used in conjunction with the literature review in the development of several conceptual designs, which will be presented next.

4.2 – Design Synthesis

The purpose of this section is to select the best possible design concepts from a group of candidate designs in order to advance to the process and material selection. Many insert designs were considered, however, many of them did not meet the criteria discussed in the previous section, and will not be presented. The two families of inserts that displayed the best potential and are presented are the plug & sleeve and pin & collar designs.

An important design consideration is whether the insert should be installed before or after panel manufacturing. The study by Bianchi et al. [14], summarized in section 2.1 concluded that hot bonded inserts (installed prior to sandwich panel curing) have higher pullout strengths than cold bonded inserts (installed after sandwich panel curing). This is expected since the source of strength for the insert in this loading scenario is the potting compound. For plug and sleeve inserts, the shear strength and bending strength are heavily influenced by the mechanical design itself and less so by the potting compound used to install them. For this reason it is not possible to conclude that hot bonded plug

and sleeve inserts will be stronger than cold bonded ones without an additional study. This research will focus on cold bonded inserts for the following reasons:

- More efficient test coupon manufacturing: It is advantageous to be able to manufacture both the inserts and the panels simultaneously in separate processes.
- Removes uncertainty about infusion defects in the vicinity of the joint.

The plug and sleeve design was introduced in section 2.1.2, as a common insert method for joining monolithic composite panels together. Figure 4-1 illustrates the elements of the design adapted to a sandwich panel. Figure 4-2 shows the cross section of a typical plug and sleeve joint assembly, the load paths in bearing and bending are illustrated.

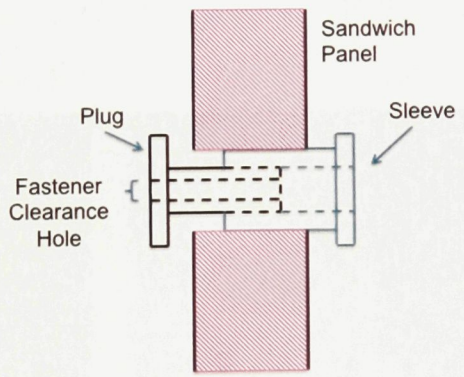

Figure 4-1 - Plug and sleeve insert design for a sandwich panel.

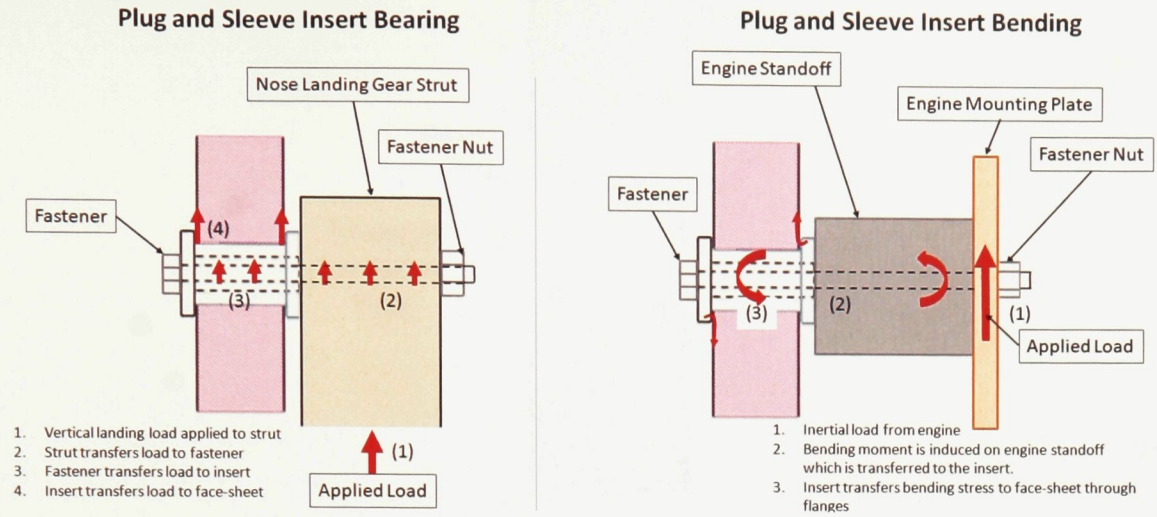

Figure 4-2 - Cross-section view of the plug and sleeve insert assembly, illustrating the load paths under bearing and bending loads.

As the name suggests, this insert design features two components; a plug and a sleeve that come together and lock in place either by threading or bonding. A solid model of the plug and sleeve assembly is shown in Figure 4-3. A variation on the design is shown in Figure 4-4.

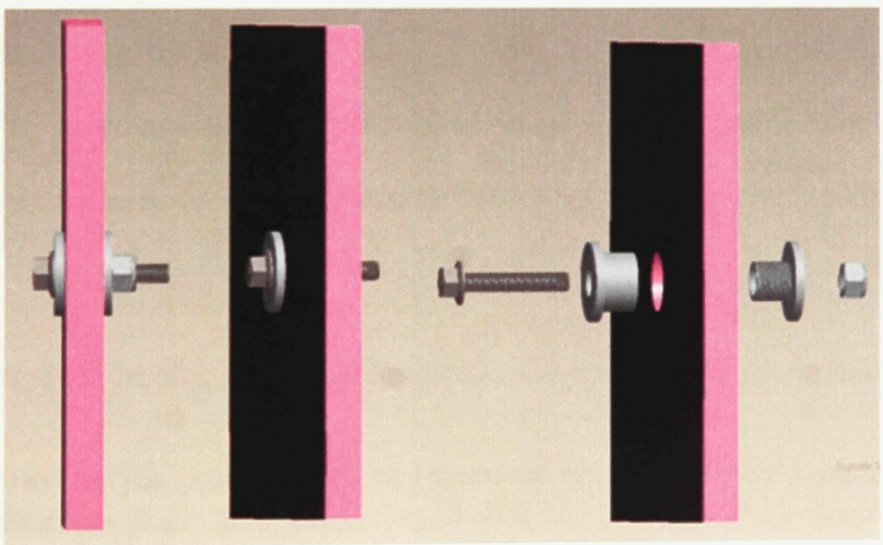

Figure 4-3 - Plug and sleeve insert design v.3.1.

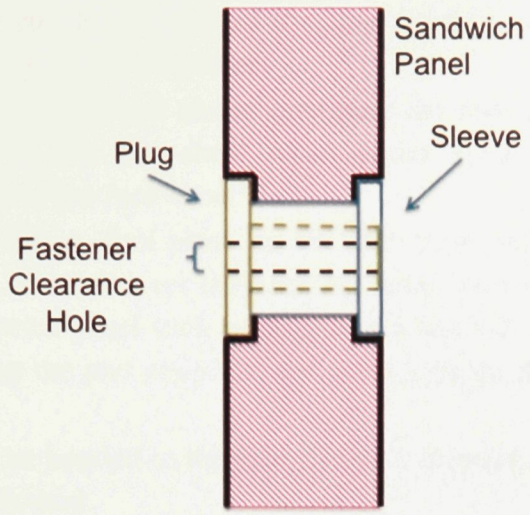

Figure 4-4–Recessed Plug and sleeve insert design v.3.2.

The difference between these two designs is that in v.3.2 (Figure 4-4) the flanges are recessed in the sandwich panel. This allows the insert to be flush with the face-sheet and not protrude out of the sandwich structure. This is desirable in some applications such as the nose landing gear where the strut should be flush against the front bulkhead when attached to help distribute the load on the front bulkhead. The design it is more complicated from a manufacturing point of view, the foam core would need to be machined to accommodate the thickness of the recessed flanges. For this added complexity to the manufacturing of coupons for testing it will not be considered in this research.

Advantages of the plug and sleeve design over the previous designs include:

- Allows for the possibility of the insert to be mechanically fastened and not bonded into place. This feature would allow for in-field replacement to be quick and simple to do in the event of an insert being damaged in service. In addition to in-service replacement capabilities, a mechanically fastened insert system would remove the issues commonly associated with bonding. Problems with bonding include: proper preparation, bond-line thickness control, compatible materials,

proper adhesion etc. In the case of dynamic loading, nuts and washers will be holding the plug and sleeve together.

- The flanges of the plug and sleeve compress the face-sheet to the core, adding lateral stability to the face-sheet when under shear loading, increasing the buckling strength of the face-sheet.
- The flanges provide a 'foot print' on the face-sheet which acts to distribute the load in bending. This removes the need for large, heavy metal washers on either side of the sandwich panel such as designs v.1 and v.2. (See Figure 3-18). As a result of reducing the part count for the insert system, there are potential weight savings.
- The flanges can be bonded to the face sheets to increase the shear load capability of the inserts if desired.
- If the insert system were not bonded into place then theoretically it would make inspection of the insert itself and the surrounding structure possible.

Disadvantages of the plug and sleeve design include:

- The insert is more complex and therefore will require additional manufacturing steps.
- Due to the higher complexity, the cost of the insert system could potentially be higher.
- If bonded instead of mechanically fastened, the design has the same problem with regards to inspection and easy replacement of the insert in-situ.

The pin and collar design is similar to the plug and sleeve design; however, it features a single pin that transfers the bearing load to the face-sheets. The pin is held in place by a collar, which aids in transferring the bending load into the sandwich structure. Figure 4-5 shows a schematic of the pin and collar design. The pin and collar design is similar to the HI-Lok metallic fastener presented in section 2.1.2, adapted to a sandwich structure.

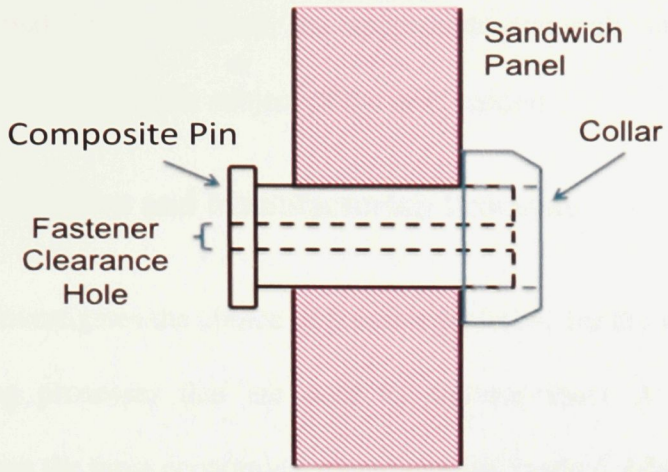

Figure 4-5 - Pin and collar insert design.

The pin and collar design shares many of the same advantages as the plug and sleeve design, however in addition to these this design features:

- A simpler design from a manufacturing standpoint. It could be possible to find a supplier of standard threaded collars (lock nut, hex nut etc.), which would make production of this insert system simpler.

Disadvantages include:

- Collars with the desired configuration may not be readily available and may have to be manufactured.
- Collar will be larger than the flanges of the plug and sleeve design, which would increase the weight of the insert system.
- To simplify manufacturing, the collar will likely be metallic.
- Smaller surface area to bond or thread together as compared to the plug and sleeve design, which could affect the insert's load carrying capability.
- The collar would likely protrude further than the flanges of the plug and sleeve design.

Although both of the presented designs could be potentially developed into working solutions, the plug and sleeve design was chosen as the best candidate for the new insert system. The new design will be identified as v.3.

With the conceptual design selected, the appropriate materials and manufacturing processes must be chosen; this is the subject of the next section.

4.3 – Material Selection and Manufacturing Processes

This section investigates the choice of possible materials for the v.3 inserts as well as the manufacturing processes that are used to produce them. A cost analysis is performed to determine the most economical manufacturing method. Manufacturing trials aimed at assessing different materials workability were performed as well as strength testing of those materials in order to see how they behave under applied loads.

4.3.1 – Material and Manufacturing Process Selection

There are various factors to consider when selecting a suitable material, some of these factors include:

- **Weight:** The material should be as light as possible; (v.1 inserts are 0.10 lb including washers).
- **Material compatibility:** Localized corrosion can develop with dissimilar materials (galvanic) and should be controlled or avoided wherever possible.
- **Minimal magnetic signature:** For geomagnetic applications the magnetic signature should be kept as low as possible (i.e. avoid the use of ferromagnetic components).
- **Manufacturability:** The material should be easily formed, cast machined etc.
- **Cost:** Material and manufacturing process should both be cost effective.
- **Fatigue/damage resistance:** The selected material should be damage resistant and be able to withstand dynamic loads (fatigue/vibration).

With these criteria in mind, the materials presented in Table 4-1 were identified as possible candidates. Manufacturing methods are also presented for each material.

Table 4-1 also presents the estimated cost per insert for each of the materials/ manufacturing processes. All prices were obtained from the same supplier (McMaster-Carr) to maintain consistency. Low volume purchases (raw material enough to manufacture 1-12 inserts) were used for pricing. The diameter of the inserts was assumed to be 0.75-in for the purposes of this exercise. Please refer to Appendix C for the insert cost calculations.

Table 4-1 - Possible materials and manufacturing processes for v.3 inserts along with their respective price per insert (see Appendix C for insert cost calculations).

Material	Manufacturing Process	Parent Materials	Cost Per Insert $ (approximate)
Carbon fibre - Epoxy	Casting	Chopped fibre/ Epoxy	0.85
Fibreglass - Epoxy	Casting	Chopped fibre/ Epoxy	0.77
Fibreglass - Polyurethane	Casting	Chopped fibre/ Polyurethane	2.66
Carbon fibre – Epoxy	Machining	Carbon-Epoxy Round Stock	7.33
Fibreglass – Epoxy	Machining	Fibreglass-Epoxy Round Stock	0.35
Wood (Birch)	Machining	Round Stock	0.45

Casting and machining were chosen as suitable processes for manufacturing the v.3 inserts. Table 4-2 and Table 4-3 present the detailed manufacturing steps for both machining and casting of the v.3 inserts. The estimated time it takes for each step and the overall time per insert is outlined as well.

The times shown in Table 4-2 were determined from machining trials using a 0.75-in aluminum round and timing each machining step independently. The times were rounded-off and are approximate. The step times presented in Table 4-3 were obtained in a similar manner to those of Table 4-2; each step was individually timed and rounded up to the nearing multiple of 5 for simplicity as the manufacturing step was performed.

Table 4-2–Manufacturing process times for machining the plug and sleeve insert components.

Process step	Illustration of machining step	Time to complete process step (min)	Description of process step
1	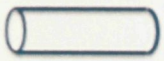	5	Lathe Setup
2		5	Drilling clearance hole
3	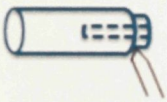	5	Turning down stock
4		5	Changing to parting tool and parting off sleeve
5	Repeat steps 2-4 for insert plug	15	To make multiple sleeves
Final Product		10 + 30x	Time it takes to make x amount of inserts

Table 4-3 - Manufacturing steps and process times for casting v.3 inserts.

Process step	Illustration of machining step	Time to complete process step (min)	Description of process step
1		30	Create solid models of cast moulds
2		60	Machine the cast moulds
3	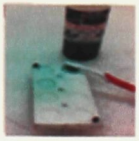	5	Apply release agent
4		10	Mix fibre and resin
5	 	10	Apply mix to mould and clamp
6	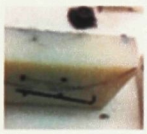	5	Remove inserts from mould
7		5	Lathe setup
8	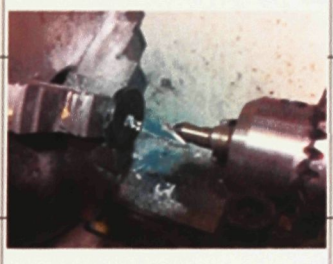	5	Drilling clearance hole on each sleeve
9		5	Drilling clearance hole on each plug
Final Product		$90 + x\left(\frac{30}{n} + 15\right)$	Time it takes to make x amount of inserts

From Table 4-2 and Table 4-3, the time it takes to manufacture x amount of inserts by machining and casting is governed by the following two equations:

$$t = 90 + x\left(\frac{30}{n} + 15\right) \qquad \text{(Casting)}$$

$$t = 10 + 30x \qquad \text{(Machining)}$$

Where t is in minutes, x represents how many inserts are being manufactured and n is the number of inserts that are simultaneously produced by each cast.

If a labour rate of $20/h is assumed, then by combining the labour rate, the time it takes to produce inserts via either casting or machining and the material cost per insert (Table 4-1), a total cost to produce each insert can be calculated. Figure 4-6 shows the net cost versus number of inserts produced for each of the materials and processes presented in Table 4-1.

Although the casting process has more manufacturing steps and a higher initial time investment, the process becomes more economical than machining fibreglass or wood after approximately 13 inserts (3-4 if compared to machining carbon-epoxy). If the casting moulds are modified to allow for 10 inserts to be made simultaneously then this is reduced from 13 inserts to 8. The inserts when cured and removed from the moulds, are required to be separated from each other as they are attached together by a thin film of epoxy which cures between the two moulds. The inserts are easily separated with scissors.

To check for sensitivity to labour costs, Figure 4-7 was regenerated with an hourly wage of $40/h to see the effect of labour costs on the viability of the

manufacturing processes. It can be seen that casting becomes more economical than machining at 11 inserts, and if the casting moulds are modified to produce 10 inserts simultaneously, then casting becomes more economical at 7 inserts.

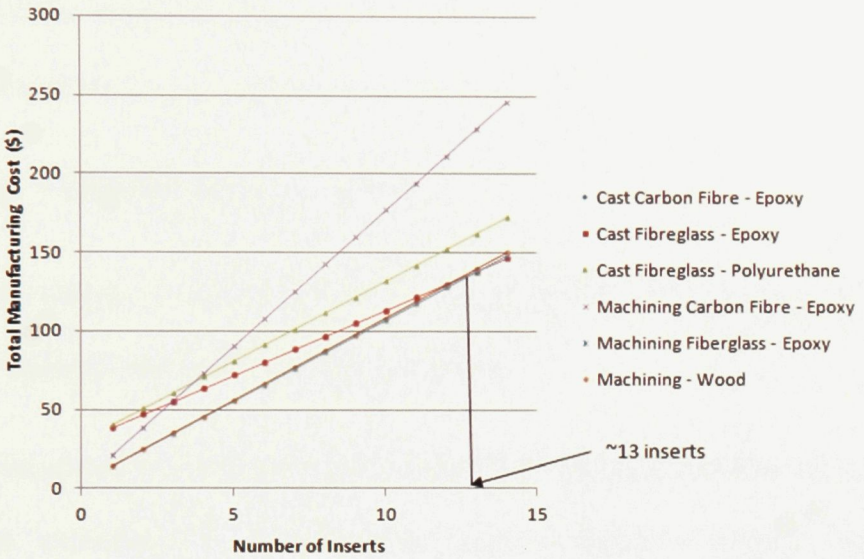

Figure 4-6–Cost analysis: Net cost vs. number of inserts manufactured for machining and casting assuming $20/h labour rate.

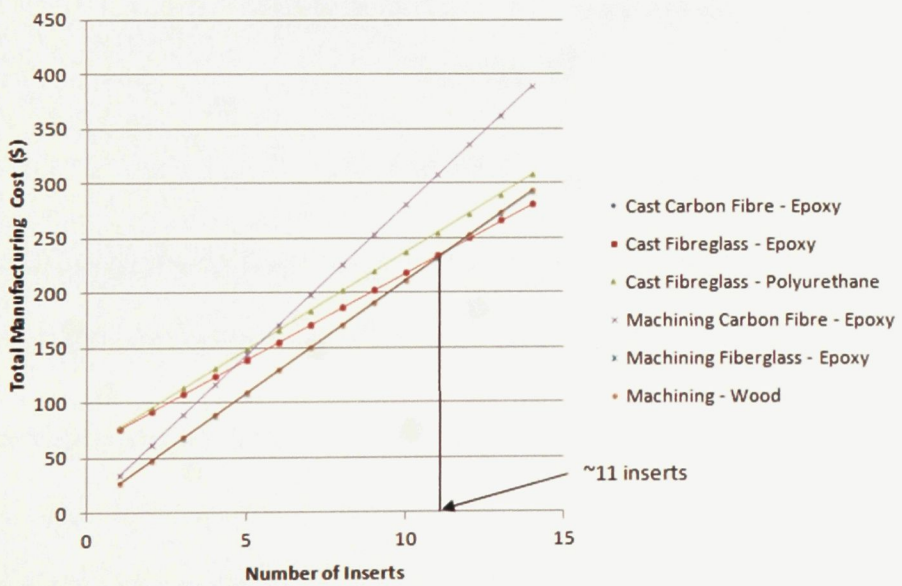

Figure 4-7 - Cost analysis: Net cost vs. number of inserts manufactured for machining and casting assuming $40/h labour rate.

This cost analysis study demonstrates that casting is more economical than machining and is more sensitive to labour costs (i.e. the higher the labour costs, the sooner casting becomes more economical over machining).

To further refine the selection of materials for the v.3 inserts, material strength tests were performed to assess the performance of the three candidate materials.

4.3.2 - Material Strength Testing

Since casting is determined to be the preferred manufacturing method, this narrows the choice to the three composite materials.

It is necessary to investigate and compare how the materials behave under applied loading. Six specimens for each material were subjected to bearing loading. The following numbering system was used to identify each of the 18 specimens:

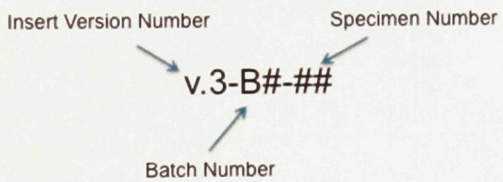

The plug and sleeve inserts were bonded together using West Systems 105 epoxy kit, Figure 4-8 shows a typical insert system assembly on a test coupon.

The experimental setup was consistent with the bearing testing outlined in Chapter 3. The only deviation from the previous procedure was that the axial displacement rate was set to 0.0028 in/s for a total displacement of 0.5 in. This was done to ensure that the inserts failed and that a significant amount of data was collected after the insert failure. Figure 4-9 shows a test specimen in the MTS frame.

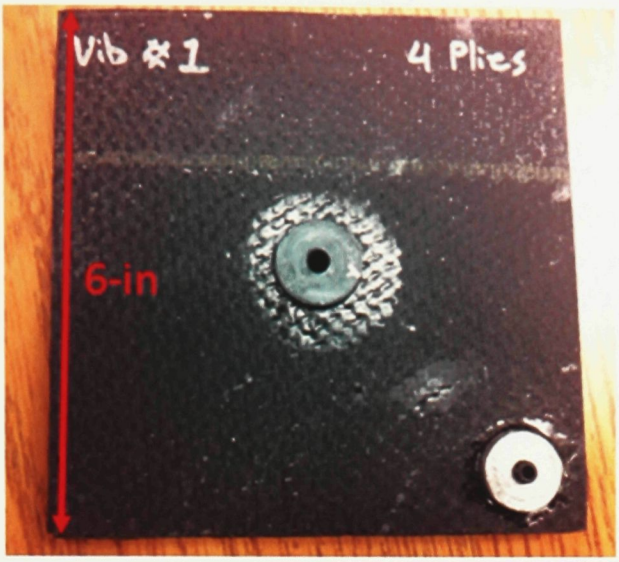

Figure 4-8 - Typical v.3 insert test coupon.

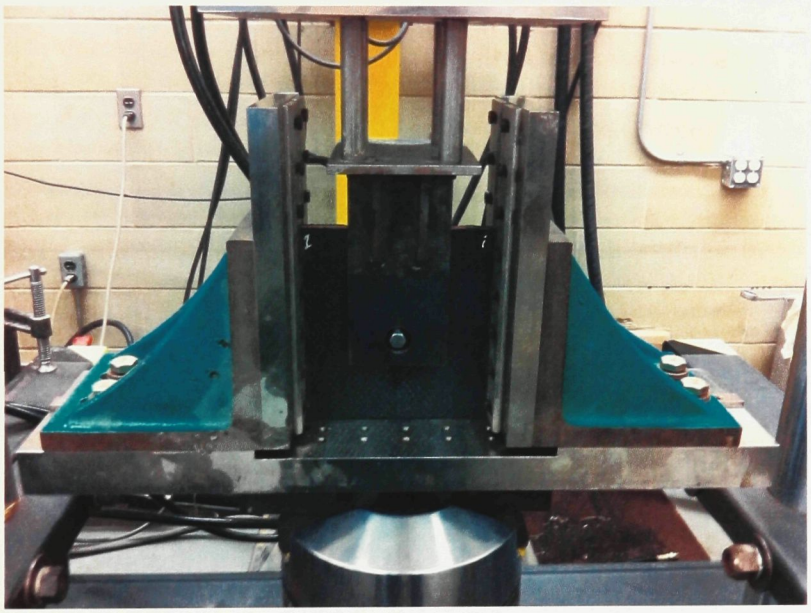

Figure 4-9 - v.3 insert in the bearing test frame.

Table 4-4 presents the test matrix along with the results of the bearing tests. The stiffness values, maximum load achieved for each coupon and the weight of each insert are included.

Table 4-4 - Test matrix and results of the material strength tests.

Specimen #	Face-sheet Layup	Insert Material	Stiffness (lb/in)	Max Load (lb)	Weight of Insert Including Washers (lb x10^{-2})
v.3-B1-1	(+-45,0/90)	Chopped Carbon Fibre - Epoxy	28473	1309	0.041
v.3-B1-2			22512	1201	0.041
v.3-B1-3			29908	1051	0.041
v.3-B1-4			27669	1106	0.040
v.3-B1-5			29578	1146	0.041
v.3-B1-6			27969	1195	0.041
v.3-B2-1		Chopped Fibreglass - Epoxy	12604	936	0.048
v.3-B2-2			25424	1134	0.048
v.3-B2-3			41574	1267	0.048
v.3-B2-4			36724	1077	0.048
v.3-B2-5			34373	1139	0.048
v.3-B2-6			39625	1424	0.048
v.3-B3-1		Chopped Fibreglass - Polyurethane	18530	707	0.045
v.3-B3-2			15283	702	0.045
v.3-B3-3			25337	766	0.044
v.3-B3-4			19754	721	0.044
v.3-B3-5			20982	776	0.044
v.3-B3-6			18470	673	0.044

The stiffness values were determined by approximating a line of best fit on the linear portion of the force displacement curves. Figure 4-10 shows a typical force-displacement curve for a Batch 1 specimen with a line of best fit added to determine the stiffness. The region of data used to construct the line of best fit was taken to be between the 100 lb and 800 lb mark. This was done for each specimen to ensure consistency in determining the stiffness for each specimen.

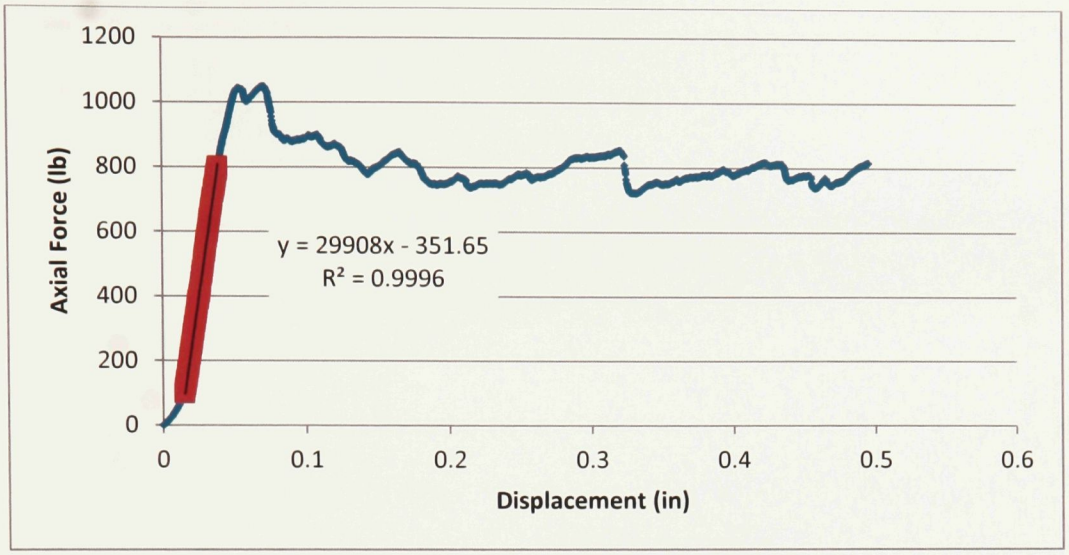

Figure 4-10 - Typical force-displacement curve for a batch 1 specimen.

Figure 4-11 shows the mean load-displacement curves for each of the three insert batches and Figure 4-12 summarizes the average maximum applied loads for each Batch.

It can be seen from Figure 4-11 that Batches 1 & 2 have similar stiffnesses, which are evidently higher than Batch 3. This is expected as the polyurethane used has a lower modulus of elasticity as compared to epoxy.

Batch 1 exhibited more consistency (less scatter) in the specimen force-displacement curves, as well as displaying a higher average maximum load value (see Figure 4-12).

From the material strength testing of the three candidate materials it was determined that the chopped carbon fibre – epoxy v.3 inserts had the highest average strength, the lowest weight, and the least scatter in the stiffness and strength values. Therefore, chopped carbon (Batch 1) is the material selected for the v.3 inserts.

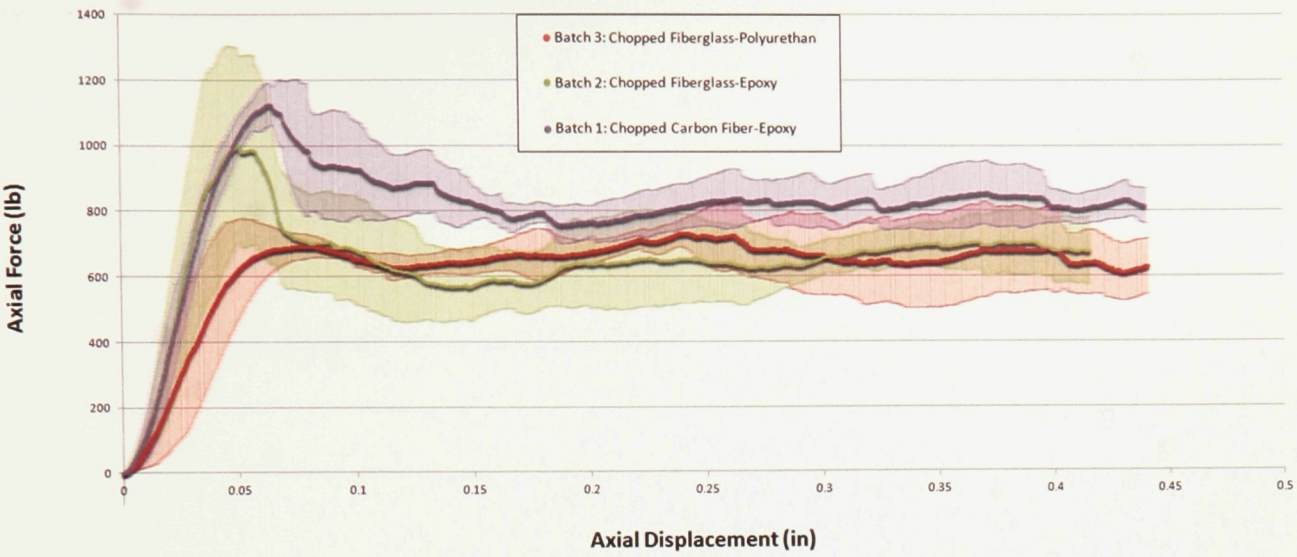

Figure 4-11 - Mean force versus displacement curves for the three insert batches.

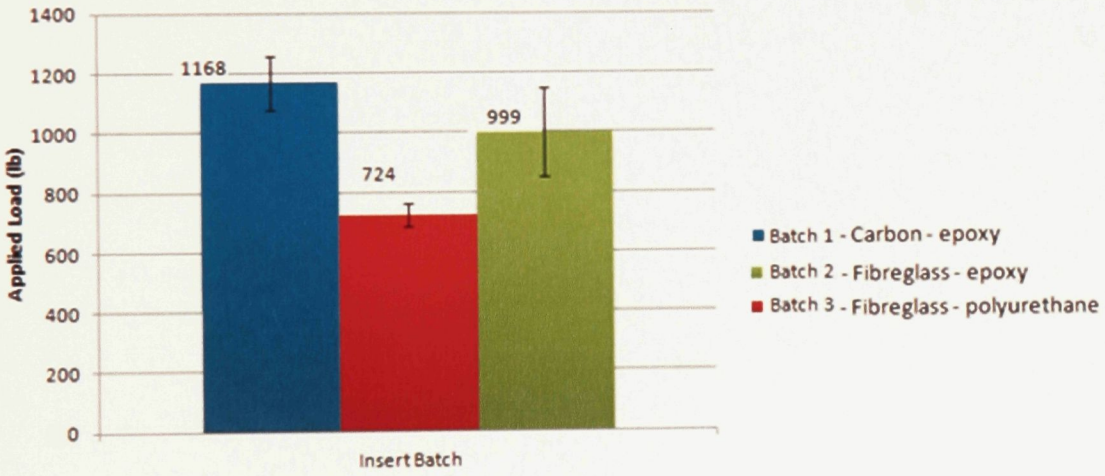

Figure 4-12 - Average maximum axial loads for each insert batch.

This chapter presented the development of the v.3 insert design. The design, manufacturing process and the materials were selected. It was shown that the plug and sleeve design had the best characteristics for the new insert system. Casting was shown to be more economical than machining for the production of the v.3 inserts. Chopped

carbon fibre – epoxy was demonstrated to yield the best performance out of the candidate materials.

With the design, manufacturing process and material selected for the v.3 insert system, the next phase of this research will be to determine the effects of dynamic loading on the performance of the v.3 insert system.

Chapter 5 – The Effects of Vibration on the v.3 Insert Joint Strength

The effects of dynamic loading have not been considered in this research thus far. Although static loads are important, the fatigue due to vibration can dramatically reduce the service life of a component and should be taken into consideration when designing inserts [17].

The GeoSurv II Prototype serves as the test bed for this study. The source of the vibration on the GeoSurv II Prototype is the engine; the effects of this vibration on the load carrying capability of the v.3 inserts are studied. The vibration of the engine will be characterized, and coupons with v.3 inserts installed will be subjected to vibratory loads simulating the engine vibration. Residual static strength tests will be subsequently performed to assess the effects of the vibration.

This study is not a comprehensive fatigue assessment of the composite sandwich structure insert assembly. Rather, it is an exploratory look into the possible effects that vibrational loads can have on the v.3 insert assembly and foam core sandwich structures in general. The results will highlight areas that should be investigated more closely.

5.1 - Engine Vibration Classification and Signal Processing

To quantify the vibration experienced by the inserts, an accelerometer was installed on the rear bulkhead of the fuselage of the GeoSurv II and the vibration was recorded while the engine was run at various throttle settings.

Since the accelerometer outputs voltage, it is necessary to correlate this output to accelerations, velocities and displacements. This was achieved by attaching the accelerometer to a Brüel & Kj□r calibration exciter (specifications shown in Figure 5-1) and recording the output. Since the acceleration, velocity and displacement of the calibration exciter are known, it is possible to relate the voltage output to those parameters which are more suitable for characterizing the signal. The calibration setup is shown in Figure 5-2.

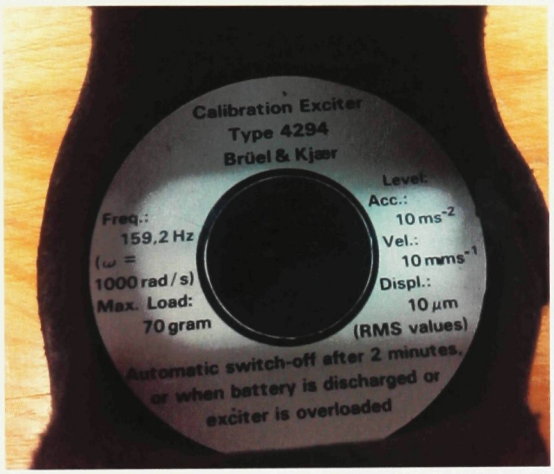

Figure 5-1 - Calibration exciter specifications.

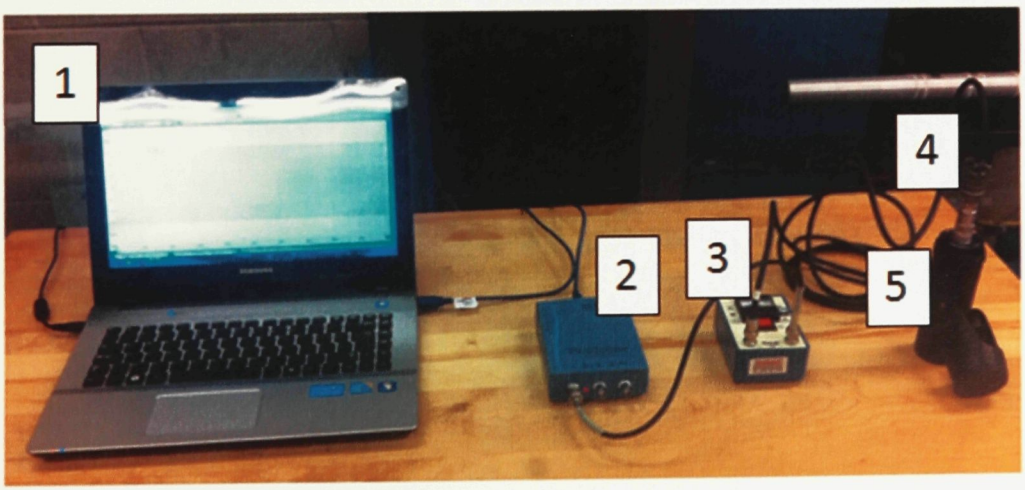

Figure 5-2 - Calibration Setup: (1) laptop (2) oscilloscope (3) signal conditioning unit (4) accelerometer (5) calibration device.

A calibration signal was generated from the exciter and a portion of it is shown in Figure 5-3. The accelerometer used is a Brüel & Kj□r (model number: 603C01) sensor attached to a PCB model 480C02 ICP® sensor signal conditioner. The signal conditioner is connected to a PicoScope 2204 portable oscilloscope which is connected to a notebook computer for monitoring and data logging purposes. The data logging was accomplished through the PicoLogger software package.

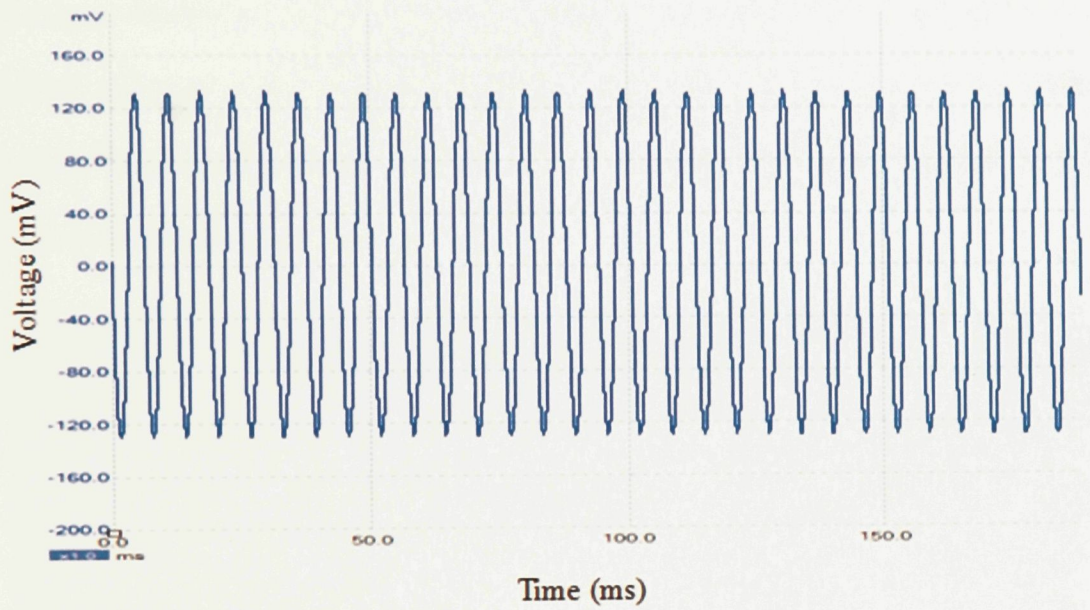

Figure 5-3 - Calibration curve generated from the calibration exciter.

By relating the voltage output of approximately 130mV to the known exciter displacement of 10 μm (3.94×10^{-4} in) the following relationship was determined between the output of the accelerometer and displacement in inches:

$$1 \text{ mV} = 3.03 \times 10^{-6} \text{ in}$$

The data acquisition setup for the GeoSurv II engine can be seen in Figure 5-4. The engine is a 3W-342iB2 30HP 2 stroke engine [24]. The sensor was attached to the inside of the rear bulkhead near the insert where the engine standoff is located.

Figure 5-5 shows a close-up view of the engine mounting system. The engine is mounted via engine standoffs which are attached to the rear bulkhead of the fuselage (review Figure 3-6 for engine to rear bulkhead connection). The mounts feature vibration isolating grommets; as well, the plywood panels on either side of the bulkhead sandwich structure will have a vibration damping effect. Since the accelerometer was mounted on the inside of the bulkhead, the recorded vibration signal will include all of the damping effects from the mounting system.

Figure 5-4 - Vibration measurement setup: (1) engine (2) laptop (3) accelerometer (4) USB oscilloscope (5) signal conditioning unit.

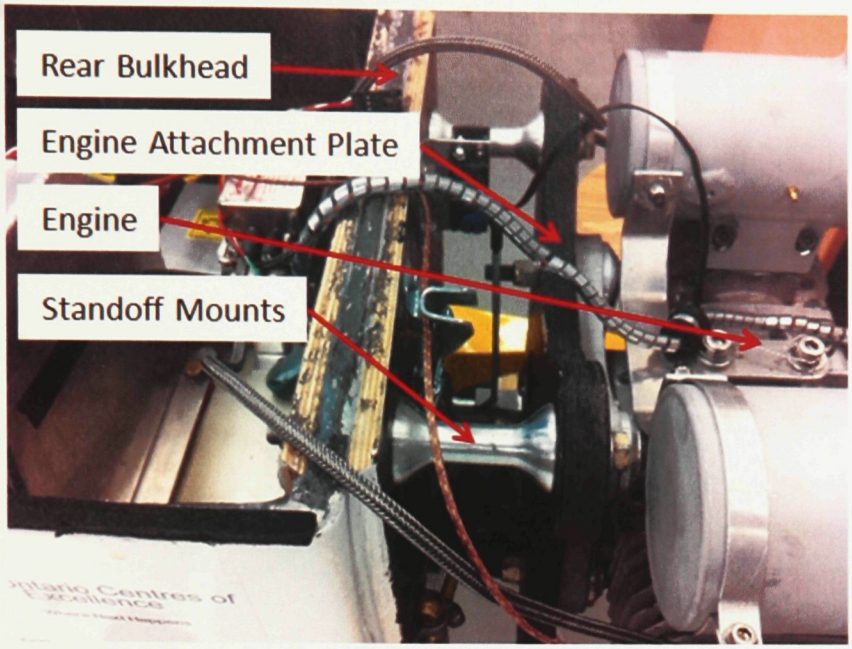

Figure 5-5 - Engine mounting system on the GeoSurv II Prototype.

Vibration data was gathered in 20-second intervals at a sampling rate of 1ms. Data was collected from idle up to 75% throttle setting. A typical recorded signal is shown in Figure 5-6. The signal is un-uniform, and it is difficult to determine the dominant frequency.

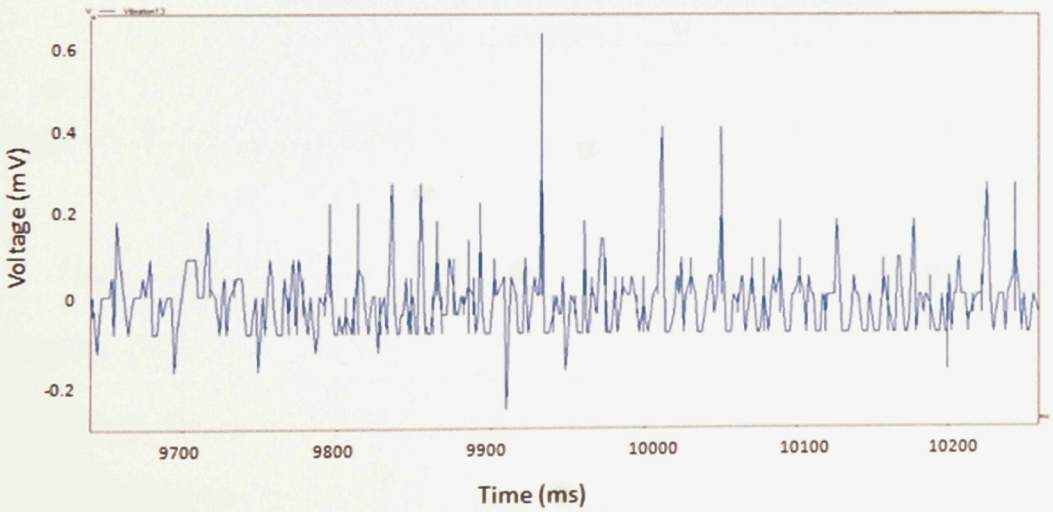

Figure 5-6 - Snapshot of the vibration data sample taken from the GeoSurv II engine at 75% throttle setting.

It was determined that the highest amplitude signal was produced at the 75% engine throttle setting, and therefore represented the 'worst case' for engine vibration. This was the signal chosen to be characterized. The engine rpm has a range of 1200-6500 [24]; at 75% throttle setting, this corresponds to an engine rpm of approximately 5175 or a frequency of 86 Hz.

In order to clean up the signal and discern the dominant range of frequencies, a Fast Fourier Transform (FFT) analysis was performed on the data set [25]. Figure 5-7 shows the result of performing an FFT analysis on the 75% throttle signal shown previously in Figure 5-6.

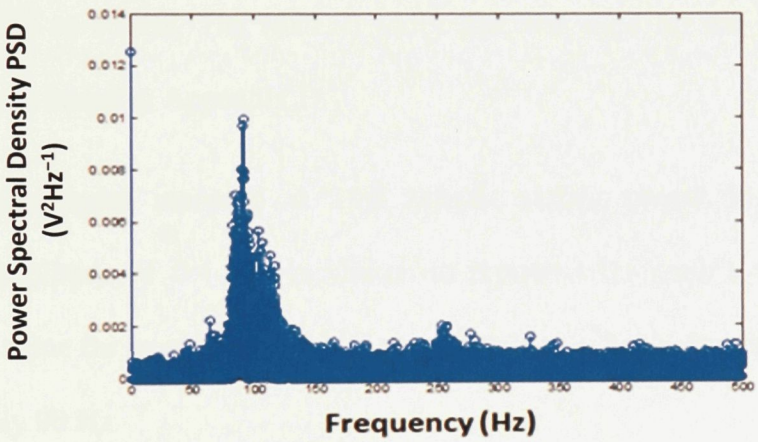

Figure 5-7 - Frequency contribution to the GeoSurv II engine vibration signal at 75% throttle.

From Figure 5-7 it can be seen that there is a range of frequencies that is dominating the signal. The highest contribution to the overall signal is caused by frequencies in the range of approximately 75-125 Hz. If power contributions of below 0.004 are ignored, the signal can be cleaned up and the dominant frequency range is more discernible. The result of this can be seen in Figure 5-8.

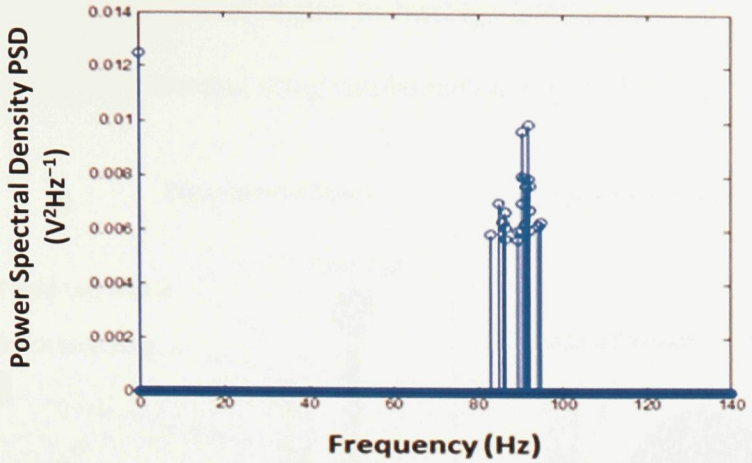

Figure 5-8 - Further processing of the GeoSurv II engine vibration signal at 75% throttle setting.

The frequency range that dominates the vibration of the engine lies between approximately 80 to 95 Hz. The MatLab script that was used for the FFT and signal processing can be found in Appendix D.

From the signal recorded at 75% throttle setting shown in Figure 5-6, a conservative amplitude of 0.4 V was chosen to represent the engine vibration of the GeoSurv II. A value for amplitude of 0.4 V corresponds to a displacement of 1.18×10^{-3} in at approximately 90 Hz.

The following section outlines the test method, and experimental setup of the coupon vibration testing.

5.2 - Experimental Setup and Test Method

With the vibration of the engine characterized, the signal was input into a load frame to simulate its vibration. Test coupons were subjected to this vibration signal in order to observe its effects on the strength of the v.3 insert joints. A comparison of the

experimental setup and the actual engine to fuselage interface can be seen in Figure 5-9 and the image of the experimental setup can be seen in Figure 5-10.

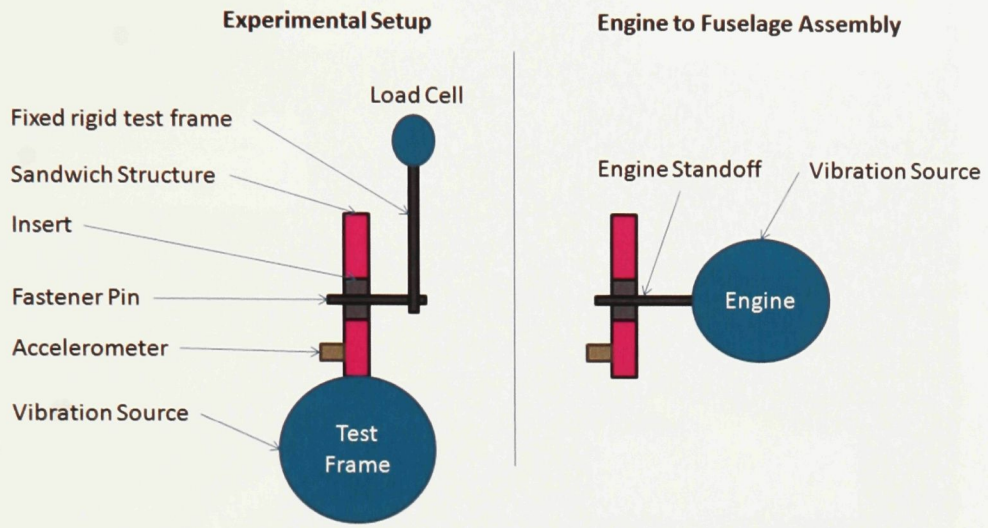

Figure 5-9 - Illustration of the experimental setup versus the actual engine to fuselage interface on the GeoSurv II fuselage.

The experimental setup differs from the actual engine to fuselage configuration; the two setups are reversed. In the case of the engine to fuselage assembly, it is the engine that is the vibration source and the load is transferred to the fixed fuselage sandwich structure. In the experimental setup, the bottom piston of the load frame is the vibration source which vibrates the sandwich structure directly. The insert is attached to the fixed top half of the test fixture via a ¼ in bolt. The experimental setup is very similar to the bending test configuration described in Chapter 3.

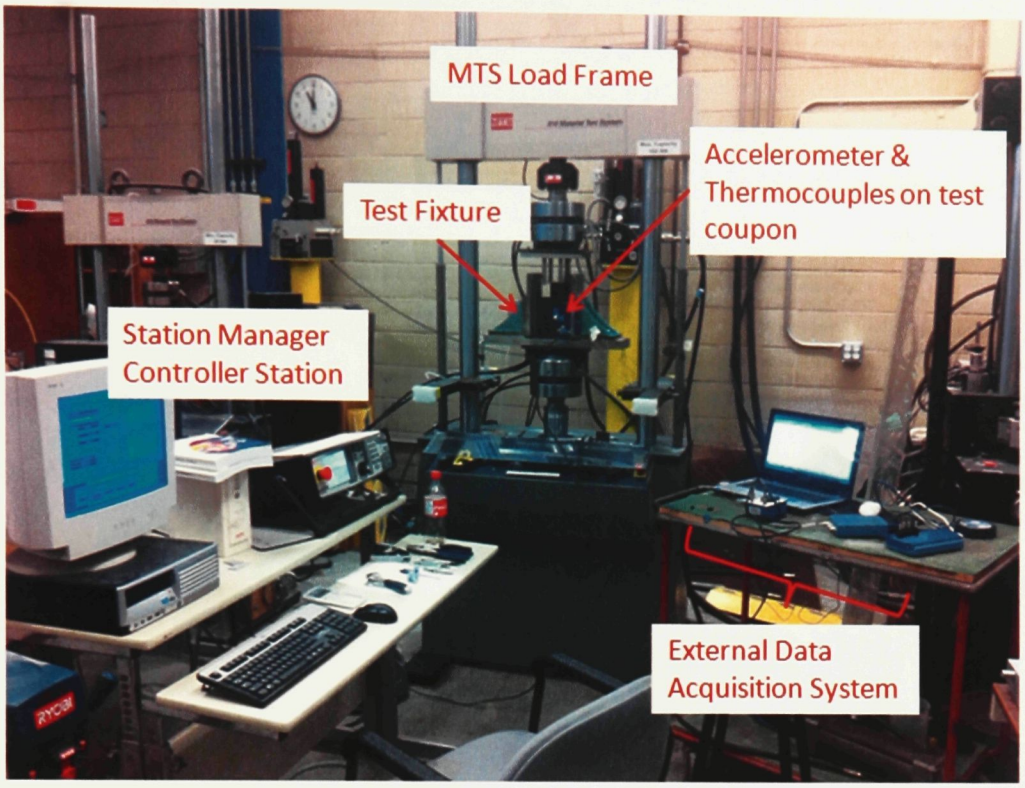

Figure 5-10 - Experimental setup for vibration testing of v.3 inserts.

The same load frame that was described in Chapters 3 & 4 for the static performance testing of bending and shear was used for this study. The data acquisition system was again used to monitor the vibration of the test coupon. The reasons why the vibration was measured externally at the insert were:

- The vibration input by the bottom piston of the load frame may differ from the vibration measured at the insert of the test coupon. This due to the amplification of the input frequency throughout the test apparatus. Since this study is concerned with the vibration at the joint, that is where it was measured.
- Since the experimental setup and actual engine to fuselage interface are reversed, it is important to make sure the vibrations measured at the joint for each set-up can be related.

The accelerometer was attached to the lower corner of the test coupon and three thermocouples were placed to record any changes in temperature due to the dynamic loading. One thermocouple was also used to record ambient temperature. The configuration of the accelerometer and thermocouples on the test coupon can be seen in Figure 5-11 the type J thermocouples were connected to a TC-08 Omega Data Acquisition (DAQ) 8 channel USB device, which was then connected to a notebook computer. The temperatures were recorded using the same Pico Logger software that was used in the previous section to record the engine vibration.

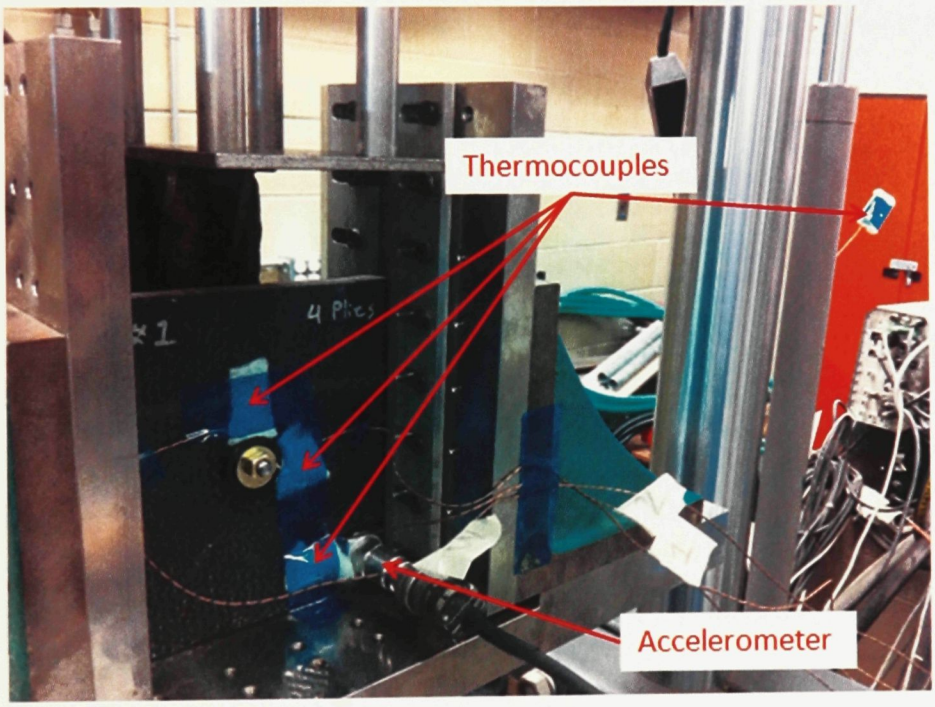

Figure 5-11- Test coupon with the accelerometer and thermocouples attached.

The first test coupon was used to tune the system to achieve an output that when measured by the external data acquisition system, matched the signal recorded from the engine characterization study.

A sinusoidal input of 80 Hz and amplitude of 0.028 in was entered into the load frame controller; the output recorded by the accelerometer on the test coupon was 250 Hz with amplitude of 0.0012 in. There was a frequency shift and damping effect in the test frame assembly, and as was hypothesized, the input into the load frame did not match the output measured by the accelerometer at the insert joint. Although the frequency shifted, the amplitude was eventually matched with that of the recorded vibration of the GeoSurv II engine.

The subsequent testing would be performed with these specifications. Since the frequency of the tests was increased to 250 Hz from 80 Hz, the time to achieve the same number of cycles would be reduced and thus test times would be decreased.

The first 5 specimens were subjected to 1 million cycles which, at 250 Hz corresponds to a test time per coupon of approximately 66 minutes and represents 3 hours of flight time on the GeoSurv II Prototype. The last coupon was to be tested for 16 hours which corresponds to 50 hours of flight time.

Residual strength tests were subsequently performed for each specimen and compared to the quasi-static load tests used in the correlation development work discussed in the next chapter.

The peak-to-peak values of the applied force and axial displacement along with time were recorded. The next section will analyze and discuss the results of the vibration and residual strength testing.

5.3 - V.3 Insert Vibration Study Test Results and Analysis

This section presents the results of the 6 vibration tests performed on the v.3 inserts. As was mentioned in the previous section, the coupons were subjected to a sinusoidal input with a frequency of 250 Hz and amplitude of 1.18×10^{-3} in. Table 5-1 shows the test matrix for the vibration testing along with the results of the residual strength tests.

Table 5-1 - Vibration and residual strength test matrix and results.

Specimen #	Ply Layup (per face)	Number of Cycles	Length of Test (hr:min)	Residual Strength Failure Load (lb)	Stiffness (lb/in)
1	(+-45,0/90)	1.00E+06	1:06	198	1279
2			1:06	195	1748
3			1:06	202	721
4			1:06	210	660
5			1:06	247	1059
6		1.40E+07	16:00	-	-

The peak force per load cycle were recorded during the test and plotted against time to see if trends suggesting the onset and progression of damage could be identified. The force versus time plot for the entire duration of test specimen #3 is shown in Figure 5-12 as recorded from the load cell of the load frame. The plot displays a very uniform trend, which does not suggest any reduction in strength during testing.

Maximum load values of approximately +250 lb and -200 lb can be seen from Figure 5-12. The externally measured peak acceleration at the insert joint was found to be approximately 101.03 ft/s^2. With the mass of the vibration source (bottom part of test

fixture) of 2.98 slugs, this corresponds to a force of 301.1 lb which is similar to the forces measured by the load cell.

Since the mass of the engine is significantly less than the test fixture (approximately 0.93 slugs including the muffler, mounting plate etc.) [24] the expected force is only 94.2 lb. The significance of this difference in mass will be discussed later in this section.

The discrepancy between the peak load values of +250 and -200 could be caused by the sandwich coupon being held in place by friction on its sides only when the vibration source (load frame piston) is on its down stroke (negative displacement). When the piston is on its up stroke (positive displacement) the specimen has a hard contact with the bottom of the test fixture and thus the entire load is transferred to the load cell. This explains why the positive peak load value is higher than the negative one.

Figure 5-13 shows a small time slice of the plot shown on Figure 5-12. A trend line was added to help visualize how the max/min peaks are linked together. This trend was similar to the output seen on the MTS control station. The trends seen in Figure 5-12 and Figure 5-13 were typical of all the vibration tests. The peak load values vary slightly from specimen to specimen, and can be attributed to slight changes in the installation of the test coupons in the test fixture. Also there are slight variances in the manufacturing of the test panels (geometry, imperfect edges etc.) which may contribute to slight variances in the transferring of loads to the load cell.

There was no discernible increase in temperature in the specimens; a typical temperature versus time plot for a test can be seen in Figure 5-14.

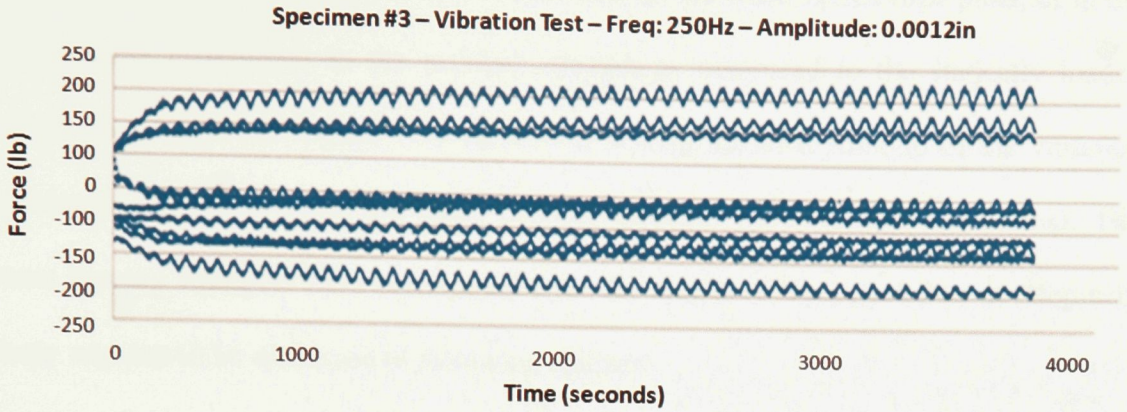

Figure 5-12 - Peak force per cycle vs. time plot for the vibration test of specimen #3.

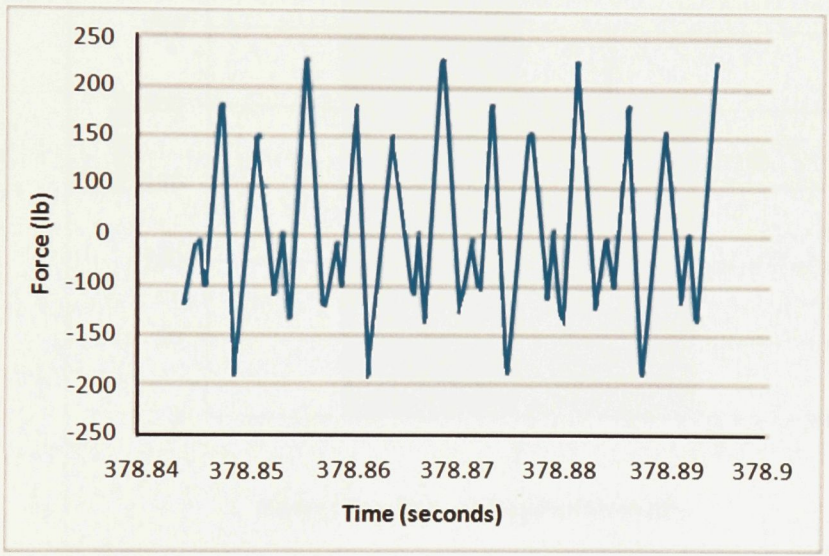

Figure 5-13 - Magnified slice of Figure 5-12 with a trend line added between max min points.

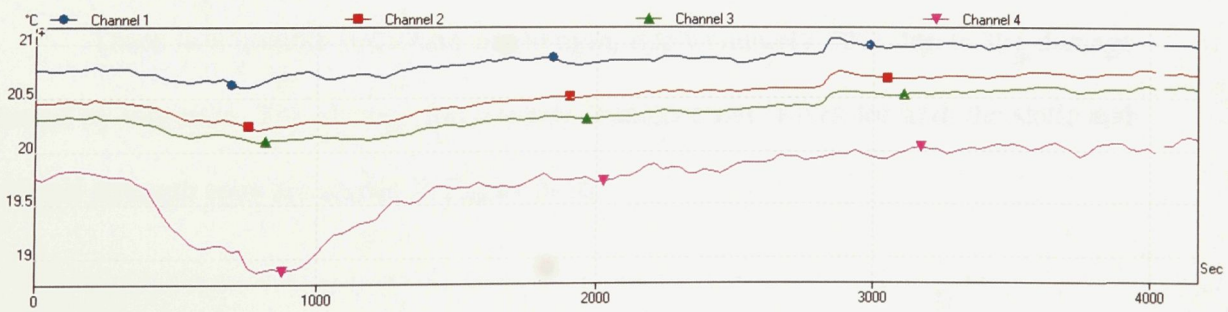

Figure 5-14 - Typical thermocouple readings during a vibration test.

Although there were no observable trends in the force versus time plots, or in the temperature, differences in the residual strength as compared to the statically loaded inserts were apparent. Figure 5-15 shows the average residual strength of the vibration specimens compared with the static bending strength (non-vibrated specimens). The static bearing strengths were determined from the results of the correlation development study which will be discussed in following chapter.

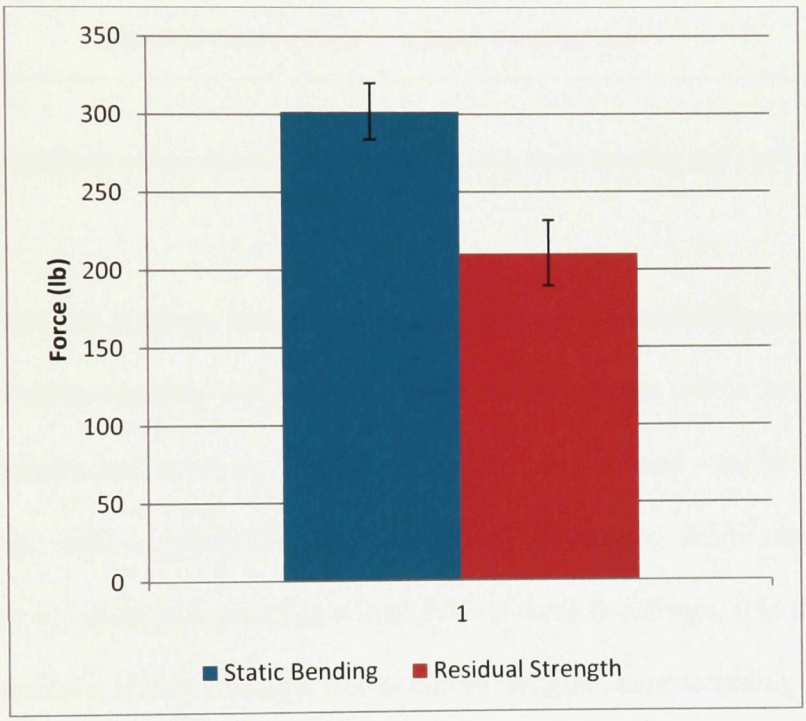

Figure 5-15 - Static Bending strength compared to residual strength after vibration testing.

There is a notable reduction in strength, approximately 30% due to the damage caused by vibration. The average force versus displacement curves for both the static and residual strength tests are shown in Figure 5-16.

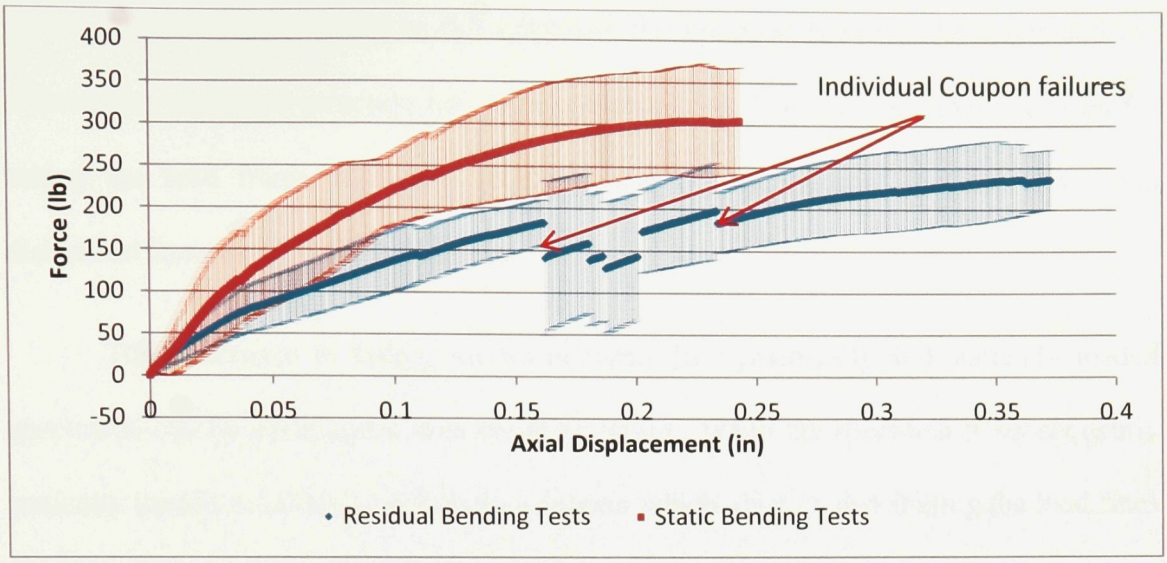

Figure 5-16 - The mean force versus displacement curve for both static bending and residual strength vibration tests.

Furthermore, the washers and nuts on either side of the insert squeeze the plug and sleeve components together and keep the insert intact and the whole insert system (plug, sleeve, washers and nuts) is therefore able to carry a load despite the insert components (plug, sleeve, sandwich structure) being disbonded from one another. Although it is able to continue supporting a load even if there is damage, it is difficult by inspection to determine if any damage has occurred without disassembling the insert system.

The discontinuities in the residual bending test curve in Figure 5-16 are due to the specimens failing at different load values and at different displacements. Interestingly, all but one of the residual bending test specimens fractured with a sharp drop in the measured load value, this behaviour was not seen in the static bending tests, further evidencing that the vibration degrades the performance of the v.3 inserts.

After being subjected to the vibration, the bondline between the insert and the surrounding sandwich structure had been compromised. The specimen that was used for tuning the load frame was cross-sectioned and it was apparent that the insert had disbonded from the sandwich structure.

The difference in failure modes between the dynamically and statically loaded specimens can be attributed to this bondline failure. When the specimen is subsequently statically loaded to failure, this bondline support which aided in distributing the load from the insert flanges to the sandwich structure evenly is no longer present. Since the sandwich structure and the insert do not have a perfectly even contact surface, local stresses in the insert flanges develop and fracture occurs. Figure 5-17 shows the fractured flange on the insert which is not present in the specimens that were not dynamically loaded.

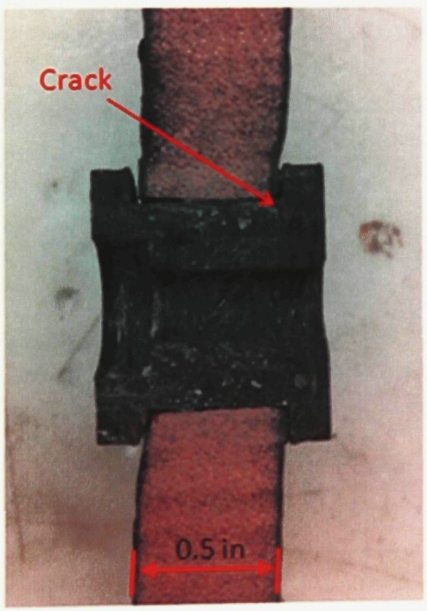

Figure 5-17 - Fractured v.3 insert after residual strength testing.

The final specimen was intended to be subjected to 16 hours of vibration to simulate approximately 50 hours of flight on the GeoSurv II Prototype. 10.8 hours into testing, however, the fastener bolt connecting the test coupon to the top portion of the test fixture failed due to the cyclic loading. Figure 5-18 shows the fractured bolt.

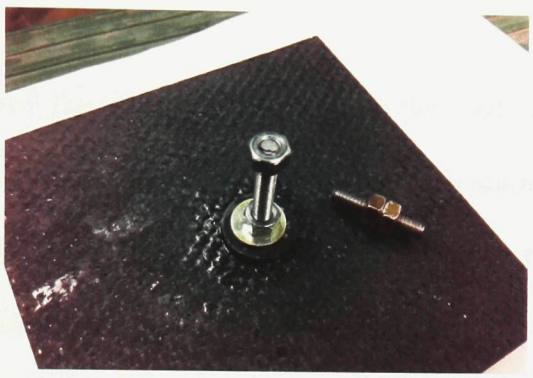

Figure 5-18 - Lifetime test specimen bolt failure.

There was no apparent trend indicating the onset of failure in the peak-to-peak, force versus time graph. The failure was very sudden, as can be seen from Figure 5-19 which displays the final cycles before failure. The condition of the insert was similar to previous vibration specimens.

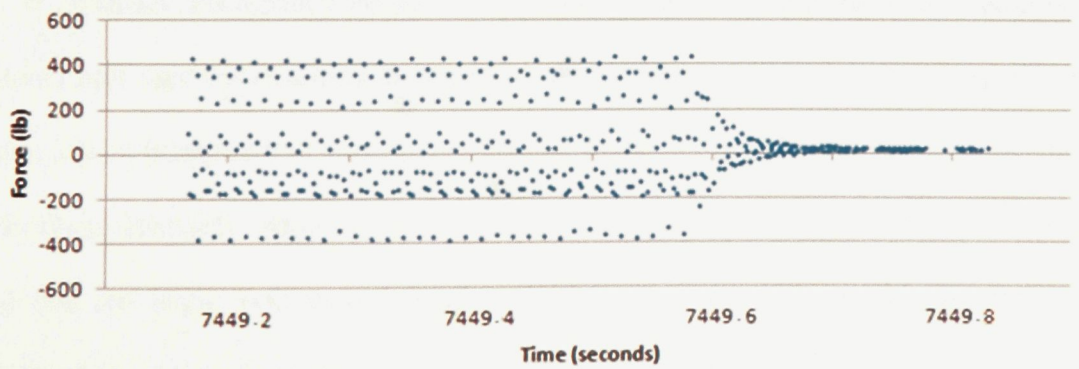

Figure 5-19 - Force versus time graph showing the final cycles before failure of the fastener bolt.

Due to the length of the lifetime test, the experiment had to be conducted in separate blocks of time, and in each new block, the time counter was restarted. The 7449.8 seconds in the x-axis of Figure 5-19 corresponds to the end of the final test block and when added to the previous test blocks, cumulatively adds up to 10.8 hours of total testing.

This Chapter discussed the effects of vibration on the load carrying capability of the v.3 inserts, using the GeoSurv II as a test bed. The vibration of the engine was characterized and attempted to be replicated using a load frame. Problems were encountered, however, with the experimental setup.

Though the accelerations at the insert were matched for both the experimental setup and the actual engine-to-fuselage assembly, the masses of the vibration sources are very different, resulting in different forces. The consequence is that although this study did in fact show that there was a reduction in the strength of the joint as a result of the applied vibrational loads, it cannot answer for certain if the inserts would be affected by the vibration generated by the GeoSurv II engine.

Another discrepancy between the experimental setup and the actual setup is the fastener bolt used for attaching the insert to the test frame. In the case of the experimental setup, a ¼-in diameter bolt was used compared to the 3/8-in bolt used in the actual engine to fuselage assembly. Although the ¼-in bolt failed during the lifetime test, it cannot be said that the larger bolt in the GeoSurv II Prototype assembly would also fail when subjected to a lower load than that observed during the experimental testing. Due to the more conservative design of the GeoSurv II Prototype as compared to the experimental

setup in this experimental work, it is deemed unlikely that the GeoSurv II engine vibration would cause a failure such as the one seen in Figure 5-18.

The 1/4 in bolt was used instead of the engine bolt diameter so that the residual strength tests could be compared to the static tests in the correlation development testing performed in Chapter 6.

In order to address the problems with the experimental testing and revisit this testing, a few changes to the experimental setup are necessary.

The bottom part of the test fixture that attaches to the lower piston of the load frame should be redesigned to match the weight of the vibration source (GeoSurv II engine).

Figure 5-20 shows a proposed design for a new tests fixture. The engineering drawings can be found in Appendix E. The new test fixture has a total mass of 0.622 slugs. While this is less than the weight of the GeoSurv II engine, mass attachment points have been incorporated into the design to allow for the mass of the fixture to be variable. With this feature, the test fixture can be used for a wider array of vibration tests such as testing the vibration effects of engines with different masses.

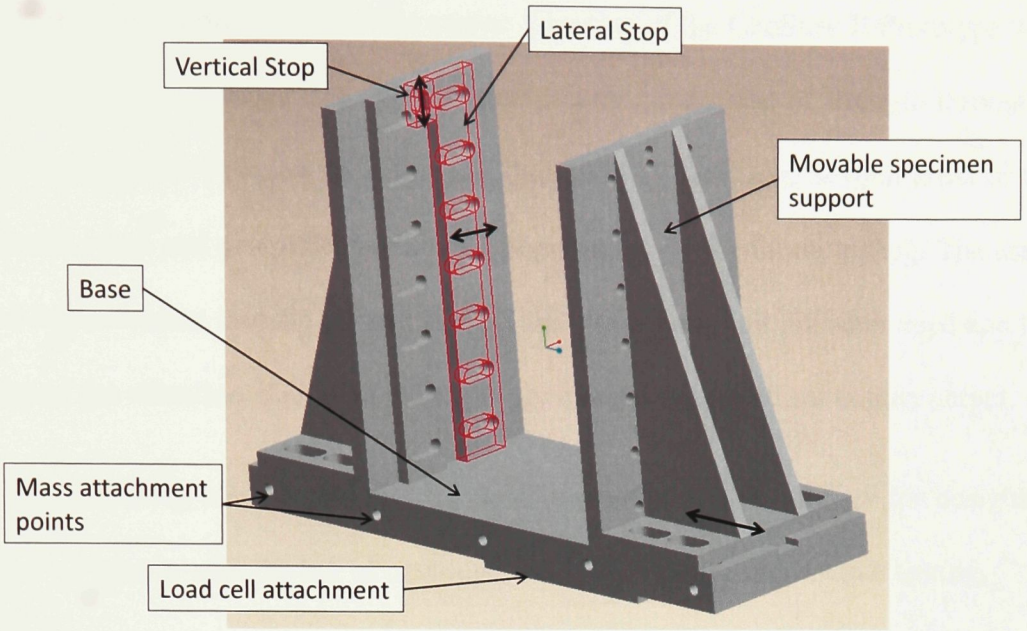

Figure 5-20 - Redesigned test fixture for the v.3 vibration testing.

The bolt diameter should be matched to that of the actual engine mount assembly to ensure that the load transfer will be the same for both situations.

There is not much information on the strain rate sensitivity of sandwich structures, and it may be useful to focus some attention on determining its effects. Until the effects are more fully understood, the frequency of vibration should be more closely matched for future testing.

Despite the flaws in the testing, the results provide useful insight into the possible effects that excessive vibration can have on the v.3 inserts. It was determined that the vibration caused a bondline failure between the insert and the sandwich structure which decreased the load carrying capacity of the insert system. It is also useful to note that this damage is not visible by visual inspection of the joint, and requires the coupons to be sectioned in order for the damage to become apparent. Despite final fracture of the insert, the washers and nuts in the assembly maintain the integrity of joint.

In summary, a brief study of the engine vibration of the GeoSurv II Prototype was conducted. It was determined that the vibration causes a reduction of strength through a failure in the bondline between the insert and the sandwich structure. Several areas of the experimental setup and procedure need to be improved upon for future testing. The areas that need improvement include the test fixture, the attachment bolt diameter used and the frequency of the vibration should be more closely matched to the actual engine output.

The following chapter presents the development of a methodology for designing optimized v.3 inserts with the use of computer simulations and experimental testing.

Chapter 6 – Methodology Development for Sizing Inserts

Joints are often subjected to different loading conditions. It would be useful to develop a methodology for quickly designing optimized inserts given a set of design parameters. This chapter develops such a methodology; the roadmap is shown in Figure 6-1.

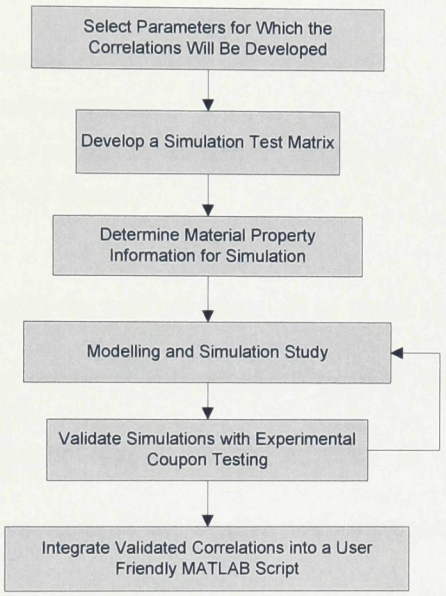

Figure 6-1 - Roadmap for the development of a methodology for quickly producing optimized inserts given a set of design parameters.

Design parameters were chosen in order to develop correlations between design variables. Simulations with realistic material property values were used to develop the relationships between the selected design parameters. The simulations were validated with experimental coupon testing and the results were integrated into a MATLAB script. This program enables designers to enter their design specifications; load values and the insert geometry are computed.

6.1 - Selection of Design Parameters to Correlate

There are many design variables to consider when designing a sandwich structure airframe joint; several of these parameters are listed below in no particular order:

- Expected service loads
- Load cases (bearing, bending, torsion, 'pull-out' etc.).
- Layup (quasi-isotropic, balanced, symmetric etc.)
- Number of plies
- Core height
- Face-sheet material
- Core density and material
- Attachment bolt (material, diameter, length etc.)
- Dimensions of v.3 Insert

Although it is tempting to try and correlate all of these variables together, it would be difficult to do so within the scope of this research project. Instead, a few of the above variables were chosen to ensure that a useful number of design scenarios can be accounted for. Table 6-1 shows each of the design variables presented above, along with justification on whether that parameter will be held as constant or allowed to be variable. Some of the justifications will be reiterations of findings already presented in earlier chapters and are included in Table 6-1 for completeness.

Table 6-1 - Synthesis of parameters for the development of correlations.

Parameter	Variability	Justification of Variability and Limitations
Expected Service Loads	Variable	The loads expected during operation will be different from joint to joint and from airframe to airframe. The variability of the loading is central to the value of any methodology for designing optimized inserts. The limitations include the geometry of the v.3 insert.
Load Cases	Fixed	The two load cases that have been the focus in this research have been bearing and bearing + bending; those will be the two load cases considered (see section 1.1). Bearing and bending loads were determined to be the most predominant load cases in the GeoSurv II Prototype.
Layup	Fixed	The stacking sequence will be limited to quasi-isotropic. Quasi-isotropic layup patterns are close to the optimum for providing maximum fastener strength [21] (see section 3.2.1).
Number of Plies	Variable	It is important for the thickness of the face sheet to be variable as it is the parameter of the sandwich structure which most influences the bearing load strength of the joint (see section 2.1.1).
Core Height	Fixed	Although the core height influences the bending strength of the sandwich structure, it has no effect on the bearing strength (see section 2.1.1). For the purposes of this study, the core height will be held constant at 0.5 in to limit the complexity of the correlation development.
Face-sheet Material	Fixed	As was discussed in Chapters 1 and 2, the scope of this research focuses on carbon-epoxy laminates. The principles discussed in this research however, could be applied to sandwich structures with different face-sheet materials.
Core Density	Fixed	The effects of core density on the bending strength of inserts has not been investigated. From section 2.1.1 it is clear that the core density has no clear effect on the bearing strength. In order to further simplify the correlation study, the core density will be held fixed at 6.7 lb/ft^3, the same PVC foam used throughout this research.
Attachment Bolt Diameter	Variable	Since the attachment bolt will be transferring the load to the insert system, it is important that it can handle the associated loads which will vary depending on the joint requirements.
Insert Dimensions	Variable	The most important dimension affecting the load carrying capability of a v.3 insert is its diameter, and therefore will also be variable in this study. The thickness of the flanges of the plug and sleeve were held constant at 0.125-in. This was done to reduce the complexity of the simulation test matrix needed to correlate the design parameters. Since the bending strength will increase as a function of the insert diameter, the flange width was held constant.

After identifying the fixed and variable design parameters, the relationships among them were established.

While designing a sandwich structure airframe, the expected service loads are established and each joint is designed to support the loads. The main design requirements for the purposes of this research are the service loads in bearing and bending. The

dependent variables are those which determine the load carrying capacity of the insert (face-sheet thickness, insert diameter and fastener diameter). The illustration in Figure 6-2 depicts how the variables are related.

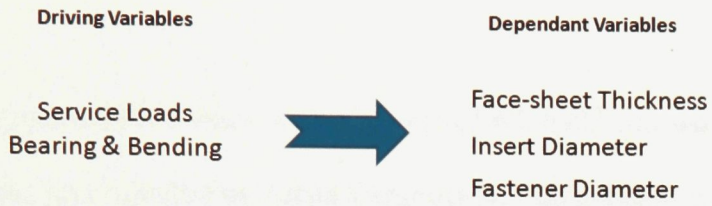

Figure 6-2- Relationship between the variable parameters.

With the relationship between the design parameters established, a test matrix was developed which links the driving variables to the dependant ones. The test matrix along with the results of the simulation and experimental work are presented in Table 6-3 in Section 6.3.3.

6.2 – Material Properties

This section covers the material properties along with the modelling of both the bearing and bending load cases.

Four components are included: the insert, the foam core, the face sheet and the fastener pin. They are summarized in Table 6-2.

Version 3 Insert

As was described in Chapter 4, the insert material is comprised of chopped carbon fibre reinforced with epoxy. The rule of mixtures was applied to estimate the tensile modulus of the insert material which was subsequently used in the material property

definition in ABAQUS. The calculation can be found in Appendix F. From the rule of mixtures, the tensile modulus was found to be 4.8×10^5 psi, and assumed to be an isotropic material as the chopped fibres are randomly oriented within the matrix.

Foam Core

Airex C structural PVC foam with a density of 6.2 lb/ft^3 was used throughout this research. The foam was supplied by Alcan Composites. The material was assumed to be isotropic with a Poisson's ratio of 0.32. This is a simplification as PVC foams do not obey the relationship between the ν, E and G. A more thorough explanation on the isotropic assumption of PVC foam can be found in M. Mahendran's thesis work, section 7.1.2, *Material Properties* [11].

Fastener Bolt

The fasteners used were a 316 stainless steel bolts, chosen for its high strength, corrosion resistance and non-magnetic properties.

Sandwich Face-sheet

The fabric used for the face-sheet is a Style #94132 (plain weave) fabric featuring T300 fibres with 3k tows provided by Hexcel Corporation. This fabric was chosen as it is the fabric used on the latest GeoSurv II Prototype fuselage and was readily accessible for this research. Hart Smith's 10% rule for preliminary sizing of fibrous composites was applied to calculate the E_2, G_{12}, and G_{13} and is based on the rule of mixtures [26].

The material properties for the components of the insert system are summarized in Table 6-2. Significant work has been done on characterizing the face-sheet material properties by M.Mahendran [11]. Those properties have also been included in Table 6-2.

Table 6-2 - Summary of material properties for the components of the insert system [11], [27].

Component	Available/Estimated Properties	Source	Knock Down Factor and Rationale	Derived properties
Face Sheet: AGP370 5H Satin Carbon fibre fabric /SC-780 epoxy	E 1 = 9325900 psi	In-house coupon testing	N/A: T 300 and AS4C fibres have similar moduli values [11]	E 1 = 9325900 psi
	G_{12} = 102250	In-house coupon testing	N/A: In plane shear is a matrix dominated property [11]	G_{12} = 102250 psi
	E2 = 932590	Hart Smith's 10 % rule	N/A	E2 = 932590 psi
	G_{13} = 10225			G_{13} = 10225 psi
	G_{23} = 10225			G_{23} = 10225 psi
	υ = 0.3	Typical for carbon-epoxy composites		υ = 0.3
	Tensile Strength/Yield Strength = 122400 psi	In-house coupon testing	-10% (T300 vs. AS4) +10% (Crimp Angle 3k vs. 6k) -10% (Fabric = Unidirectional Lamina assumption in the FEA) [11]	Tensile Strength/Yield Strength = 101160 psi
	Strain to failure (Tension) = 0.013		+10% (T300 vs. AS4) -20% (Fabric = Unidirectional Lamina assumption in the FEA and additional safety factor of 10%) [11]	Strain to failure (Tension) = 0.011
	Shear Strength = 8600 psi		15% of the tensile strength typical for carbon epoxy composites [11]	Shear Strength = 15174 psi
	Strain to failure (In-plane shear) = 0.05		-20% (Fabric = Unidirectional Lamina assumption in the FEA and additional safety factor of 10%) [11]	Strain to failure (In-plane shear) = 0.04
Insert: Chopped Carbon -Epoxy	E = 2313939 psi	Rule of mixtures (see appendix F)	N/A	E = 2313939 psi
	υ = 0.3	Typical for carbon-epoxy composites		υ = 0.3
	Tensile Strength/Yield Strength = 7846 psi	Manufacturers Specifications	Due to low fibre volume fraction and in the absence of test data, tensile strength will conservatively be chosen to be equal to the matrix strength	Tensile Strength/Yield Strength = 7846 psi
Foam Core: Airex C structural PVC foam	E=18850	Manufacturers Specifications	N/A	E=18850
	υ = 0.32	Manufacturers Specifications		υ = 0.32
Fastener Bolt: 316 Stainless Steel	E= 27195 ksi		N/A	E= 27195 ksi
	υ = 0.28			υ = 0.28
	Tensile Strength = 70ksi	ASTM Standard F-593-02 [27]		Tensile Strength = 70 ksi

With the material properties of the components of the insert system defined, the assembly was modeled in ABAQUS. The following two sections cover the modelling and simulation setup for the bearing and bending load cases.

6.3 Simulation Study

The following sections describe the modelling of the v.3 inserts. The results of the simulation work and experimental validation testing are discussed. The correlation development between design variables is covered along with their integration into an easy-to-use computer program to aid future insert designers.

6.3.1 Modelling Bearing Tests

Figure 6-3 shows the v.3 bearing insert assembly modelled in ABAQUS 6.10. The face-sheet was modelled two ways: as an isotropic material and as a 3D laminate, see Figure 6-4. Both modelling techniques were used and compared against one another; the results are presented later in the chapter. For the 3D laminate, the plain weave fabric was assumed to be unidirectional. This is an idealization and a knockdown factor was used on the tensile strength of the composite face-sheet. The knockdown factor used as a result of this idealization was derived from in-house coupon testing [11]. The v.3 insert was modelled as one homogeneous component, the plug and sleeve were assumed to be one part. This idealization was made to simplify the model, reduce computational time and eliminate additional constraint definitions. The foam core, v.3 insert and pin were each modelled as isotropic materials.

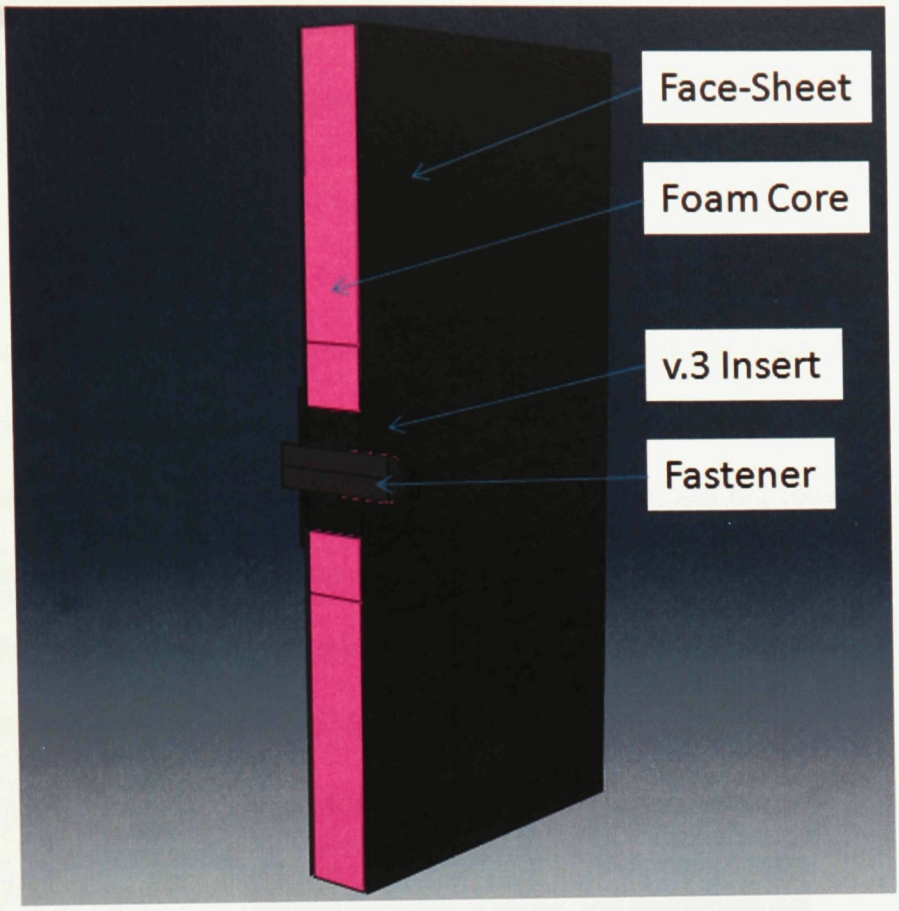

Figure 6-3- v.3 insert system assembly modelled in ABAQUS 6.10.

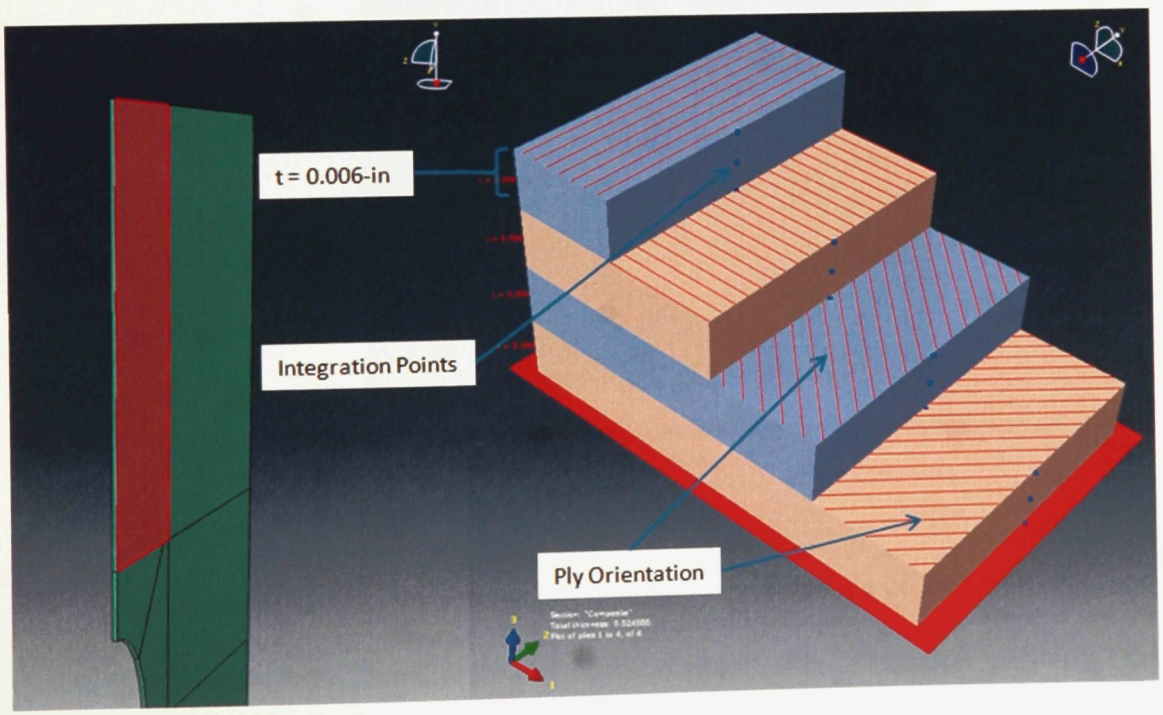

Figure 6-4 - Face-sheet modelled as a three dimensional laminate.

The bondline between the face-sheet and foam core was simulated using a tie constraint. This tie constraint assumes a perfect bondline, which is adequate for this model.

Three general, surface-to-surface contact constraints were used to model the v.3 insert. The first constraint was between the inner surface of the insert flanges and the outer surface of the face-sheet, view Figure 6-5. The interaction property was defined as a 'hard' contact. Hard contact constraint assumes no damping and the transfer of pressure between the defined surfaces is instantaneous. This constraint is also an idealization as in reality there will be some damping effects; however, since both components are made of brittle materials it is deemed an adequate assumption.

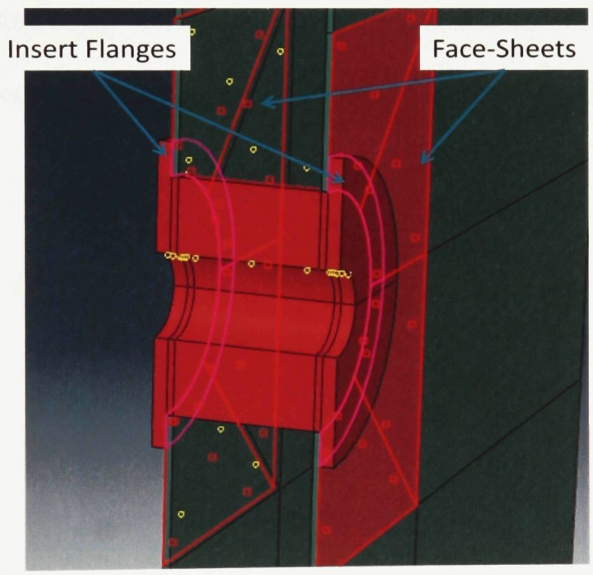

Figure 6-5 - Surface-to-surface general contact constraint between the insert flanges and the outer surface of the facesheet.

The second insert interaction is between the bearing surface of the insert and face-sheet (view Figure 6-6). Similar to the first constraint, the interaction property was defined as a 'hard' contact.

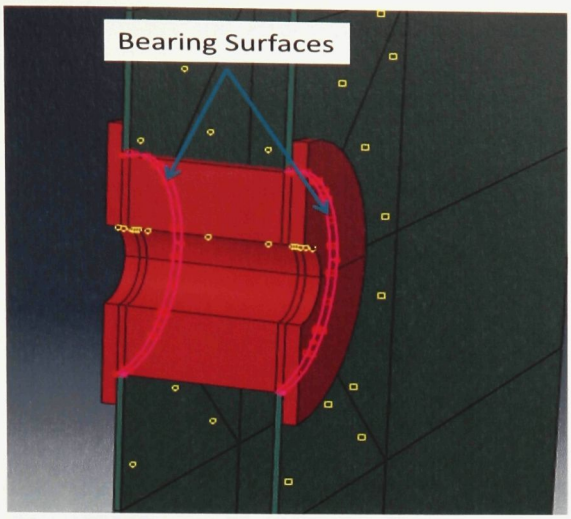

Figure 6-6 - Surface-to-surface general contact constraint between the bearing surfaces of the insert and the face-sheets.

The final contact constraint used was between the bearing surfaces of the insert and the foam core. A geometrical contact constraint was used with finite sliding which assumes little relative movement between the contacting surfaces (view Figure 6-7).

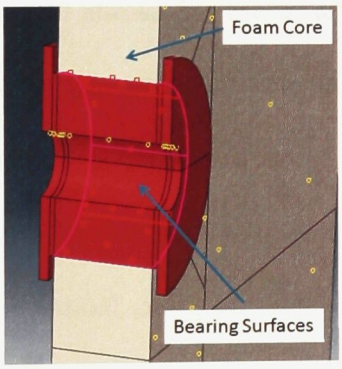

Figure 6-7 - Surface-to-surface general geometrical contact constraint between the bearing surfaces of the insert and foam core.

The pin was tied to the insert in the manner shown in Figure 6-8. Only the top halves of the mated surfaces between the insert and fastener pin were mated together as the bearing load acts in this direction. In the physical model, the fastener pin is not

bonded to the inner surface of the insert and thus tying the bottom surfaces would not be representative of the physical model.

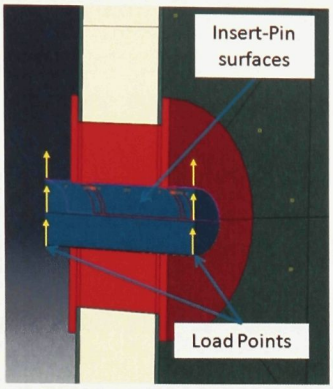

Figure 6-8 - Tied surface constraint between the fastener pin and the v.3 insert and the concentrated load points for the simulation of bearing loading.

The bearing load was applied as six concentrated load points on the fastener pin in the configuration shown in Figure 6-8. The pin was also constrained to only translate in the direction of the load value (y-direction view Figure 6-9). This simplification greatly reduces the computational time and allows for the solution to converge. In reality, the alignment of the assembly (pin, insert, sandwich structure etc.) will not be perfect, and rotations and translations in other directions will occur. Despite this simplification, in general, the rotations and out of plane translations due to misalignments and manufacturing flaws should be minimal, and this simplification will thus be maintained for the purposes of this study.

Half of the insert system was modelled and a symmetry constraint was invoked in order to reduce the number of computations and reduce simulation times. The model could have been further reduced to a quarter-model with another plane of symmetry added, however, for visualization purposes it was decided that the half model was

sufficient. The outer surface of the insert system assembly was also fixed in place to simulate the bearing experimental setup used in the previous chapters. Figure 6-9 shows the symmetry and the encastre constraint on the assembly.

A structured mesh was used for each of the components in the assembly, with C3D8R hexahedral elements. The C3D8R element is a general purpose three-dimensional, continuum, 8-node linear brick element (reduced integration - 1 integration point). Hexahedral elements were used to give better visualization of the results over triangular (tri) and tetrahedral (tet) elements. Also, since the C3D8R element is a reduced integration element, it computes average strain values using uniform strain formulation which yields more accurate results than fully integrated elements such as triangular or tetrahedral elements.

In addition to higher accuracy, computational time is reduced, as a result of the fewer number of integration points [28]. Figure 6-10 shows the fully meshed insert assembly with 30164 elements. Finer meshes on slave components compared to the master components were used for discretizing the assembly. To reduce computational time, the mesh was refined near the insert area, and remained coarse in non-critical areas further away from the zones of interest.

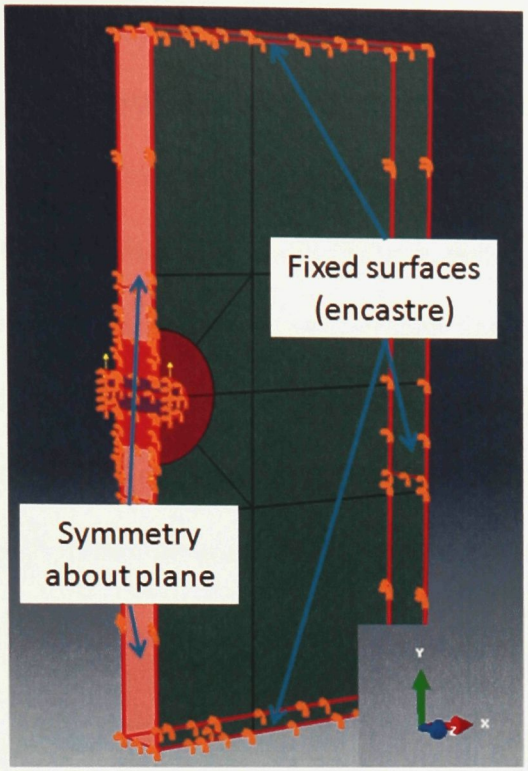

Figure 6-9 - Modelled insert system assembly showing the encastre constraint and the symmetry invoked about the YZ plane (x-direction).

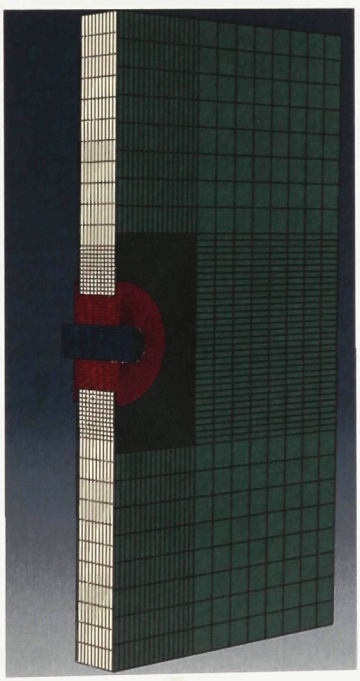

Figure 6-10 - Fully meshed insert system assembly with a total of 30164 C3D8R elements.

The simulations were performed for the combination of parameters presented in Table 6.3. Failure during the simulations was taken to be when the first component of the assembly displayed a stress level exceeding its tensile strength. In all of the bearing tests, failure was observed in the face-sheet as a result of the bearing load transferred from the insert. Figure 6-11 shows the typical displacement progression of a bearing test with the fastener pin removed for clarity. As the insert is displaced upward into the face-sheet, the face-sheet collapses and buckles into the foam. The pressure of the face-sheet on the bearing surface of the insert forces the insert flanges inward towards the face-sheet.

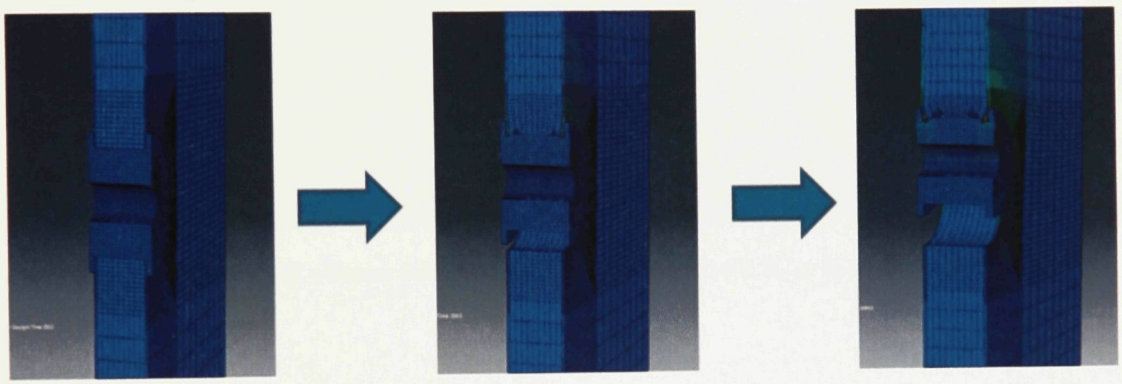

Figure 6-11 - Progression of the displacement of the bearing simulation test (displacement is magnified for visualization)

As was mentioned earlier in the chapter, the bearing tests were performed with two face-sheet modelling techniques. Both the isotropic and three dimensional lamina models failed at similar load levels; the stress fringe plot of a typical face-sheet and insert are shown in Figure 6-12. The lamina model, however, did produce more accurate results when compared to experimental validation; this is due to the fact that the isotropic assumption averages the stress out over the whole laminate, whereas the lamina model considers the stress state in each of the plies in the laminate. In reality, the first ply will

fail, and subsequently the remaining plies will pick up the load, once the first ply fails, the layup no longer becomes quasi-isotropic.

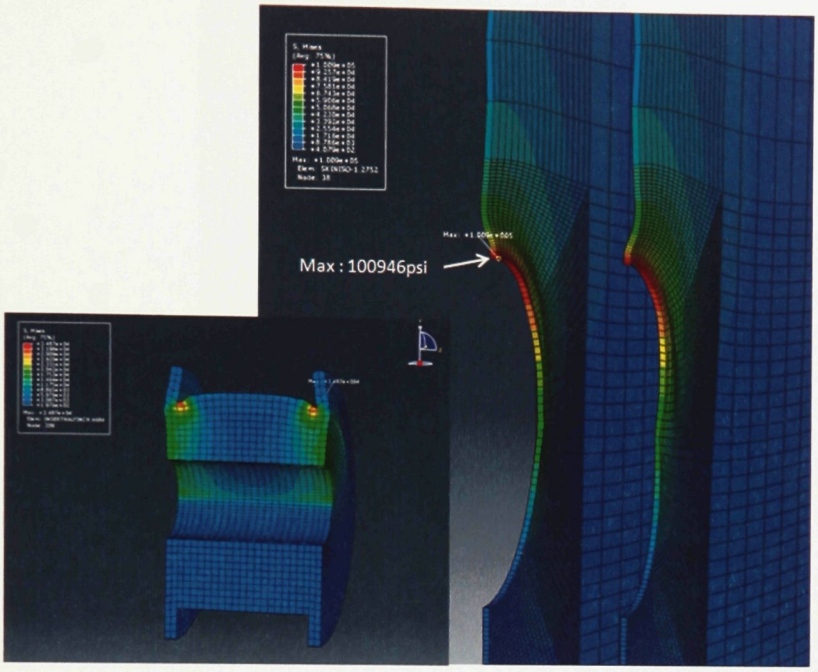

Figure 6-12 - Stress fringe plot of the 4-ply isotropic face-sheet and insert

6.3.2 - Modelling Bending Tests

Figure 6-13 shows the bending v.3 insert assembly model in ABAQUS. It is similar to the bearing model, the difference being the geometry of the fastener pin. The distance from the flange of the insert to the end of the pin where load is applied measures 2.4 in, which corresponds to the length of the engine standoff mount on the GeoSurv II Prototype.

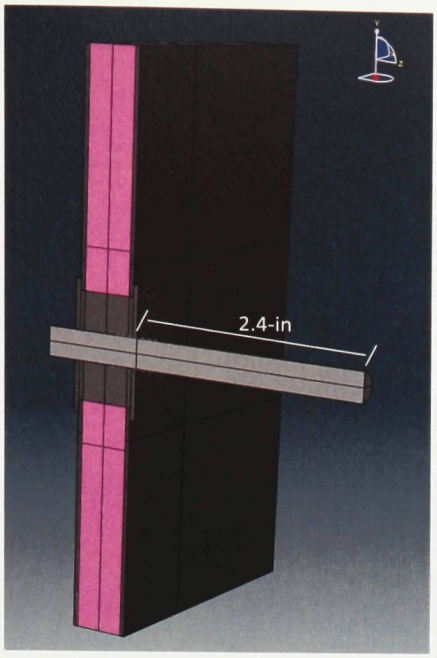

Figure 6-13 - Bending v.3 insert assembly model

For the bending load case, the face-sheet was only modelled as a three dimensional composite laminate (refer to Figure 6-4). The constraints were also applied differently:

- The only contact constraint used was between the bearing surfaces of the insert and the face-sheet (refer to Figure 6-6).
- The pin was constrained to the inner surface of the insert in the manner shown in Figure 6-14.
- The surfaces that were in contact due to the applied load were tied together and the surfaces that tended to separate were not constrained.
- Figure 6.15 shows how the flanges of the insert were tied to the face-sheet.

Tying the flanges of the insert to the face-sheet in the manner shown in Figure 6-15 is justified because there is little relative motion between those tied surfaces. The pin was removed from Figure 6-15 for illustration purposes.

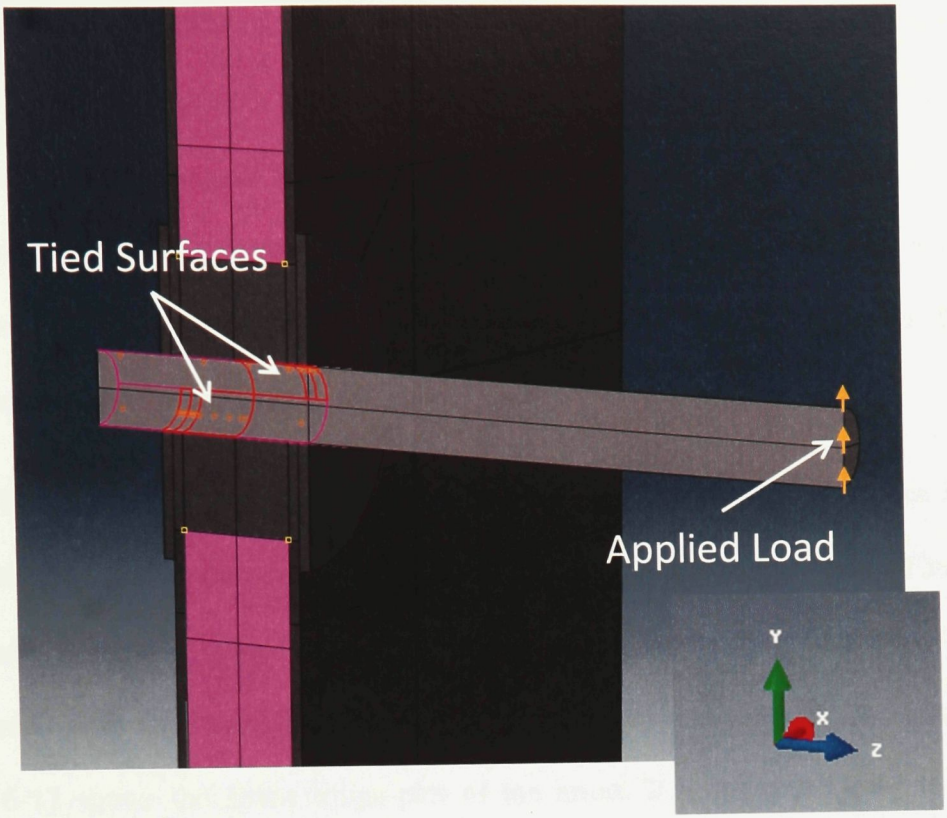

Figure 6-14 - Tie constraint between the fastener pin and the v.3 insert

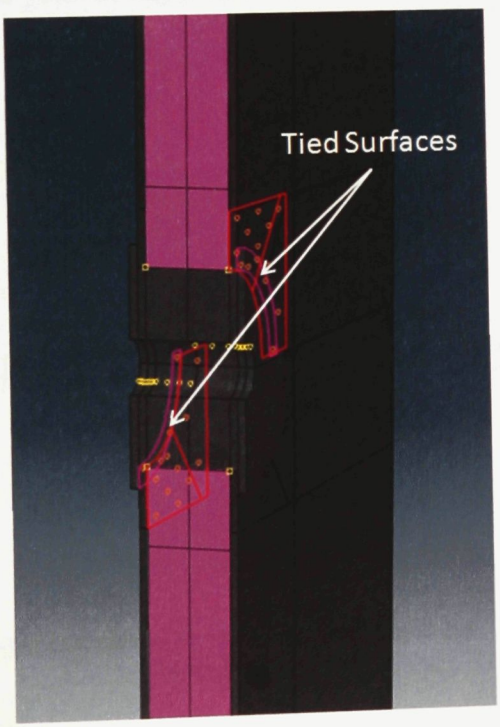

Figure 6-15 - Tie constraint between the insert flanges and the face-sheet

The skin was tied to the foam core in the same manner as the bearing simulations, also, the same encastre and symmetry constraints were used. The pin and insert were constrained to only translate in the direction of the load (y-direction), normal to the load (z-direction) and rotate about the axis of symmetry (x-axis) (refer to Figure 6-14). The load was applied as a point load through three nodes (on the y-axis) on the end of the pin at the location shown in Figure 6-14.

The displacement progression can be seen in Figure 6-16. As can be seen from the figure, the bending is transferred from the insert flanges to the face-sheet. The critical component in these simulations were the inserts. All of the bending simulations had the same result with the insert reaching its yield stress before the rest of the components. Figure 6-17 shows the stress fringe plot of the insert. It is important to note that the diameter of the steel fastener pin was held fixed at a diameter of 0.25 in. The stress level in the pin did not reach the yield strength of the steel.

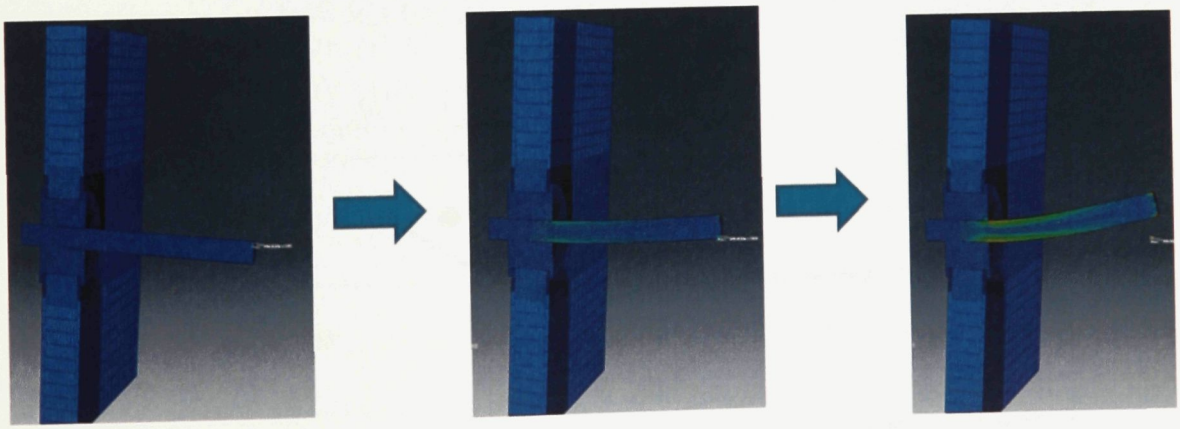

Figure 6-16 - Displacement progression of the bending simulation test (displacements are magnified for visualization).

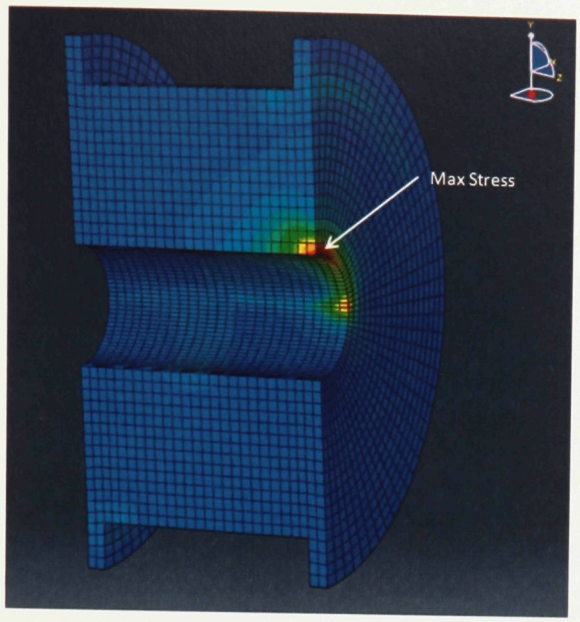

Figure 6-17 - Stress fringe plot of the v.3 insert.

A convergence study was performed for each of the bearing and bending simulations studies. It verified that the simulation results converge on a particular solution and that no further changes to that solution occur as the mesh is refined. Figure 6-18 shows the plot of maximum stress in the face-sheet against element count in the assembly mesh for the bearing simulation. Figure 6-19 shows the same plot for the 4-ply bending simulation.

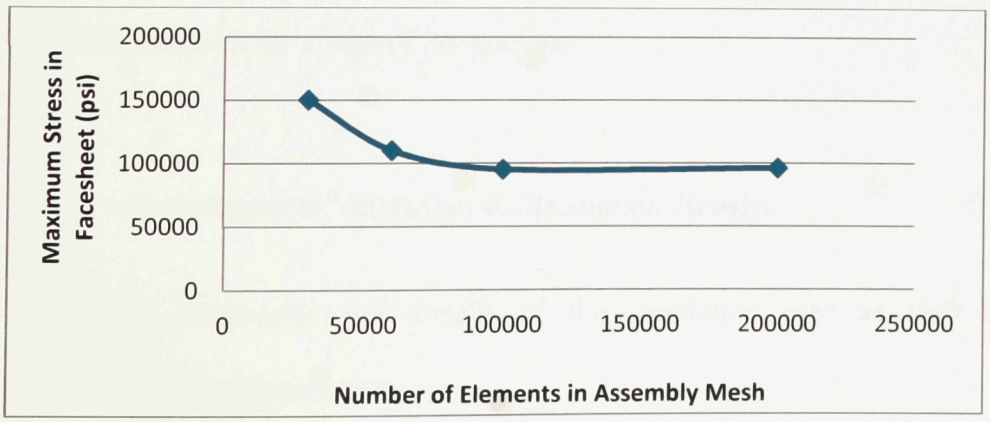

Figure 6-18 - Plot of maximum stress versus assembly mesh element count for 4-ply bearing simulation.

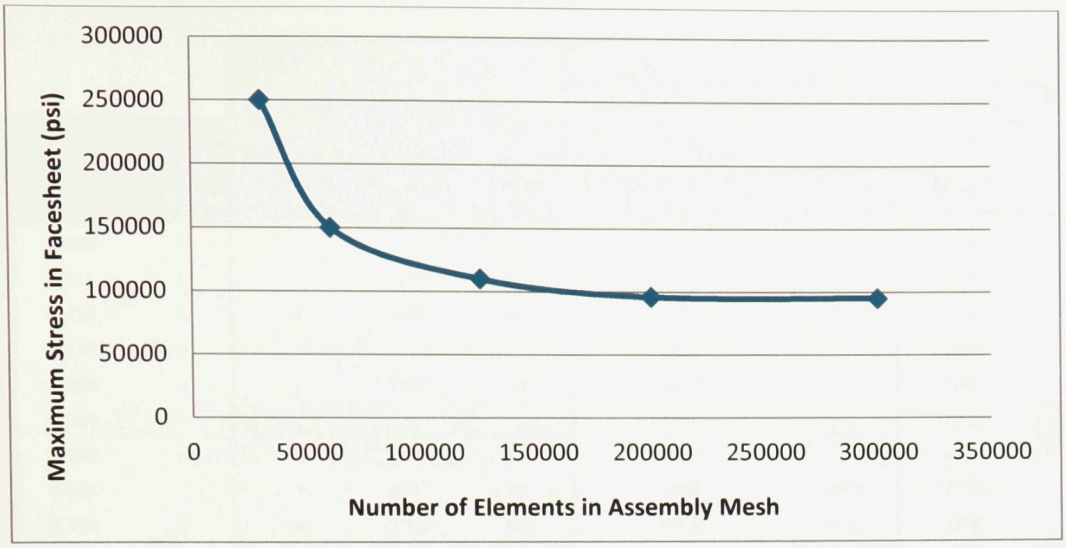

Figure 6-19 - Plot of maximum stress versus assembly mesh element count for 4-ply bending simulation.

Experimental Validation

In order to validate the simulations, experimental coupon tests were performed in both bearing and bending. The experimental setup and testing procedures used in Chapters 3 and 4 were used again for the validation testing.

Three different insert diameters were tested (0.625, 0.75 and 1.00 in) along with two face-sheet ply counts (4 and 8 plies) in bearing and bending. Three coupons were tested for each data point for a total of 36 coupons.

6.3.3 - Experimental Validation & Simulation Results

Table 6-3 summarizes the results of the simulation tests as well as the experimental validation coupon tests.

Table 6-3 - Database showing the results of the simulation study and experimental validation coupon tests.

			Experimental Coupon Tests			3D Lamina Face-Sheet Simulation Tests		Isotropic Face-Sheet Simulation Tests	
	Insert Diameter	Number of Plies	Number of Test Coupons	Failure load (lb)	Standard Deviation	Failure load (lb for bearing, lb-ft for bending)	Percent Error (%)	Failure load (lb)	Percent Error (%)
Bearing Tests	0.500	4				800		800	
	0.625	4	3	1003	44	1000	0.3	1000	0.3
	0.750	4	3	1168	89	1150	1.6	1300	-10.1
	0.875	4				1400		1550	
	1.000	4	3	1747	33	1650	5.9	1700	2.8
	1.125	4				1750		2000	
	0.500	8				1400		1400	
	0.625	8	3	1277	53	1700	-24.9	1700	-24.9
	0.750	8	3	1958	220	2000	-2.1	2100	-6.8
	0.875	8				2250		2700	
	1.000	8	3	2393	25	2700	-11.4	3200	-25.2
	1.125	8				2950		3500	
	0.500	12				2000		2000	
	0.625	12				2400		2400	
	0.750	12	No Experimental Tests Performed			2850		2925	
	0.875	12				3100		3850	
	1.000	12				3740		4725	
	1.125	12				4150		5000	
Bending Tests	0.500	4				89			
	0.625	4	3	248	17	153	62.1		
	0.750	4	3	302	18	210	43.8		
	0.875	4				273			
	1.000	4	3	584	71	336	73.9		
	1.125	4				405			
	0.500	8				120			
	0.625	8	3	342	25	184	85.8		
	0.750	8	3	391	34	251	55.6		
	0.875	8				315			
	1.000	8	3	677	38	379	78.5		
	1.125	8				443			
	0.500	12				152			
	0.625	12				215			
	0.750	12	No Experimental Tests Performed			295			
	0.875	12				360			
	1.000	12				425			
	1.125	12				480			

6.3.4 - Bearing Simulation Test Results

A plot of the bearing failure load versus the v.3 insert diameter for the following items are presented in Figure 6-20:

- Isotropic simulation model
- 3D Lamina simulation model
- Experimental testing

As can be seen from the graph, there is good agreement between the experimental results and both bearing simulation models. Both simulation models are within approximately 10% of the experimental values for the 4-ply face-sheet sandwich structure.

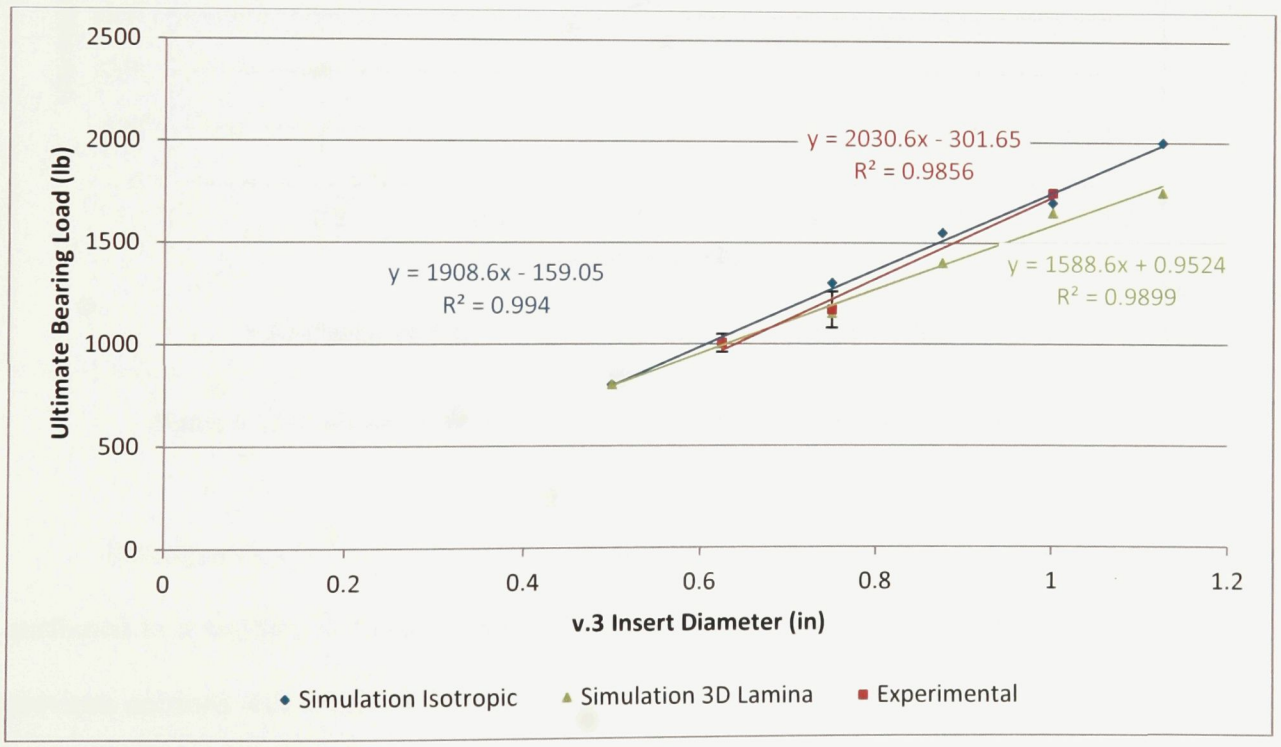

Figure 6-20 - 4-ply face-sheet - bearing failure load versus v.3 insert diameter

Figure 6-21 shows the bearing failure load versus the insert diameter for the 8-ply load case. The simulation models become more divergent from one another and over predict the strength of the insert by approximately 10-25%. The 3-D Lamina face-sheet model represents the insert strength more closely when compared to the experimental testing. In the 12-ply simulation, the two models further diverge from each other; however, there is no experimental data for validation. The 12-ply bearing failure load versus insert diameter is presented in Appendix G.

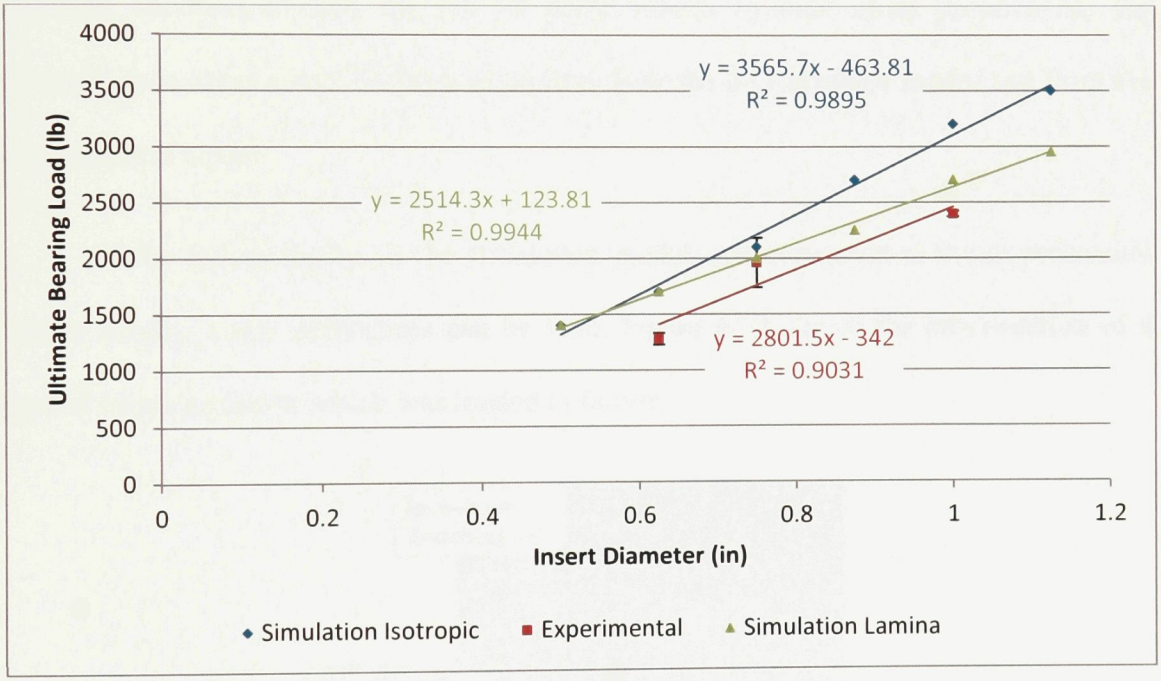

Figure 6-21- 8-ply face-sheet - bearing failure load versus v.3 insert diameter

Discrepancies between the simulation models and the experimental results can be attributed to a number of factors. Many of the simplifying assumptions presented in the previous sections will tend to over predict the strengths of the inserts. These assumptions include the use of unidirectional fibres (in the case of the 3D lamina face-sheet model)

instead of a plain weave layup. In a plain weave layup, the tows are kinked, which reduces the mechanical properties of the laminate. The tie constraints assume perfect bonding between the mating surfaces, where in reality the bond surfaces can be the area of weakness, due to manufacturing defects (poor surface preparation, poor bondline thickness control etc.). Although the load case is in bearing and the layup is quasi-isotropic, the insert flanges apply pressure out-of-plane as the pin is displaced and the face-sheet is strained. Modelling the face-sheet as a purely isotropic material does not properly capture the out-of-plane effects in the laminate. This could explain why, as the laminate becomes thicker, the out of plane effects become more pronounced; the isotropic face-sheet model deviates more from both the 3-D laminate model and from the experimental model.

If the failure modes in the simulation models are compared to the experimental failure results, a few differences can be seen. Figure 6-22 shows the cross-section of a typical bearing coupon which was loaded to failure.

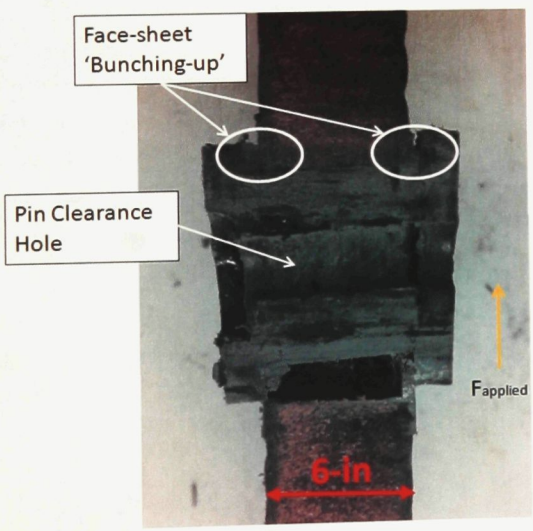

Figure 6-22 - Cross-section of a typical bearing coupon which was strained to failure

As can be seen from the figure, as the face-sheet is loaded past failure, it buckles and bunches between the face-sheet and the insert flanges. This material build-up applies an outward pressure on the flanges and eventually leads to the insert cracking and failing where the flanges meet the bearing surface. These effects are not captured by the simulation model because the simulation only captures the onset of failure and not the subsequent deformation.

Despite the discrepancies between the experimental and simulation models, the 3D lamina model was determined to best represent the experimental results.

6.4.2 - Bending Simulation Test Results

For the simulation of the insert assembly in bending, the isotropic assumption was not used as out-of-plane effects cannot be neglected. The only modelling technique used for the bending simulations was the 3D lamina approach.

Figure 6-23 shows the bending moment plotted against the insert diameter for a 4-ply face-sheet.

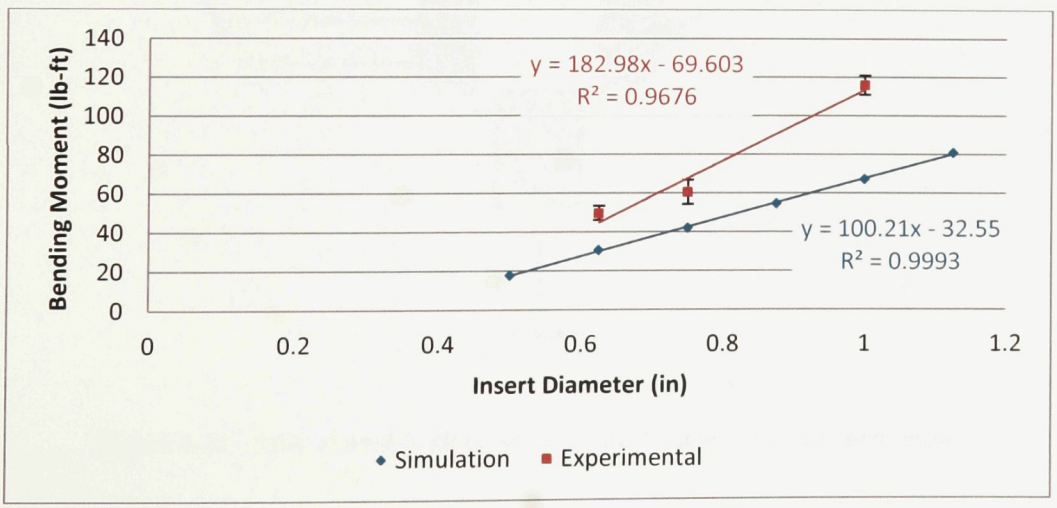

Figure 6-23 - 4-ply face-sheet - Bending Failure Load versus v.3 Insert Diameter

The simulation results do not agree as well with the experimental testing as did the bearing tests. The simulation results under predicted the strength of the insert by approximately 40-85% for the 4 and 8 ply specimens when compared to the experimental test results. The divergence between the experimental and simulation results was similar between the 4 and 8 ply assemblies. The axial force versus insert diameter plots for the 8 and 12 ply insert assemblies can be seen in Appendix G.

There are a number of reasons that contribute to the discrepancy between the experimental and simulation results. The most obvious are the differences between the experimental setup and the simulation assembly. In the experimental setup, the fastener pin is secured to the v.3 insert assembly with the use of nuts and washers on either side of the insert (view Figure 6-24).

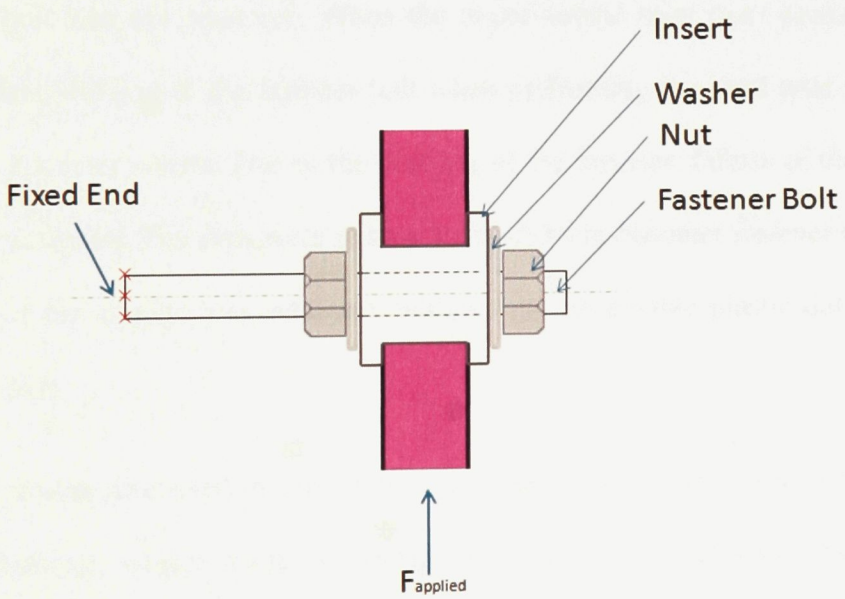

Figure 6-24 - Joint assembly illustration for the bending experimental testing

In the simulation model (view Figure 6-14) there are no such washers or nuts holding the assembly together. Since the nuts are tightened prior to the testing, the insert joint is compressed and all the components behave as one and bend together in unison. The insert itself is not carrying the whole load into the sandwich structure; the nuts and washer are contributing to the overall strength in bending. Since the simulation does not take these extra components into account, the strength of the insert joint is under predicted.

Other factors that could contribute to the differences in the results are the simplifying assumptions such as assuming unidirectional plies and the tie constraints assuming perfect bonding between surfaces.

Due to the low failure loads in the simulation trials, yielding of the 0.25-in attachment bolt was not observed. When the experimental tests were performed, there was significant yielding of the fastener bolt when performing the bend tests for the 0.75 and 1.00-in diameter inserts. Due to the yielding of the fastener, failure of the insert was not initially achieved. The tests were redone with a 5/16-in diameter fastener bolt instead, and failure of the coupon was achieved, without any observable plastic deformation of the fastener bolt.

The results discussed in this section were used to develop correlations between the insert diameter, service loads in bearing and bending and face-sheet thickness. The following section presents the correlations and incorporate the results into a user friendly computer program for designers to utilize.

6.4 – Insert Size Calculator

The equations that relate the insert diameter to the bearing, bending and face-sheet thickness were determined from the trend lines of the bearing/bending load versus insert diameter plots (view Figure 6-20, Figure 6-21). All of the previously mentioned plots can be found in Appendix G.

Table 6-4 lists the aforementioned equations, the variables and also the source of equation (experimental results, simulation or otherwise).

Table 6-4 - Correlation equations between the bearing and bending loads, face-sheet thickness and insert diameter.

Load Case	Face-sheet Thickness	Correlation Equations: Y = Failure load (bearing) or moment (bending) X = Insert Diameter (in)	Derivation
Bearing	4	y = 1908.6x - 159.05	Equation of the trend line from the 3D lamina simulation Failure load versus insert diameter plot (Figure 6-20)
	8	y = 3565.7x - 463.81	Equation of the trend line from the 3D lamina simulation Failure load versus insert diameter plot (Figure 6-21)
	12	y = 5234.3x - 769.52	Equation of the trend line from the 3D lamina simulation Failure load versus insert diameter plot view Figure G- 1 in Appendix G
Bending	4	y = 182.98x - 69.603	Equation of the trend line from the experimental testing plot of the failure load versus insert diameter (Figure 6-23)
	8	y = 185.67x - 53.063	Equation of the trend line from the experimental testing plot of the failure load versus insert diameter view Figure G- 2 in Appendix G
	12	y = 186.29x - 35.143	Extrapolation of the experimental testing results for the 4 and 8 ply face-sheet thicknesses view Figure G- 3 in Appendix G

For the bearing load case, the three-dimensional lamina simulation results were close to the experimental coupon testing results. The trend line equation relating failure load with insert diameter were extracted from the simulation results (Figure 6-20, Figure 6-21 and Figure G-1 in Appendix G).

For the bending load case, the simulation results did not match well with experimental testing. The trend line from the bending moment versus inserts diameter

plots for the experimental results were taken from Figure 6-23, and Figures G-2 and G-3 in Appendix G.

Experimental testing was not performed for the 12-ply face-sheet thickness, and instead its values were extrapolated by plotting the failure moment versus number of plies (4, 8) for each of the insert diameters. Where the trend lines for each insert diameter crossed the 12-ply value was where the failure load was 'determined' to be (see Figure 6-25).

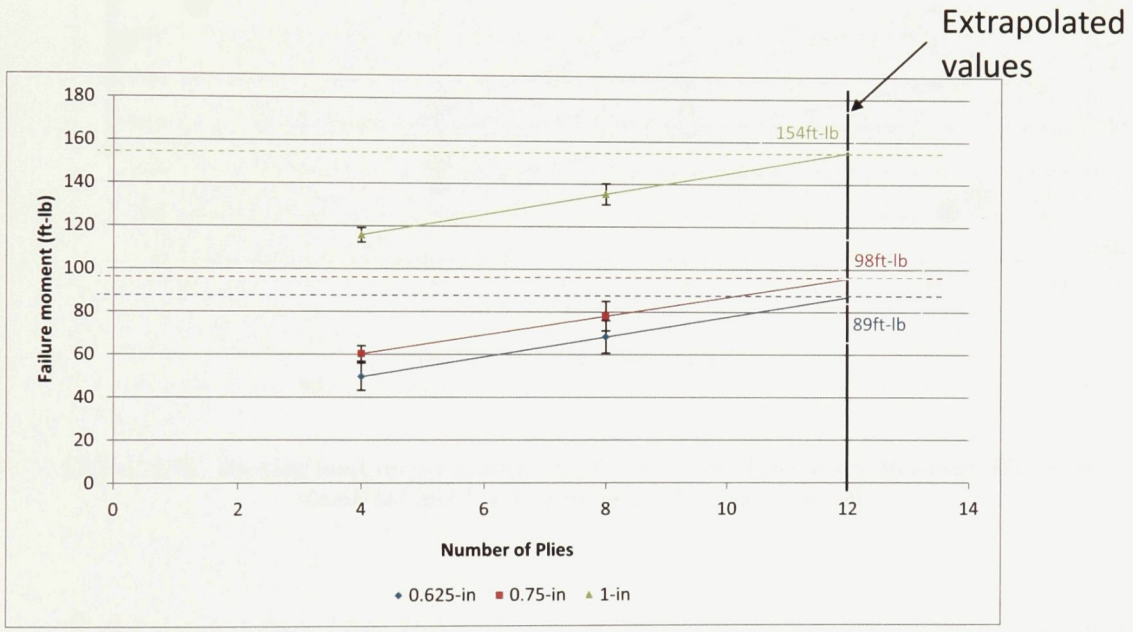

Figure 6-25 - Bending moment versus number of plies for each of the insert diameters that were experimentally tested

From Figure 6-25, the maximum bending moment was found to be 154 ft-lb which corresponds to the 1-in diameter insert. The same plot was made for the bearing load case (Figure 6-26).

From Figure 6-26, the maximum bearing load that can be used in the correlation calculations is 4150 lb. Bearing load or moment values above those mentioned above will lie outside the range of values that were simulated and/or experimentally verified, and therefore will be neglected.

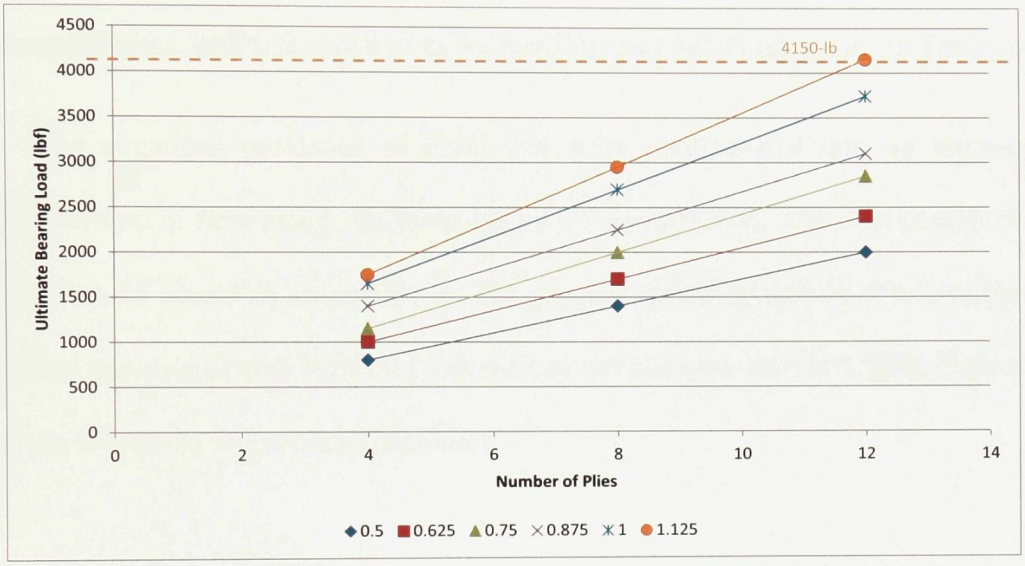

Figure 6-26 - Bearing load versus number of plies for each of the insert diameters that were simulated in ABAQUS using the 3D lamina model.

For load values less that 500 lb (bearing) or 49.6 ft-lb (bending) the insert diameter will be restricted to 0.5-in. Manufacturing v.3 insert with diameters less than 0.5-in becomes challenging using the manufacturing process developed in Chapter 4.

The insert diameter is calculated based on the most critical load case using the correlations from Table 6-4. The optimized insert diameter is calculated separately for the bending and pure bearing load cases, the larger of the two insert diameters that are calculated is the final insert diameter.

The bending load case correlations in Table 6-4 are not pure bending but also includes a bearing force element. The bearing force component of the bending + bearing load case is less than 50% of the loads in the pure bearing load case. This assumption of neglecting the bearing effects will yield slightly more conservative result (i.e. calculate slightly larger inserts than needed). The reason for this is the shear effects of the bending load case contributed to the maximum stress in the insert when performing the bending experimental tests, which is captured in the bending correlation equations in Table 6-4.

The equations presented in Table 6-4 were incorporated into an input-output program written in Java using NetBeans IDE 7.1.1 environment. The source code for the program can be found in Appendix H. The purpose of the program is to combine the correlation equations from Table 6-4 into an easy-to-use user interface (UI). Figure 6-27 shows the UI for the Insert Size Calculator.

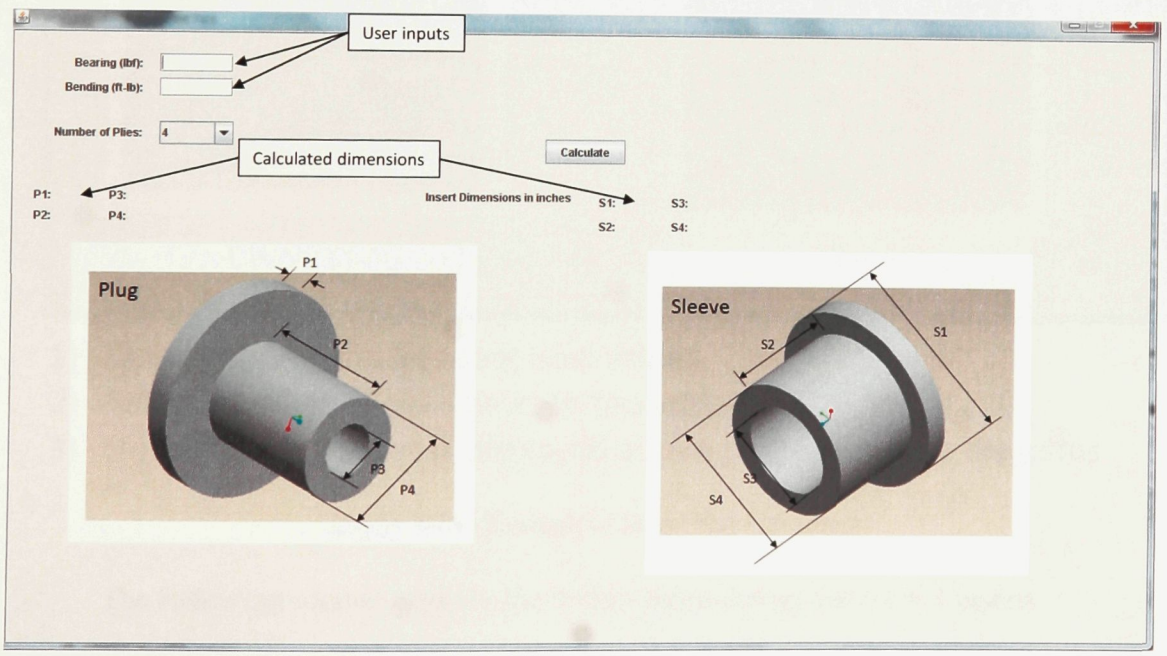

Figure 6-27 - Insert Size Calculator UI

As can be seen from the program UI, the user inputs include the loads in bearing and bending along with the number of plies on each face-sheet of the sandwich structure. The user can input the in-service loading conditions and the program will calculate the geometry of the plug and sleeve components necessary to handle the applied loading. The calculated geometry can then be used in the mould manufacturing process described in Chapter 4. Figure 6-28 shows an example of sizing inserts using the Insert Size Calculator. With an input bearing load of 1500 lb, bending load of 350 ft-lb and 8 ply face-sheets, the dimensions of the v.3 insert required to handle the above load value/condition is displayed above the plug and sleeve diagram.

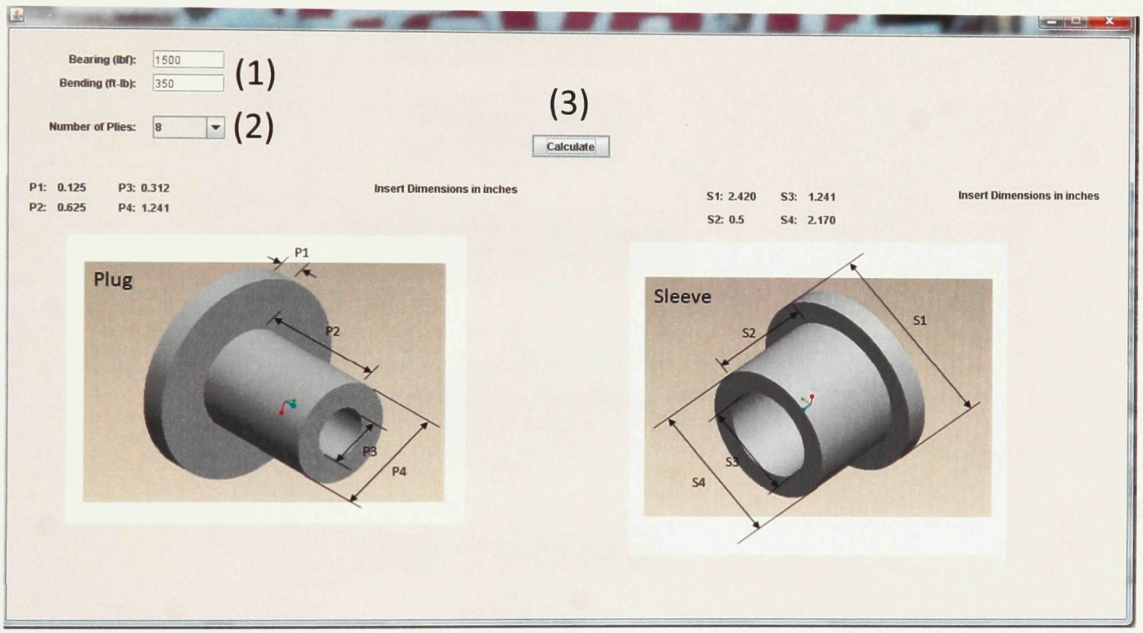

Figure 6-28 - Example of Insert Size Calculator.

The following section outlines the design methodology for the v.3 inserts.

6.5 – Insert Design Methodology

Chapters 4 and 6 covered the design, manufacturing and parameter correlation development of the v.3 insert system. The overall methodology for designing v.3 inserts is presented in Figure 6-29.

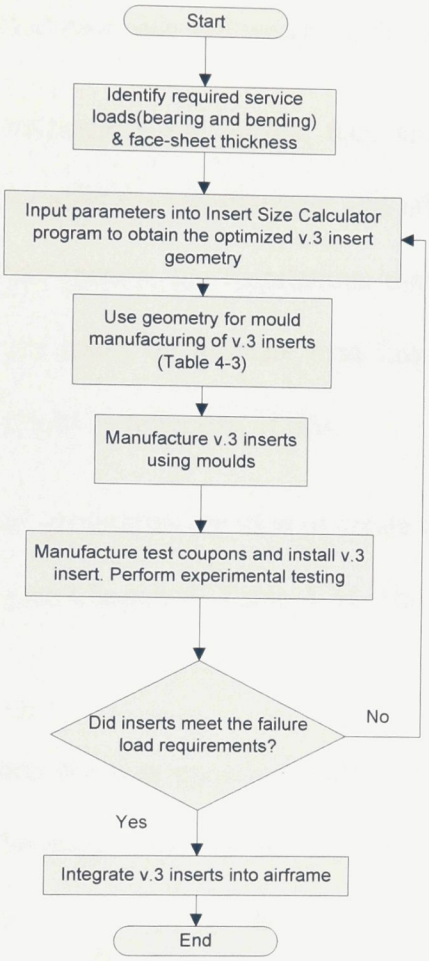

Figure 6-29 - V.3 inserts design and manufacturing methodology

Figure 6-29 summarizes the work from the previous chapters and organizes it into a flowchart illustrating the methodology for quickly designing an optimized v.3 insert system for sandwich structures.

The first step in designing the insert system is to identify the required service loads in bearing and bending along with the desired face-sheet thickness. The designer can choose to compare the results of selecting different face-sheet thicknesses and then deciding which solution is most desirable to their application. The advantage of choosing a thicker face-sheet is that the diameter of the insert will be decreased; however, increasing the face-sheet thickness may add weight to the overall structure.

Once the design parameters are chosen, they are entered into the Insert Size Calculator program, which calculates the diameter and other insert dimensions. As was mentioned previously in this section, the correlations that are integrated into the Insert Size Calculator program are based on ultimate load failure data. The load parameters entered into the program should be reflective of this.

The optimized insert geometries are used to create the solid models of the moulds for mould manufacturing (see Chapter 4, Table 4-3). The plastic moulds are then CNC machined.

The optimized inserts are then experimentally tested to validate the design. The same static bearing and bending tests that were performed for the validation of the simulation work is required.

If the tests are successful then the inserts can be integrated into the airframe. If they are not successful, then further optimization will be required. If the inserts are under designed (i.e. they fail prematurely) then a solution could be to locally reinforce the face-sheet to reduce the stress concentration, or to revisit the loading parameters and generate a more robust geometry for the insert. If the insert is over-designed, it is up to the

designer to make the decision on whether or not to revisit the design and attempt a second iteration, or whether to accept the weight penalty.

A disadvantage of this design methodology is if the experimental testing reveals that a second iteration of the design is required (i.e. the insert geometry is inadequate), then new moulds must be machined. A possible alternative solution, is the use of rapid prototype machines to manufacture inserts, such as the one shown in Figure 6-30.

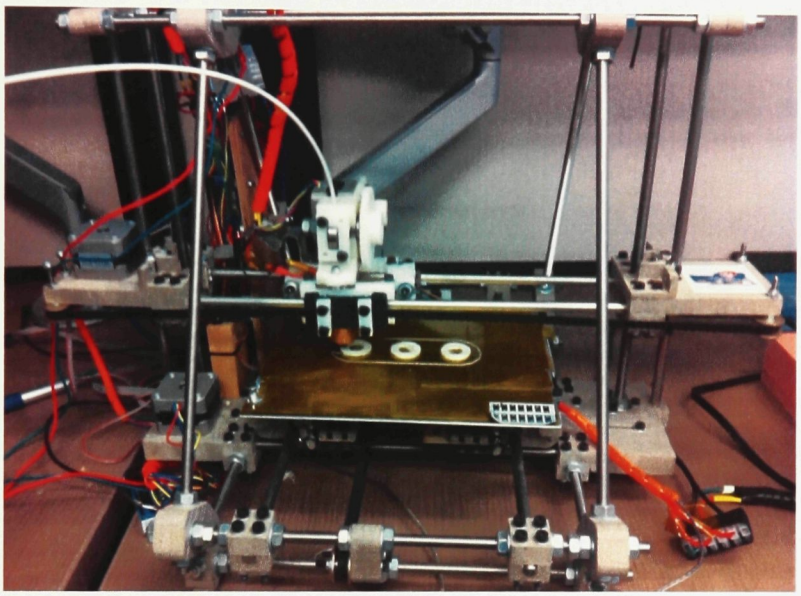

Figure 6-30 - 3D rapid prototype printer (RepRap Mendel) in the process of printing three v.3 insert plugs simultaneously.

The 3D printer can take a solid model or assembly of inserts and rapidly 'print' them using various polymers such as Polycaprolactone (PCL) or Acrilonitrile Butadien Styrene (ABS). More structural materials such as reinforced thermoplastics could potentially be used in such a 3D printer which would greatly increase the strength of any inserts printed using this technique. Using this technique removes the necessity of using a CNC mill to manufacture moulds which will lower the capital and operating costs. In

addition, if it is determined through experimental testing that the inserts do not meet the load requirements, the solid models can easily be changed and submitted to the 3D printer. The modified inserts could then be printed in minutes. Figure 6-31 shows three v.3 inserts printed with PCL polymer. Figure 6-32 shows the potential design and manufacturing methodology if the manufacturing process were changed from cast inserts to printed ones.

Figure 6-31 - Three v.3 inserts printed with PCL using the 3D rapid printer.

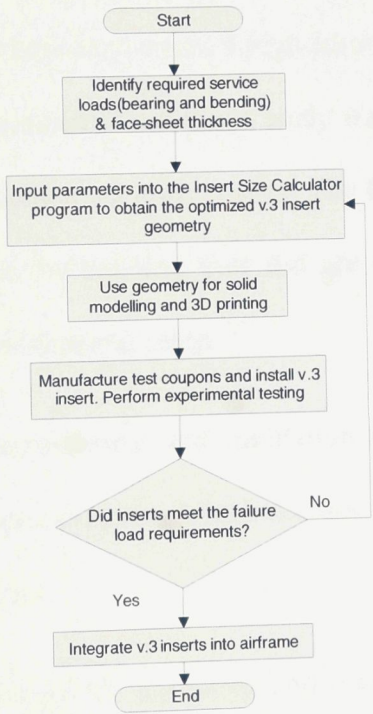

Figure 6-32 - Modified insert and design methodology using 3D printing as the manufacturing process.

Despite the apparent advantages to switching to this manufacturing process, there are still several design challenges that must be overcome in order for this to be a viable solution. Some of these design challenges include:

- **Dimensional tolerances:** The printed inserts shown in Figure 6-31 are not within the dimensional tolerances required for the insert system to be assembled properly without additional manufacturing steps being required.
- **Strength:** Since the printer is laying down strips of polymer the overall structure is very porous and could weaken the structure. PCL or ABS are relatively weak when compared to the chopped carbon fibre-epoxy. The use of thermoplastics alone or reinforced has not been attempted in the 3D printer and would require development.

Despite the challenges, there are enough potential benefits to make investigating this manufacturing process worthwhile.

This chapter outlined the work of simulating the bearing and bending tests in order to develop correlations between certain design parameters such as service loads and face-sheet thickness. An experimental validation study was performed in order to confirm that the simulation results yielded accurate results. The bearing tests matched well with the experimental results, but the bending tests did not due to differences between the simulation model and the experimental setup.

The results of the experimental and simulation work produced correlations that were integrated into a computer program, which accepts design parameters and calculates optimized v.3 insert geometries.

The overall methodology for designing and manufacturing v.3 inserts was also presented in this chapter. The following chapter will discuss the areas for future work in

the area of insert design and manufacturing as well as discuss the conclusions that pertain to this thesis work.

Chapter 7 – Conclusions & Future work

Foam-core sandwich structures are attractive for UAV airframes for their combination of strength, stiffness and low weight. Although sandwich structures are quite capable of handling distributed loads such as aerodynamic forces, they are susceptible to concentrated loads in areas such as attachment points or joints. Inserts must be included to safely introduce the required flight loads into the airframe.

A review of the literature and of the previous insert systems revealed that a more systematic approach for designing inserts in sandwich structures was required. The previous inserts that were used in the GeoSurv II Prototype were benchmark tested and design deficiencies were found. A new insert system was developed (v.3) along with a methodology for rapidly sizing inserts for a range of design variables and sandwich structure configurations. As a result of this research work the following conclusions were drawn:

- The v.3 inserts are 60% lighter than the v.1 and v.2 inserts.
- The v.3 inserts display less variability in strength and stiffness as compared to the v.1 and v.2 inserts.
- Manufacturing the v.3 inserts using chopped carbon fibre – epoxy with casting moulds is more economical when making more than 13 inserts as compared to machining the inserts from bar stock.
- Chopped carbon fibre-epoxy was found to have a lower variability in strength and stiffness and lower weight than chopped fibreglass-epoxy and chopped fibreglass-polyurethane.
- Simulating inserts in bearing and bending is possible using ABAQUS CAE software and is a useful tool for predicting the failure loads of insert systems with a given set of parameters.
- Developing correlations between design parameters is an effective way of rapidly designing inserts for a range of applications.

7.1 –Future Work

Simulation modelling using CAE software to predict failure loads of insert systems was very useful in the correlation development work. The bearing load case was successful when compared to experimental testing; however the bending case was not.

Differences between the modelling and the experimental setup were identified as the reasons for the disagreements between the results. An area to improve upon would be to further develop the bending simulation model to include the missing elements necessary to correctly simulate the experimental setup. In order to more closely model the bending experimental setup, the following items need to be developed and included in the simulation model:

- Add the washers on the outer surface of the insert flanges, apply appropriate constraints (tie constraints could be justified, see next bullet)
- Simulate the compression force that the nuts on either side of the washers impose on the insert assembly (view Figure 6-24). This pressure keeps all of the components together and increases the frictional force between them. Tie constraints may be justified as there is little relative motion between the individual components compressed together due to the high friction between the components.
- Simplify the model by adding another plane of symmetry (use a quarter symmetry models instead of the half symmetry model used in the current modelling), this will help with run times and help offset the added complexity of the additional constraints and components.

In order to further add confidence in the correlations developed and integrated into the Insert Size Calculator program, the experimental validation test matrix should be expanded to include 12 ply specimens, and validate all of the insert diameters that were simulated (fill the experimental portion of Table 6-3).

The sophistication of Insert Size Calculator would be improved by developing a correlation between the core height, and the parameters already addressed in this research work. The core height would influence the bending strength of the insert system substantially.

Areas for improvement for the vibration study presented in Chapter 5 include:

- The test fixture should be redesigned to fully constrain the specimen so as to fully transfer the vibrational load (view proposed design in Figure 5-20).
- The weight of the test fixture should match the mass of the vibration source that is being replicated. This will ensure that the forces transferred to the specimens are representative.
- The attachment bolt should be matched in order to ensure that the load transfer is the same in both the experimental setup and in the actual assembly.
- The effects of the strain rate sensitivity for the v.3 insert assembly should be investigated to see if there is a potential for the reduction of vibration test times.

7.2 – Thesis Contributions

The v.3 insert system, the manufacturing process and overall methodology for designing optimized inserts offers a practical solution for designers wishing to integrate optimized inserts into a foam-core carbon-epoxy skinned sandwich structure. This was achieved by:

- Designing a new v.3 insert system.
- Selecting an appropriate material and developing a low cost manufacturing process to produce the inserts.
- Developing correlations between insert system design parameters through simulation and experimental work.

- Integrating the correlations into an easy-to-use computer program for designers to quickly calculate optimized inserts given a set of design conditions.

References

[1] J. R. Vinson, "Sanwich Structures: Past, Present and Future," *Sandwich Structures 7: Advancing with Sandwich Structures and Materials*, vol. 7, pp. 3-12, 2005.

[2] A.S, Zahlen P. C, and Zuardy, I Herrmann, "Sandwich Structures Technology in Commercial Aviation," *Sandwich Structures 7: Advancing with Sandwich Structures and Materials*, vol. 7, pp. 13-26, 2005.

[3] Industry Week. (2007, December) Boeing 787: A Matter of Materials – Special Report: Anatomy of a Supply Chain. [Online]. http://www.industryweek.com/articles/boeing_787_a_matter_of_materials__special_report_anatomy_of_a_supply_chain_15339.aspx

[4] The Boeing Company. (2007, July) 787 Dreamliner Program Fact Sheet. [Online]. http://www.boeing.com/commercial/787family/programfacts.html

[5] D, Suong V. Hoa Gay, *Composite Materials: Design and Applications*. New York, United States of America: CRC Press, 2007.

[6] CT UM. [Online]. http://stim.obninsk.com/alumcore.jpg

[7] (2008) Nasa - Glenn Research Center. [Online]. http://www.grc.nasa.gov/WWW/RT/2006/images/RX11C-hurwitz1-f1.jpg

[8] (2008) University of Virginia - School of Engineering and Applied Science. [Online]. http://www.ipm.virginia.edu/newres/pcm.thermal

[9] (2006, July) Composites world: Lightning Strike Protection For Composite Structures. [Online]. http://www.compositesworld.com/articles/lightning-strike-protection-for-composite-structures

[10] S. Pant, "Detection and Characterisation of Low Velocity Impact Damage on Foam-core Carbon-fibre Sandwich Composite Structures," Carleton University, Ottawa, PhD Proposal 2010.

[11] M. Mahendran, "An Improved Mouldless Manufacturing Method for Foam-Core Composite Sandwich Structures," Carleton University, Ottawa, Master's Thesis 2010.

[12] J. Maley, "Composite Manufacturing," Carleton University, Ottawa, Master's

Thesis 2008.

[13] E., Lyckegaard, A. Bozhevolnaya, "Structurally Graded Core Inserts in Sandwich Panels," *Composite Structures*, vol. 68, pp. 23-29, April 2005.

[14] G., Aglietti, G.S., Richardson, G Bianchi, "Static Performance of Hot Bonded Inserts in Honeycomb Panels," in *49th Structures, Structural Dynamics, and Materials Conference*, Schaumburg, 2008.

[15] K., Choi, Ji., Kweon, J., Choi, Jin., Kim, K Song, "An experimental study of the insert joint strength of composite sandwich structures," *Composite Structures*, vol. 68, pp. 107-113, March 2008.

[16] N., Battley, M., Southward, T Raghu, "Strength Variability of Inserts in Sandwich panels," *Sandwich Structures and Materials*, vol. 11, pp. 501-517, November 2009.

[17] C. Burchardt, "Fatigue of Sandwich Structures with Inserts," *Composite Structures*, vol. 40, pp. 201-211, 1998.

[18] K.B. & Mortensen, R.K. Kristensen, "Load introduction in sandwich structures," no. 65, 1995.

[19] European Space Agency: Structures and Mechanisms Division, *Insert Design Handbook*, 1st ed. Noordwijk, Netherlands, 1987.

[20] R. M. Jones, *Mechanics of Composite Materials*, 2nd ed. Philadelphia, United States of America: Taylor & Francis, Inc., 1999.

[21] M. Y. Niu, *Composite Airframe Structures: Practical Design Information and Data*. Hong Kong, Hong Kong: Conmilit Press Ltd, 1992.

[22] M. Buschinelli, "Fuselage Load Summary," Carleton University, Ottawa, Design Report 117-17, 2009.

[23] A. Lares, "Nose Landing Gear Design and Selection," Carleton University, Ottawa, Design Report 97-14, 2009.

[24] J. Maxwell, "Engine Testing and Maintenance," Carleton University, Ottawa,

Design Report No. 83-05, 2008.

[25] (2011) MATLAB - Introductory FFT Tutorial. [Online]. http://matlabz.blogspot.com/2011/03/matlab-introductory-fft-tutorial.html

[26] Hart-Smith LJ., "The Ten-Percent Rule for preliminary sizing of fibrous composite structures. ," *51st SAWE International Conference*, pp. 29–45, May 1992.

[27] ASTM, "F 593 – 02 Stainless Steel Bolts, Hex Cap Screws, and Studs," 2004.

[28] Hirpa L. Gelgele, "Finite Element Based Dynamic Analysis of a Device in Coiled Tubing Drilling," Dept. of Mechanical and Structural Engineering and Material Technology, Stavanger, Norway, Research Paper 2009.

APPENDICES

Appendix A: CCBM Bag Manufacturing

Materials Used [11]:

Silicon - Proflex NS® silicone 850 ml tubes --> (~1hr cure time with 0.025-in thick coat)

Reinforcement fabric - Confortex® fabric

Inlet and outlet lines - Omega Flow Lines --> Airtech Corp.

Generic double sided tape

Generic wax paper

Step 1:

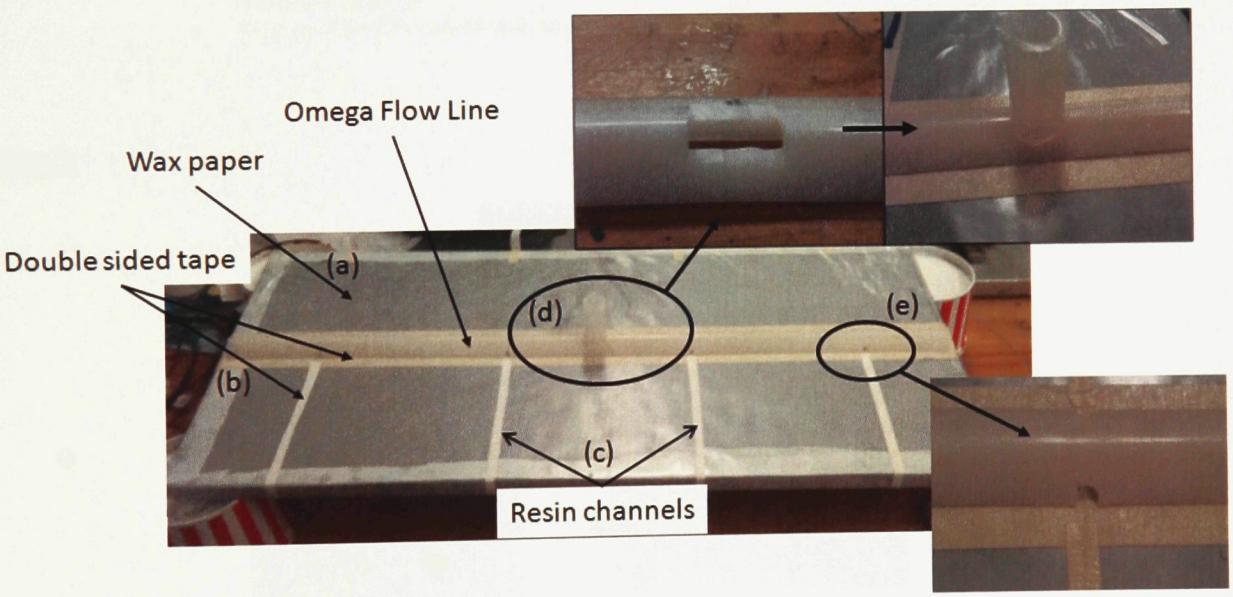

a. Sandwich structure is prepared and wrapped in wax paper.
b. Double sided tape is added in the areas shown on both sides of the wrapped part.
c. The thin sections of double sided tape are 4-in apart and will be the locations of the resin channels.
d. The inlet/outlet is formed by sectioning the Omega Flow Line (OFL) in the center and adding a vertical tube.
e. The OFL is sectioned in the areas where the resin channel will be integrated.

Step 2:

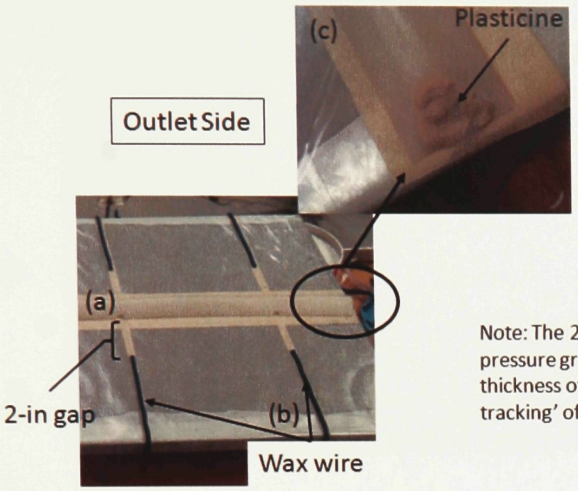

Note: The 2-in gap is to ensure a pressure gradient through-the-thickness of the layup avoiding 'race tracking' of the resin.

a. On the outlet side, there is a gap of 3-in between the resin channels and the outlet Omega flow line.
b. Wax wire is placed on the double sided tape to form the structure of the resin channels.
c. The ends of the OFL on both sides are plugged with plasticine.

Step 3:

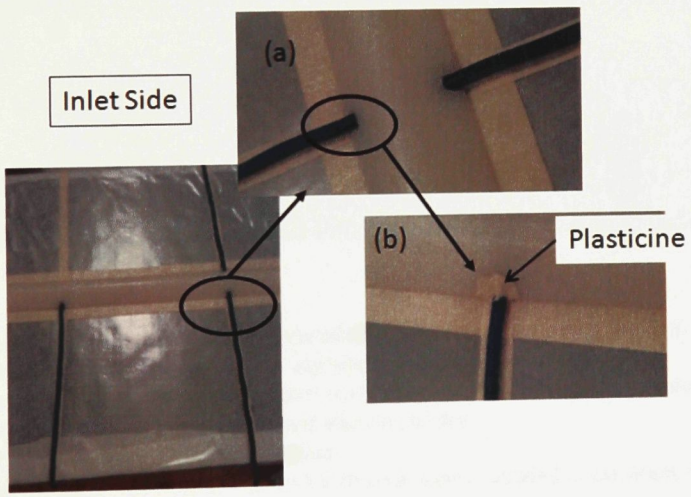

a. To integrate the resin channels with the OFL, the wax wire is fed into the sections of the OFL.
b. The interface is packed with plasticine to ensure a smooth transition from the resin channel into the inlet OFL.

Step 4

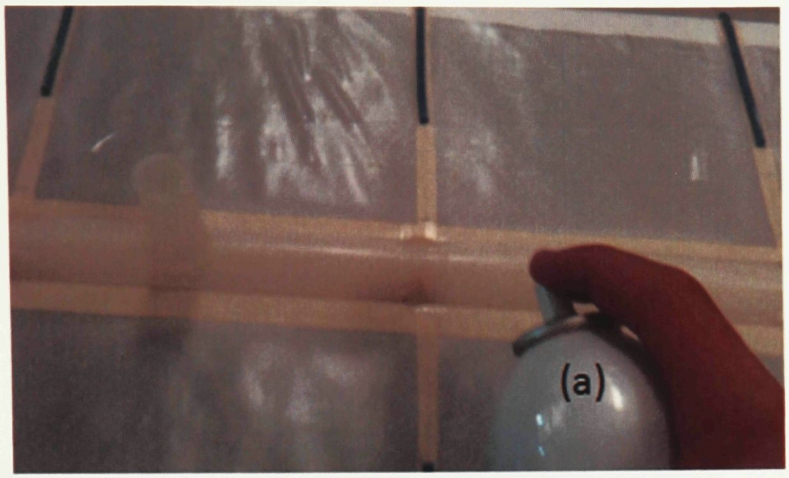

a. All surfaces are coated in release agent to ensure that the silicon does not adhere to the surface after it has dried.

Step 5

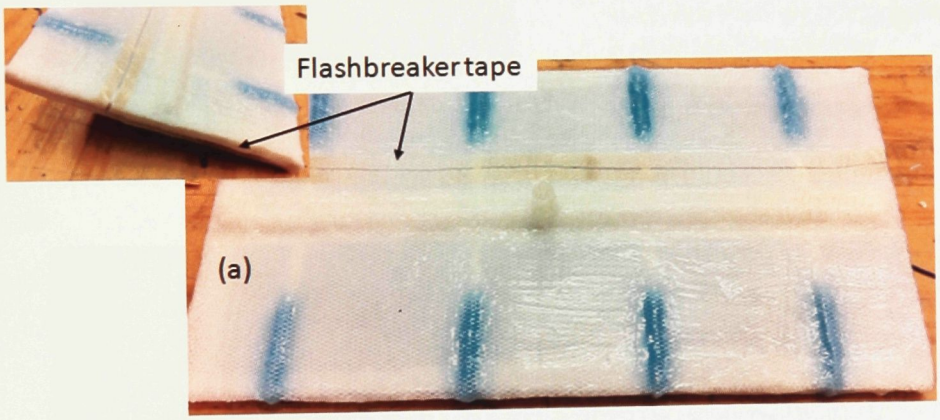

a. Two even coats of silicon are applied with a spatula over the entire surface of the bag. This was done in stages to allow for each side to dry before applying a coat to the opposite side.
b. Reinforcement mesh is applied after the second coat. This was done by applying a thin coat of silicon and then applying the fabric mesh over top and allowing to dry.
c. another coat of silicon is applied to whole surface
d. On the final coat, once applied and still wet, Flashbreaker tape is applied in the areas shown.

Step 6

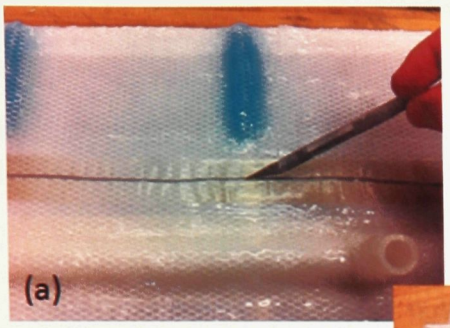

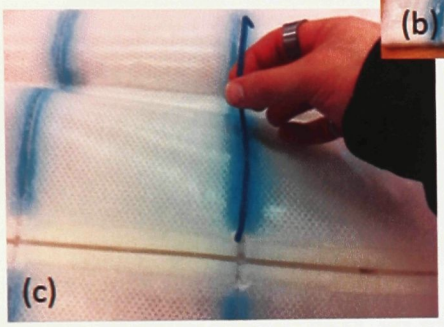

a. Once the bag has dried, the bag is cut along the middle of the flashbreaker tape
b. The bag is opened and the sandwich structure component is removed from the bag
c. The wax wire embedded on the inside of the bag is removed

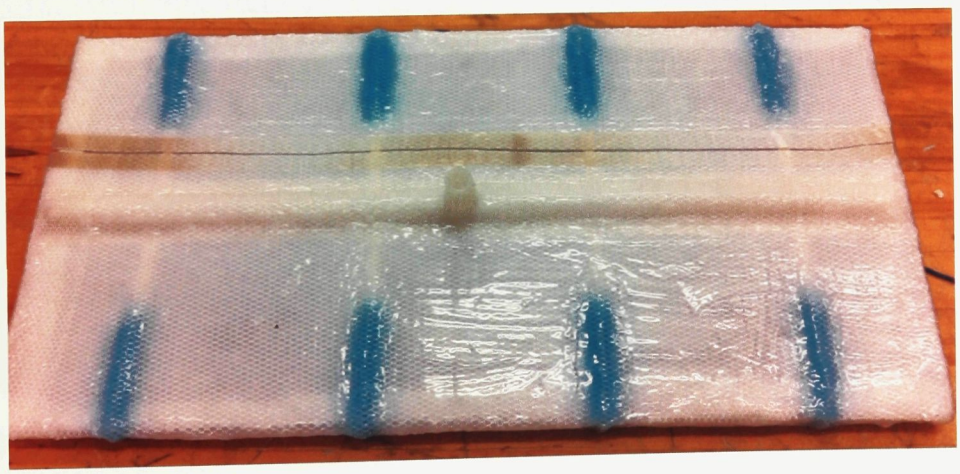

Bag is complete and ready for infusions

Appendix B: Coupon Manufacturing

Please refer to Joe Maley's Thesis *Composite Manufacturing* [12] for the procedure describing how to lay-up sandwich panels.

Step 1

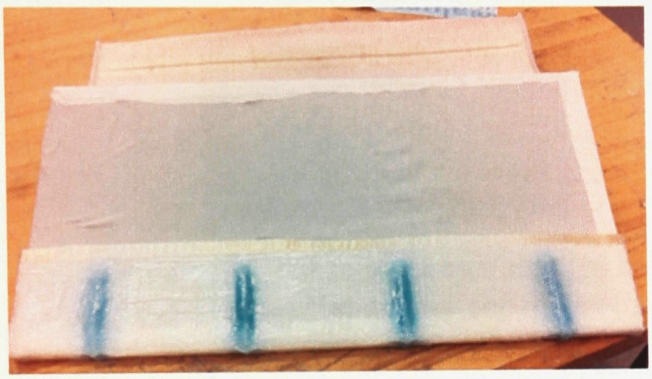

Place the prepared sandwich panel in the reusable bag

Step 2

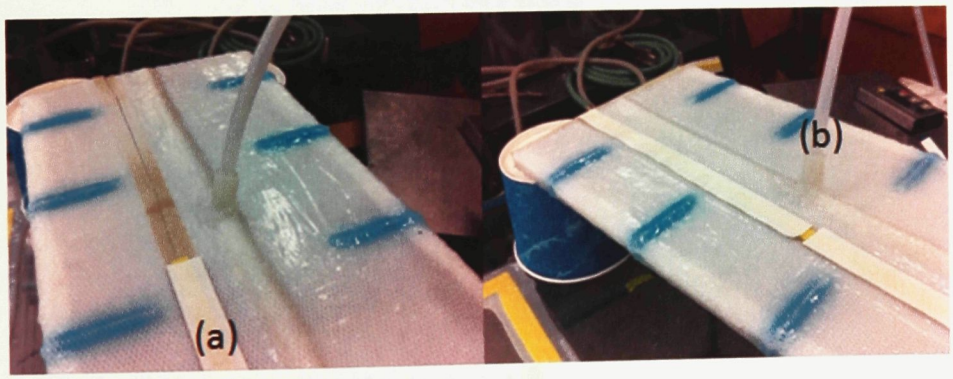

a. Place disposable sealant tape on flashbreaker tape to seal the bag
b. Place inlet and outlet tubes

Note: The bag was elevated from the table top to allow clearance for the inlet/outlet line.

Step 3

Clamps are used to ensure an air-tight seal between the plastic tubes and silicon bag

Step 4

Note: Dry spots are avoided and infusion time decreased to approximately 10 minutes if distribution media is used.

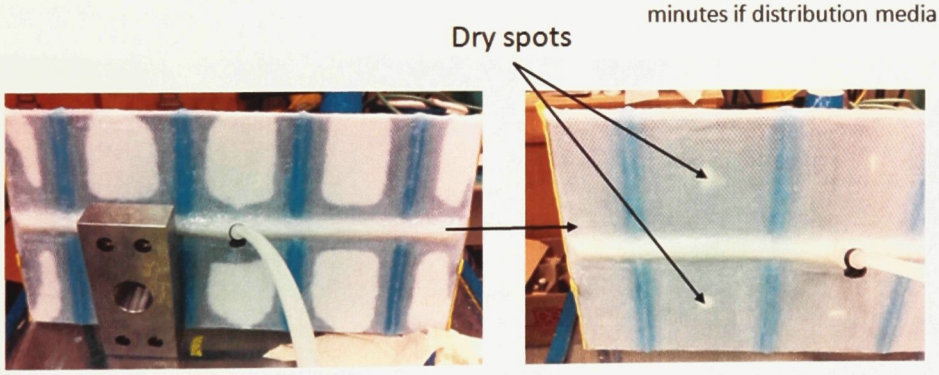

a. Attach outlet line to pump
b. Insert inlet line end into resin reservoir
c. Turn pump on, wait for complete consolidation of part
d. Once fully consolidated → reverse inlet and outlet lines
e. Clamp off inlet, allow to cure under vacuum pressure

Step 5

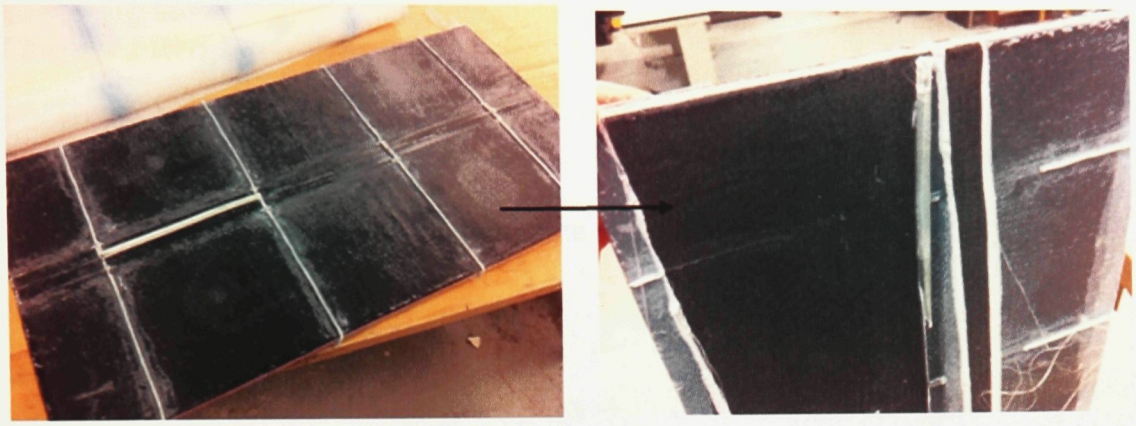

a. Remove from reusable bag
b. Remove distribution media & peel-ply

Step 6

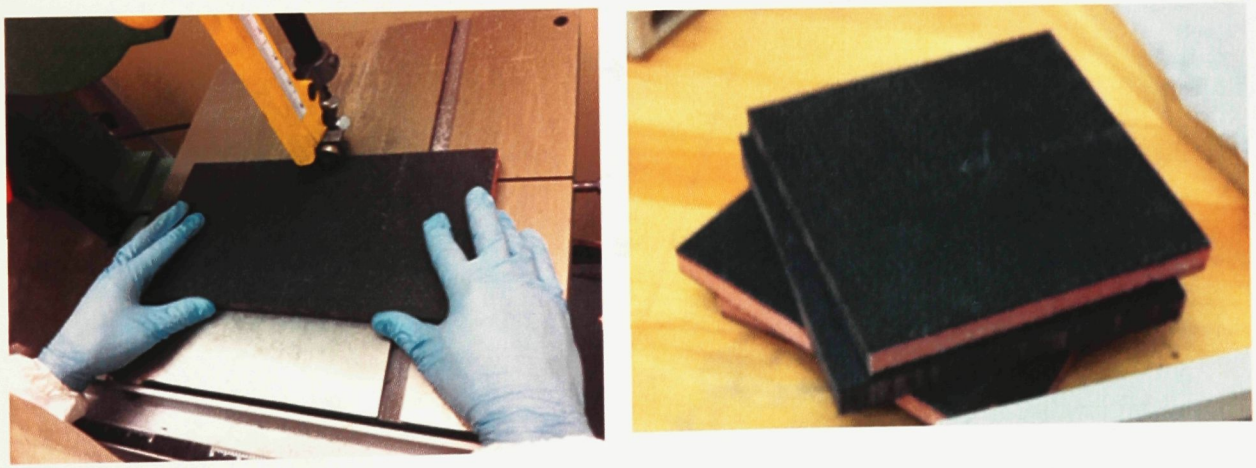

From a single cured panel → 8, 6x6-in specimens can be made

Appendix C: Insert Material Cost Calculations

Casting Processes:

Chopped Fibreglass – Epoxy:

Fibre Cost:
0.031 slugs of chopped fibre = $9.25 → *Eager Polymers Inc.*

0.00043 slugs is the required amount of fibre for each insert

= $0.13/insert

Resin Cost:
40 fl oz of West System 105 epoxy = $64.45 → *McMaster-Carr*

1 pump = 0.8 fl oz thus 50 pumps per batch = $1.29/pump

2 pumps required for batch of 4 inserts

= $0.64/insert

Total Cost:
$0.77/insert

Chopped Carbon Fibre – Epoxy:

Fiber Cost:
0.12 slugs spool of 3k carbon fibre = $384.95 → *Aircraft Spruce Canada*

1lb of carbon = $96.24

0.00027 slugs required for 1 insert

= $0.85/insert

Resin Cost:
Same as chopped fibreglass: $0.64/insert

Total Cost:
$1.49/insert

Chopped Fibreglass – Polyurethane:

Fiber Cost:
Same as chopped fibreglass – epoxy: $0.13/insert

Resin Cost:
46.00 fl oz of Shore 80D polyurethane resin = $72.78 → *McMaster-Carr*

0.4 fl oz required for each insert

= $0.73/insert

Total Cost:
= $0.86/insert

Machining Processes:

Carbon Fibre Round:

1 insert requires 1.375-in of round stock

1 ft length 0.75-in diameter round = $64 = $5/in → *McMaster-Carr*

= $7.33/insert

Fibreglass Round:

1 insert requires 1.375-in of round stock

1 ft length 0.75-in diameter round = $3 = $0.25/in → *McMaster-Carr*

= $0.35/insert

Birch Round:

1 insert requires 1.375-in of round stock

1 ft length 0.75-in diameter round = $3.96 = $0.33/in → *McMaster-Carr*

= $0.45/insert

Appendix D: FFT and Signal Processing Script

This signal processing script was developed with the help of the following tutorial: MATLAB - Introductory FFT Tutorial [25].

Function:

```
function [ X, freq ] = positiveFFT( x,Fs)
%Custom function which converts s


N=length(x);              %get the number of points in the vibration
signal
k=0:N-1;                  %create a vector from 0 to N-1
T=N/Fs;                   %get the frequency interval
freq=k/T;                 %create the frequency range
X=fft(x)/N;               %normalize the data
cutOff = ceil(N/2);       %delete second half of fft
X=X(1:cutOff);            %output first half of fft
freq=freq(1:cutOff);      %output frequency range of first half of fft
end
```

Editor:

```
%Convert signal from time domain to frequency domain
fft_v = fft(V);

%Cleans the signal, any frequency contributions that are less than a
%prescribed value are set to zero
for i = 1:size(fft_v)
    if abs(fft_v(i)) < 5

        fft_v(i) = 0;
    end;
end

%After filtering out the weaker signals or "noise" the filtered fft
signal is %converted back to the time domain for processing by the
positiveFFT function
V_clean = ifft(fft_v);

%Fs is the sampling rate
Fs = 1/1e-3;

%calculate fft of cleaned signal
[YfreqD,freqRng] = positiveFFT(V_clean,Fs);

%plot discrete data
stem(freqRng,abs(YfreqD));
```

```
AXIS([0 140 0 0.014])          %define scale
```

Appendix E: Redesigned Vibration Test Fixture

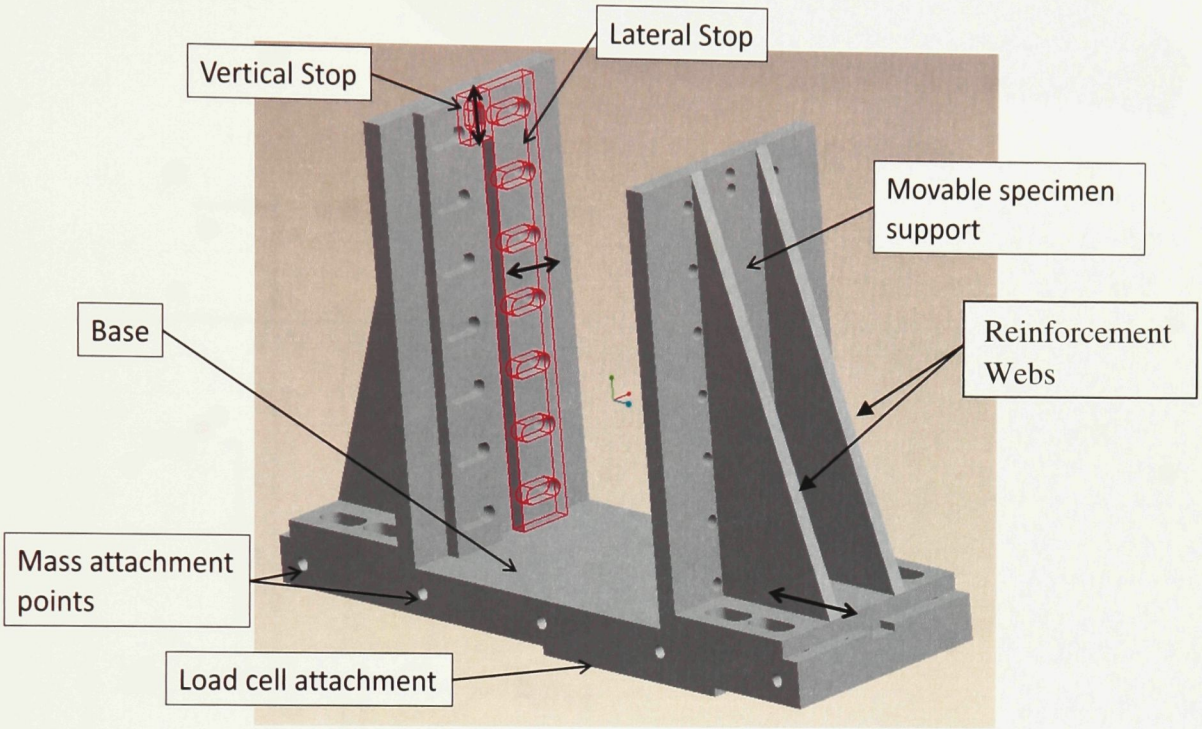

Figure E - 1 - Proposed new test fixture for vibration testing.

Design Notes:

- The 'Lateral Stops' can be used from the current test fixture.
- The load cell attachment is welded to the base..
- The reinforcement webs are to be welded to the movable specimen supports.

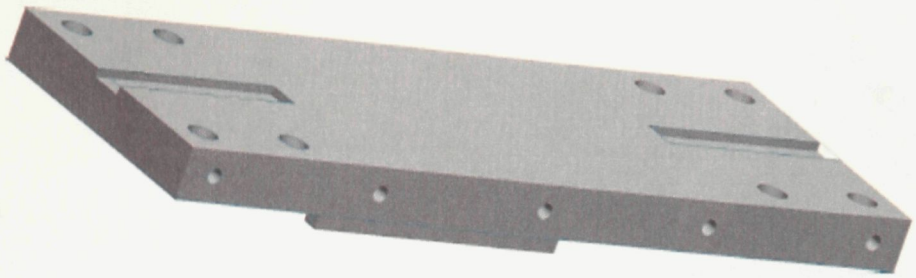

SCALE 0.500

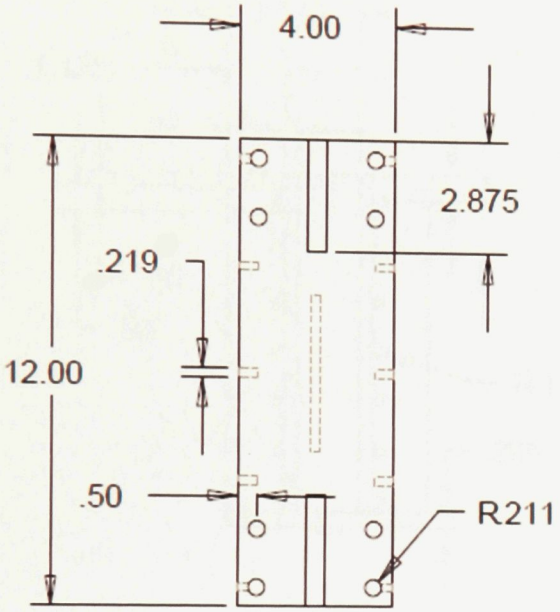

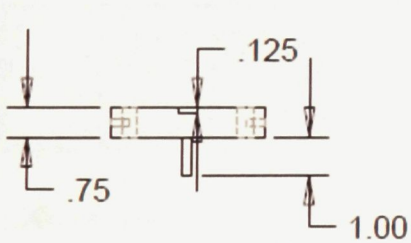

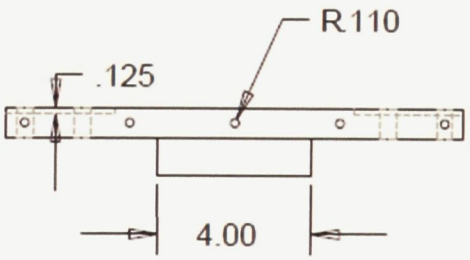

Part Name:	Material:	Dimensions :	Scale:
Bottom Plate	Mild Steel	Inches	0.25

Figure E - 2 - CAD drawing of Bottom Plate.

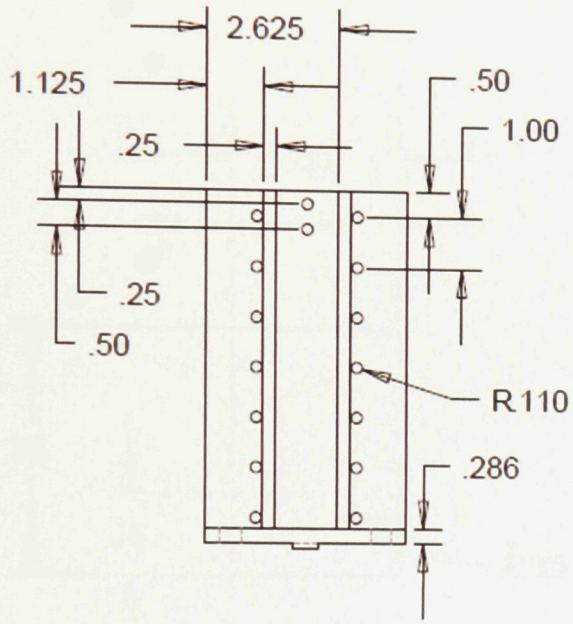

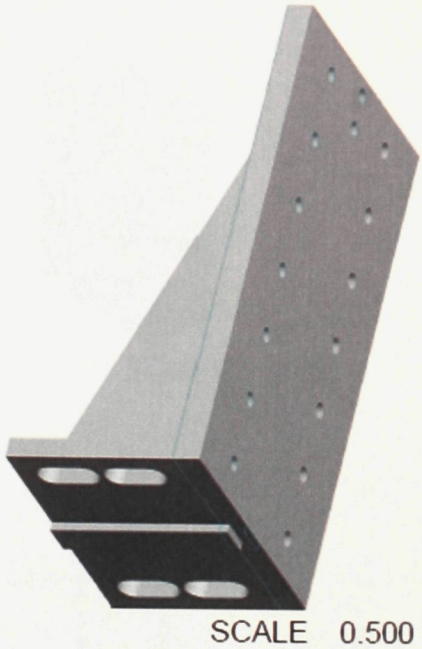

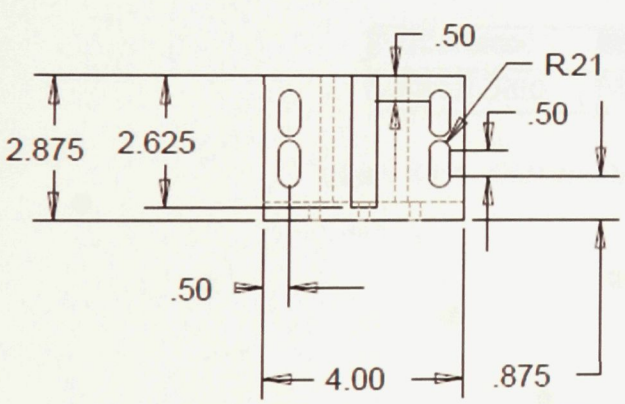

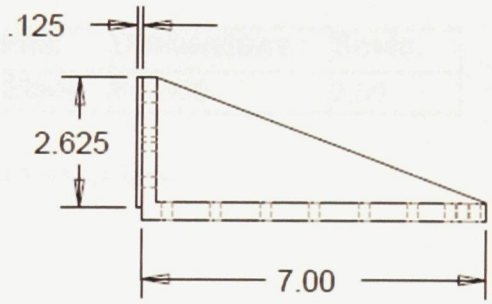

Part Name:	Material:	Dimensions :	Scale:
Support	Mild Steel	Inches	0.25

Figure E - 3 - CAD drawing of Support.

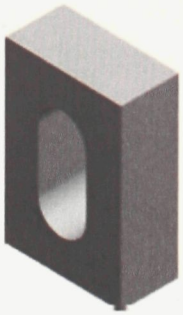

SCALE 2.00

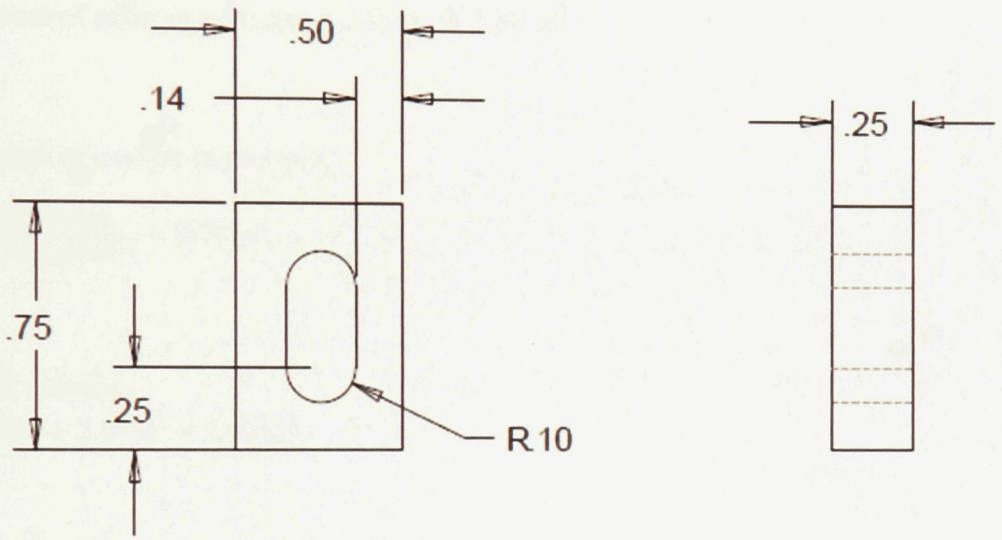

Part Name:	Material:	Dimensions :	Scale:
Vertical Stop	Mild Steel	Inches	2.00

Figure E - 4 - CAD drawing of Vertical Stop.

Appendix F: V.3 Insert Modulus Calculation

Matrix tensile modulus: 4.6×10^5 psi

Fibre tensile modulus: 93.26×10^5 psi

Density of carbon: 0.0015 slugs/in^3

Mass of carbon in mixture: 0.0011 slugs

Volume of resin in mixture: 1.6 fl oz → 2.88 in^3

Volume of carbon in mixture:

$$\frac{0.0011 slugs}{0.0015 slugs/in\text{^}3} = 0.74 \text{in}^3$$

Total volume:

$0.74\text{in}^3 + 2.88\text{in}^3 = 3.62\text{in}^3$

Volume Fractions:

$$V_m = \frac{2.88\text{in}^3}{3.62\text{in}^3} = 0.79$$

$V_f = 1 - 0.79 = 0.21$

Composite tensile modulus:

$E = E_m V_m + E_f V_f$

$= (4.5 \times 10^5 \text{ psi})(0.79) + (93.26 \times 10^5 \text{ psi})(0.21)$

$= 23.14 \times 10^5$ psi

Appendix G: Bearing and Bending Simulation and Experimental Test Results

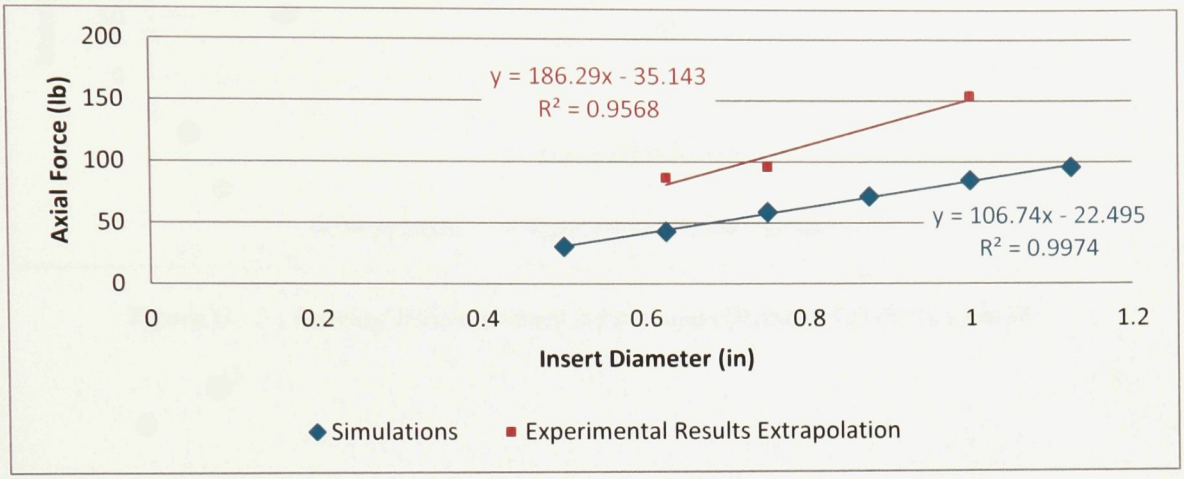

Figure G - 1- Bearing failure load versus insert diameter (12 ply face-sheet).

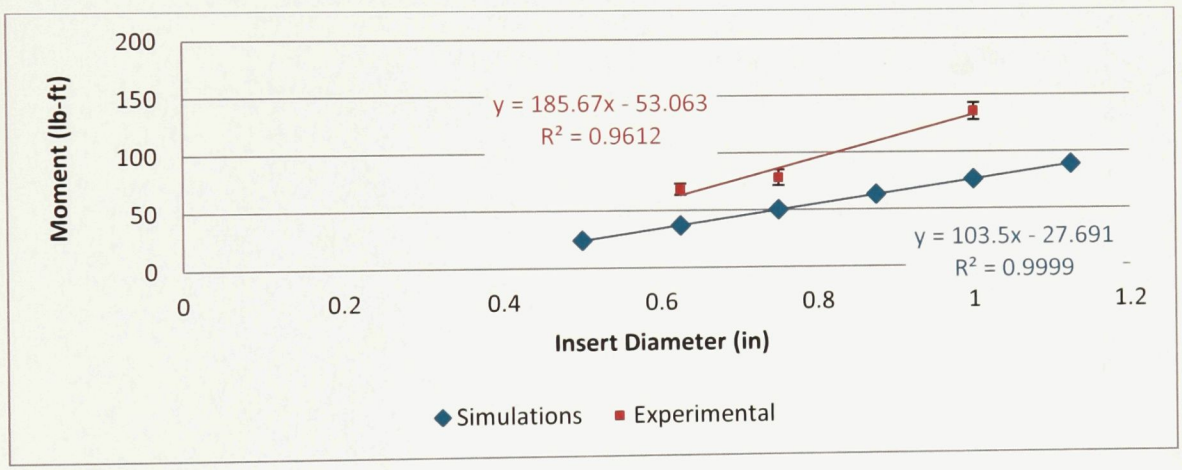

Figure G - 2 - Bending failure moment versus insert diameter (8 ply face-sheet).

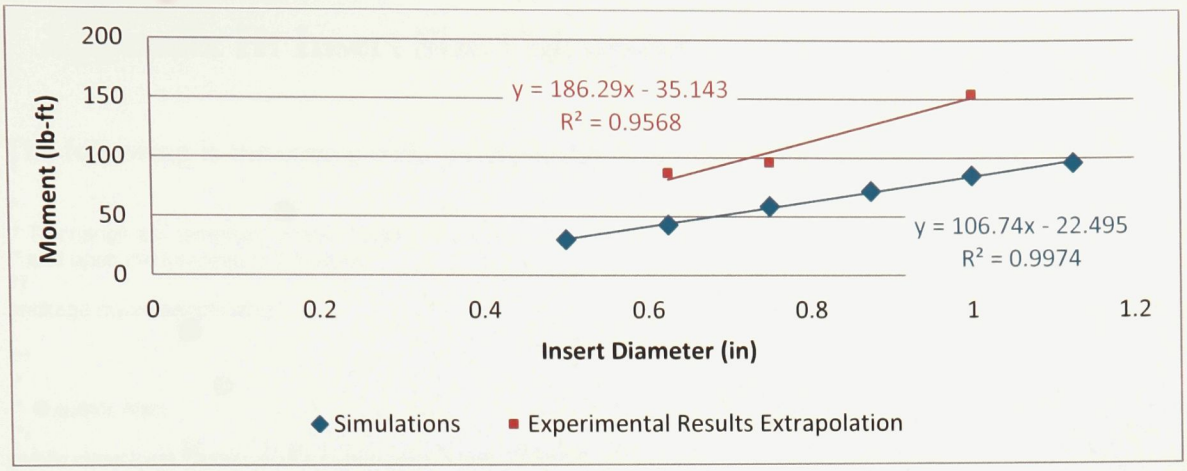

Figure G - 3 - Bending failure moment versus insert diameter (12 ply face-sheet).

Appendix H: Insert Size Calculator

The following is the source code for the Insert Size Calculator program:

```
/*
 * To change this template, choose Tools | Templates
 * and open the template in the editor.
 */
package my.insertoptimizer;

/**
 *
 * @author Alan
 */
public class InsertOptimizerUI extends javax.swing.JFrame {

    /**
     * Creates new form InsertOptimizerUI
     */
    public InsertOptimizerUI() {
        initComponents();
    }

    /**
     * This method is called from within the constructor to initialize the form.
     * WARNING: Do NOT modify this code. The content of this method is always
     * regenerated by the Form Editor.
     */
    @SuppressWarnings("unchecked")
    // <editor-fold defaultstate="collapsed" desc="Generated Code">
    private void initComponents() {

        jFrame1 = new javax.swing.JFrame();
        jFrame2 = new javax.swing.JFrame();
        jPanel1 = new javax.swing.JPanel();
        jLabelBearing = new javax.swing.JLabel();
        jLabelBending = new javax.swing.JLabel();
        jLabelNumPlies = new javax.swing.JLabel();
        bearing = new javax.swing.JTextField();
        bending = new javax.swing.JTextField();
        plyCount = new javax.swing.JComboBox();
        calcuate = new javax.swing.JButton();
        jPanel2 = new javax.swing.JPanel();
        jLabel6 = new javax.swing.JLabel();
        sleeve1 = new javax.swing.JLabel();
        sleeve2 = new javax.swing.JLabel();
        sleeve3 = new javax.swing.JLabel();
        sleeve4 = new javax.swing.JLabel();
        jLabel7 = new javax.swing.JLabel();
        jLabel8 = new javax.swing.JLabel();
        jLabel9 = new javax.swing.JLabel();
        jLabel10 = new javax.swing.JLabel();
        jLabelBearing2 = new javax.swing.JLabel();
        jPanel3 = new javax.swing.JPanel();
        jLabel5 = new javax.swing.JLabel();
        plug1 = new javax.swing.JLabel();
        plug2 = new javax.swing.JLabel();
        plug3 = new javax.swing.JLabel();
        plug4 = new javax.swing.JLabel();
        jLabel1 = new javax.swing.JLabel();
        jLabel2 = new javax.swing.JLabel();
        jLabel3 = new javax.swing.JLabel();
        jLabel4 = new javax.swing.JLabel();
        jLabelBearing3 = new javax.swing.JLabel();
```

```
        javax.swing.GroupLayout jFrame1Layout = new javax.swing.GroupLayout(jFrame1.getContentPane());
        jFrame1.getContentPane().setLayout(jFrame1Layout);
        jFrame1Layout.setHorizontalGroup(
            jFrame1Layout.createParallelGroup(javax.swing.GroupLayout.Alignment.LEADING)
            .addGap(0, 400, Short.MAX_VALUE)
        );
        jFrame1Layout.setVerticalGroup(
            jFrame1Layout.createParallelGroup(javax.swing.GroupLayout.Alignment.LEADING)
            .addGap(0, 300, Short.MAX_VALUE)
        );

        javax.swing.GroupLayout jFrame2Layout = new javax.swing.GroupLayout(jFrame2.getContentPane());
        jFrame2.getContentPane().setLayout(jFrame2Layout);
        jFrame2Layout.setHorizontalGroup(
            jFrame2Layout.createParallelGroup(javax.swing.GroupLayout.Alignment.LEADING)
            .addGap(0, 400, Short.MAX_VALUE)
        );
        jFrame2Layout.setVerticalGroup(
            jFrame2Layout.createParallelGroup(javax.swing.GroupLayout.Alignment.LEADING)
            .addGap(0, 300, Short.MAX_VALUE)
        );

        setDefaultCloseOperation(javax.swing.WindowConstants.EXIT_ON_CLOSE);
        setResizable(false);

        jPanel1.setBorder(new javax.swing.border.MatteBorder(null));

        jLabelBearing.setHorizontalAlignment(javax.swing.SwingConstants.RIGHT);
        jLabelBearing.setText("Bearing (lbf):");

        jLabelBending.setHorizontalAlignment(javax.swing.SwingConstants.RIGHT);
        jLabelBending.setText("Bending (ft-lb):");

        jLabelNumPlies.setText("Number of Plies:");

        plyCount.setMaximumRowCount(3);
        plyCount.setModel(new javax.swing.DefaultComboBoxModel(new String[] { "4", "8", "12" }));
        plyCount.setOpaque(false);
        plyCount.addActionListener(new java.awt.event.ActionListener() {
            public void actionPerformed(java.awt.event.ActionEvent evt) {
                plyCountActionPerformed(evt);
            }
        });

        calcuate.setText("Calculate");
        calcuate.addActionListener(new java.awt.event.ActionListener() {
            public void actionPerformed(java.awt.event.ActionEvent evt) {
                calcuateActionPerformed(evt);
            }
        });

        javax.swing.GroupLayout jPanel1Layout = new javax.swing.GroupLayout(jPanel1);
        jPanel1.setLayout(jPanel1Layout);
        jPanel1Layout.setHorizontalGroup(
            jPanel1Layout.createParallelGroup(javax.swing.GroupLayout.Alignment.LEADING)
            .addGroup(javax.swing.GroupLayout.Alignment.TRAILING, jPanel1Layout.createSequentialGroup()
                .addContainerGap()
                .addGroup(jPanel1Layout.createParallelGroup(javax.swing.GroupLayout.Alignment.TRAILING)
                    .addGroup(jPanel1Layout.createParallelGroup(javax.swing.GroupLayout.Alignment.TRAILING, false)
                        .addComponent(jLabelBending, javax.swing.GroupLayout.Alignment.LEADING,
javax.swing.GroupLayout.DEFAULT_SIZE, 114, Short.MAX_VALUE)
                        .addComponent(jLabelBearing, javax.swing.GroupLayout.Alignment.LEADING,
javax.swing.GroupLayout.DEFAULT_SIZE, javax.swing.GroupLayout.DEFAULT_SIZE, Short.MAX_VALUE))
                    .addComponent(jLabelNumPlies))
                .addPreferredGap(javax.swing.LayoutStyle.ComponentPlacement.UNRELATED)
                .addGroup(jPanel1Layout.createParallelGroup(javax.swing.GroupLayout.Alignment.LEADING)
                    .addComponent(bearing, javax.swing.GroupLayout.PREFERRED_SIZE, 78,
javax.swing.GroupLayout.PREFERRED_SIZE)
                    .addGroup(jPanel1Layout.createSequentialGroup()
                        .addGroup(jPanel1Layout.createParallelGroup(javax.swing.GroupLayout.Alignment.TRAILING, false)
```

```
                .addComponent(plyCount, 0, 78, Short.MAX_VALUE)
                .addComponent(bending))
            .addGap(335, 335, 335)
            .addComponent(calcuate)))
        .addContainerGap(493, Short.MAX_VALUE))
    );
    jPanel1Layout.setVerticalGroup(
      jPanel1Layout.createParallelGroup(javax.swing.GroupLayout.Alignment.LEADING)
      .addGroup(jPanel1Layout.createSequentialGroup()
        .addContainerGap()
        .addGroup(jPanel1Layout.createParallelGroup(javax.swing.GroupLayout.Alignment.LEADING)
          .addGroup(jPanel1Layout.createSequentialGroup()
            .addGroup(jPanel1Layout.createParallelGroup(javax.swing.GroupLayout.Alignment.BASELINE)
              .addComponent(jLabelBearing)
              .addComponent(bearing, javax.swing.GroupLayout.PREFERRED_SIZE,
javax.swing.GroupLayout.DEFAULT_SIZE, javax.swing.GroupLayout.PREFERRED_SIZE))
            .addPreferredGap(javax.swing.LayoutStyle.ComponentPlacement.RELATED)
            .addGroup(jPanel1Layout.createParallelGroup(javax.swing.GroupLayout.Alignment.BASELINE)
              .addComponent(jLabelBending)
              .addComponent(bending, javax.swing.GroupLayout.PREFERRED_SIZE,
javax.swing.GroupLayout.DEFAULT_SIZE, javax.swing.GroupLayout.PREFERRED_SIZE))
            .addGap(26, 26, 26)
            .addGroup(jPanel1Layout.createParallelGroup(javax.swing.GroupLayout.Alignment.BASELINE)
              .addComponent(jLabelNumPlies)
              .addComponent(plyCount))
            .addContainerGap(30, Short.MAX_VALUE))
          .addGroup(javax.swing.GroupLayout.Alignment.TRAILING, jPanel1Layout.createSequentialGroup()
            .addGap(0, 0, Short.MAX_VALUE)
            .addComponent(calcuate)
            .addContainerGap())))
    );

    jPanel2.setBorder(new javax.swing.border.MatteBorder(null));

    jLabel6.setIcon(new
javax.swing.ImageIcon(getClass().getResource("/my/insertoptimizer/PlugAndSleeve/SLEEVE.png"))); // NOI18N

    sleeve1.setText("S1");
    sleeve2.setText("S2");
    sleeve3.setText("S3");
    sleeve4.setText("S4");
    jLabel7.setText("S1:");
    jLabel8.setText("S2:");
    jLabel9.setText("S3:");
    jLabel10.setText("S4:");

    jLabelBearing2.setHorizontalAlignment(javax.swing.SwingConstants.RIGHT);
    jLabelBearing2.setText("Insert Dimensions in inches\n");

    javax.swing.GroupLayout jPanel2Layout = new javax.swing.GroupLayout(jPanel2);
    jPanel2.setLayout(jPanel2Layout);
    jPanel2Layout.setHorizontalGroup(
      jPanel2Layout.createParallelGroup(javax.swing.GroupLayout.Alignment.LEADING)
      .addGroup(jPanel2Layout.createSequentialGroup()
        .addGap(6, 6, 6)
        .addGroup(jPanel2Layout.createParallelGroup(javax.swing.GroupLayout.Alignment.TRAILING)
          .addGroup(jPanel2Layout.createSequentialGroup()
            .addComponent(jLabel7)
            .addPreferredGap(javax.swing.LayoutStyle.ComponentPlacement.RELATED)
            .addComponent(sleeve1))
          .addGroup(jPanel2Layout.createSequentialGroup()
            .addComponent(jLabel8)
            .addPreferredGap(javax.swing.LayoutStyle.ComponentPlacement.RELATED)
            .addComponent(sleeve2)))
        .addGap(40, 40, 40)
        .addGroup(jPanel2Layout.createParallelGroup(javax.swing.GroupLayout.Alignment.LEADING)
          .addGroup(jPanel2Layout.createSequentialGroup()
            .addComponent(jLabel10)
            .addPreferredGap(javax.swing.LayoutStyle.ComponentPlacement.UNRELATED)
            .addComponent(sleeve4))
```

```
                .addGroup(jPanel2Layout.createSequentialGroup()
                    .addComponent(jLabel9)
                    .addPreferredGap(javax.swing.LayoutStyle.ComponentPlacement.UNRELATED)
                    .addComponent(sleeve3)
                    .addPreferredGap(javax.swing.LayoutStyle.ComponentPlacement.RELATED,
javax.swing.GroupLayout.DEFAULT_SIZE, Short.MAX_VALUE)
                    .addComponent(jLabelBearing2, javax.swing.GroupLayout.PREFERRED_SIZE, 273,
javax.swing.GroupLayout.PREFERRED_SIZE)))
                .addContainerGap())
            .addGroup(javax.swing.GroupLayout.Alignment.TRAILING, jPanel2Layout.createSequentialGroup()
                .addContainerGap(60, Short.MAX_VALUE)
                .addComponent(jLabel6)
                .addGap(47, 47, 47))
        );
        jPanel2Layout.setVerticalGroup(
            jPanel2Layout.createParallelGroup(javax.swing.GroupLayout.Alignment.LEADING)
            .addGroup(javax.swing.GroupLayout.Alignment.TRAILING, jPanel2Layout.createSequentialGroup()
                .addContainerGap(17, Short.MAX_VALUE)
                .addGroup(jPanel2Layout.createParallelGroup(javax.swing.GroupLayout.Alignment.BASELINE)
                    .addComponent(sleeve1, javax.swing.GroupLayout.DEFAULT_SIZE,
javax.swing.GroupLayout.DEFAULT_SIZE, Short.MAX_VALUE)
                    .addComponent(sleeve3)
                    .addComponent(jLabel7)
                    .addComponent(jLabel9)
                    .addComponent(jLabelBearing2))
                .addGap(10, 10, 10)
                .addGroup(jPanel2Layout.createParallelGroup(javax.swing.GroupLayout.Alignment.BASELINE)
                    .addComponent(sleeve2)
                    .addComponent(sleeve4)
                    .addComponent(jLabel8)
                    .addComponent(jLabel10))
                .addGap(18, 18, 18)
                .addComponent(jLabel6)
                .addGap(73, 73, 73))
        );

        jPanel3.setBorder(new javax.swing.border.MatteBorder(null));

        jLabel5.setIcon(new
javax.swing.ImageIcon(getClass().getResource("/my/insertoptimizer/PlugAndSleeve/PLUG.png"))); // NOI18N

        plug1.setText("P1");
        plug2.setText("P2");
        plug3.setText("P3");
        plug4.setText("P4");
        jLabel1.setText("P1:");
        jLabel2.setText("P2:");
        jLabel3.setText("P3:");
        jLabel4.setText("P4:");

        jLabelBearing3.setHorizontalAlignment(javax.swing.SwingConstants.RIGHT);
        jLabelBearing3.setText("Insert Dimensions in inches\n");

        javax.swing.GroupLayout jPanel3Layout = new javax.swing.GroupLayout(jPanel3);
        jPanel3.setLayout(jPanel3Layout);
        jPanel3Layout.setHorizontalGroup(
            jPanel3Layout.createParallelGroup(javax.swing.GroupLayout.Alignment.LEADING)
            .addGroup(jPanel3Layout.createSequentialGroup()
                .addGroup(jPanel3Layout.createParallelGroup(javax.swing.GroupLayout.Alignment.LEADING, false)
                    .addGroup(jPanel3Layout.createSequentialGroup()
                        .addGap(53, 53, 53)
                        .addComponent(jLabel5))
                    .addGroup(jPanel3Layout.createSequentialGroup()
                        .addContainerGap()
                        .addGroup(jPanel3Layout.createParallelGroup(javax.swing.GroupLayout.Alignment.TRAILING)
                            .addComponent(jLabel1)
                            .addComponent(jLabel2))
                        .addPreferredGap(javax.swing.LayoutStyle.ComponentPlacement.UNRELATED)
                        .addGroup(jPanel3Layout.createParallelGroup(javax.swing.GroupLayout.Alignment.LEADING, false)
                            .addGroup(jPanel3Layout.createSequentialGroup()
```

```
                    .addComponent(plug2)
                    .addPreferredGap(javax.swing.LayoutStyle.ComponentPlacement.RELATED,
javax.swing.GroupLayout.DEFAULT_SIZE, Short.MAX_VALUE)
                    .addComponent(jLabel4))
                  .addGroup(jPanel3Layout.createSequentialGroup()
                    .addComponent(plug1)
                    .addGap(35, 35, 35)
                    .addComponent(jLabel3)))
                .addPreferredGap(javax.swing.LayoutStyle.ComponentPlacement.RELATED)
                .addGroup(jPanel3Layout.createParallelGroup(javax.swing.GroupLayout.Alignment.LEADING)
                  .addGroup(jPanel3Layout.createSequentialGroup()
                    .addComponent(plug3)
                    .addPreferredGap(javax.swing.LayoutStyle.ComponentPlacement.RELATED, 182,
Short.MAX_VALUE)
                    .addComponent(jLabelBearing3, javax.swing.GroupLayout.PREFERRED_SIZE, 273,
javax.swing.GroupLayout.PREFERRED_SIZE))
                  .addGroup(jPanel3Layout.createSequentialGroup()
                    .addComponent(plug4)
                    .addGap(0, 0, Short.MAX_VALUE)))))
            .addContainerGap(javax.swing.GroupLayout.DEFAULT_SIZE, Short.MAX_VALUE))
        );
        jPanel3Layout.setVerticalGroup(
          jPanel3Layout.createParallelGroup(javax.swing.GroupLayout.Alignment.LEADING)
          .addGroup(jPanel3Layout.createSequentialGroup()
            .addGroup(jPanel3Layout.createParallelGroup(javax.swing.GroupLayout.Alignment.LEADING)
              .addGroup(jPanel3Layout.createSequentialGroup()
                .addGap(72, 72, 72)
                .addComponent(jLabel5))
              .addGroup(jPanel3Layout.createSequentialGroup()
                .addContainerGap()
                .addGroup(jPanel3Layout.createParallelGroup(javax.swing.GroupLayout.Alignment.BASELINE)
                  .addComponent(plug1)
                  .addComponent(plug3)
                  .addComponent(jLabel1)
                  .addComponent(jLabel3)
                  .addComponent(jLabelBearing3))
                .addPreferredGap(javax.swing.LayoutStyle.ComponentPlacement.RELATED)
                .addGroup(jPanel3Layout.createParallelGroup(javax.swing.GroupLayout.Alignment.BASELINE)
                  .addComponent(plug2)
                  .addComponent(plug4)
                  .addComponent(jLabel2)
                  .addComponent(jLabel4))))
            .addContainerGap(103, Short.MAX_VALUE))
        );

        plug1.getAccessibleContext().setAccessibleName("");

        javax.swing.GroupLayout layout = new javax.swing.GroupLayout(getContentPane());
        getContentPane().setLayout(layout);
        layout.setHorizontalGroup(
          layout.createParallelGroup(javax.swing.GroupLayout.Alignment.LEADING)
          .addGroup(layout.createSequentialGroup()
            .addContainerGap()
            .addGroup(layout.createParallelGroup(javax.swing.GroupLayout.Alignment.LEADING)
              .addGroup(layout.createSequentialGroup()
                .addComponent(jPanel3, javax.swing.GroupLayout.DEFAULT_SIZE,
javax.swing.GroupLayout.DEFAULT_SIZE, Short.MAX_VALUE)
                .addPreferredGap(javax.swing.LayoutStyle.ComponentPlacement.RELATED)
                .addComponent(jPanel2, javax.swing.GroupLayout.PREFERRED_SIZE,
javax.swing.GroupLayout.DEFAULT_SIZE, javax.swing.GroupLayout.PREFERRED_SIZE))
              .addComponent(jPanel1, javax.swing.GroupLayout.DEFAULT_SIZE,
javax.swing.GroupLayout.DEFAULT_SIZE, Short.MAX_VALUE))
            .addGap(83, 83, 83))
        );
        layout.setVerticalGroup(
          layout.createParallelGroup(javax.swing.GroupLayout.Alignment.LEADING)
          .addGroup(layout.createSequentialGroup()
            .addContainerGap()
            .addComponent(jPanel1, javax.swing.GroupLayout.PREFERRED_SIZE,
javax.swing.GroupLayout.DEFAULT_SIZE, javax.swing.GroupLayout.PREFERRED_SIZE)
```

```
            .addPreferredGap(javax.swing.LayoutStyle.ComponentPlacement.RELATED)
            .addGroup(layout.createParallelGroup(javax.swing.GroupLayout.Alignment.LEADING)
                .addComponent(jPanel3, javax.swing.GroupLayout.DEFAULT_SIZE,
javax.swing.GroupLayout.DEFAULT_SIZE, Short.MAX_VALUE)
                .addComponent(jPanel2, javax.swing.GroupLayout.DEFAULT_SIZE,
javax.swing.GroupLayout.DEFAULT_SIZE, Short.MAX_VALUE)))
        );

        pack();
    }// </editor-fold>

    private void calcuateActionPerformed(java.awt.event.ActionEvent evt) {
        // TODO add your handling code here:
        float lBearing = Float.parseFloat(bearing.getText());
        float lBending = Float.parseFloat(bending.getText());
        Object lPlyCountItem = plyCount.getSelectedItem();
        float lPlyCount = Float.parseFloat(lPlyCountItem.toString());
        calculateGeometries(lBearing, lBending, lPlyCount);
    }

    private void plyCountActionPerformed(java.awt.event.ActionEvent evt) {
    }

    private void calculateGeometries(float bearing, float bending, float plyCount)
    {
        /*
        * BEARING AND BENDING EQUATIONS
        * 4ply bearing: x = y/1588.6 - 0.0005995
        * 8ply bearing: x = y/2514.3 - 0.0492423
        * 12ply bearing: x = y/3433.1 - 0.0729865
        * 4ply bending: x = y/182.98 + .3803858
        * 8ply bending: x = y/185.67 + .2857920
        * 12ply bending: x = y/186.29 + 0.1886467
        *
        * in the presented equations x is the insert diameter, and y
        * is the moment (bending) or force (bearing)
        */
        double insertDiameterBearing;
        double insertDiameterBending;
        double insertDiameter;
        double P1, P2, P3, P4;
        double S1, S2, S3;

        //Calculating the diameter of the bearing surface of the plug and sleeve assembly

        if (plyCount == 4)
        {
            insertDiameterBearing = (bearing/1588.6 - 0.0005995);
            insertDiameterBending = (bending/182.98 + 0.3803858);
        } else if (plyCount == 8)
        {
            insertDiameterBearing = (bearing/2514.3 - 0.0492423);
            insertDiameterBending = (bending/185.67 + 0.2857920);
        } else
        {
            insertDiameterBearing = (bearing/3433.1 - 0.0729865);
            insertDiameterBending = (bending/186.29 + 0.18886467);
        }

        if (insertDiameterBearing > insertDiameterBending)
        {
            insertDiameter = insertDiameterBearing;
        } else
        {
            insertDiameter = insertDiameterBending;
        }

        //calculate the rest of the plug and sleeve dimensions

        S1 = insertDiameter + 0.25;
```

```
        S2 = 0.5;

        P1 = 0.125;
        P2 = 0.625;

        if (insertDiameter > 0.75)
        {
           P3 = 0.3125;
        } else
        {
            P3 = 0.25;
        }

        P4 = (insertDiameter/2 + P3/2);
        S3 = P4;

        //convert dimensions to text format and print to UI
        plug1.setText(Double.toString(P1));
        plug2.setText(Double.toString(P2));
        plug3.setText(Double.toString(P3));
        plug4.setText(Double.toString(P4));


        sleeve1.setText(Double.toString(S1));
        sleeve2.setText(Double.toString(S2));
        sleeve3.setText(Double.toString(S3));
        sleeve4.setText(Double.toString(insertDiameter));
    }

    /**
     * @param args the command line arguments
     */
    public static void main(String args[]) {
        /*
         * Set the Nimbus look and feel
         */
        //<editor-fold defaultstate="collapsed" desc=" Look and feel setting code (optional) ">
        /*
         * If Nimbus (introduced in Java SE 6) is not available, stay with the
         * default look and feel. For details see
         * http://download.oracle.com/javase/tutorial/uiswing/lookandfeel/plaf.html
         */
        try {
            for (javax.swing.UIManager.LookAndFeelInfo info : javax.swing.UIManager.getInstalledLookAndFeels()) {
                if ("Nimbus".equals(info.getName())) {
                    javax.swing.UIManager.setLookAndFeel(info.getClassName());
                    break;
                }
            }
        } catch (ClassNotFoundException ex) {
            java.util.logging.Logger.getLogger(InsertOptimizerUI.class.getName()).log(java.util.logging.Level.SEVERE, null,
ex);
        } catch (InstantiationException ex) {
            java.util.logging.Logger.getLogger(InsertOptimizerUI.class.getName()).log(java.util.logging.Level.SEVERE, null,
ex);
        } catch (IllegalAccessException ex) {
            java.util.logging.Logger.getLogger(InsertOptimizerUI.class.getName()).log(java.util.logging.Level.SEVERE, null,
ex);
        } catch (javax.swing.UnsupportedLookAndFeelException ex) {
            java.util.logging.Logger.getLogger(InsertOptimizerUI.class.getName()).log(java.util.logging.Level.SEVERE, null,
ex);
        }
        //</editor-fold>

        /*
         * Create and display the form
         */
        java.awt.EventQueue.invokeLater(new Runnable() {

            public void run() {
```

```
            new InsertOptimizerUI().setVisible(true);
        }
    });
}
// Variables declaration - do not modify
private javax.swing.JTextField bearing;
private javax.swing.JTextField bending;
private javax.swing.JButton calcuate;
private javax.swing.JFrame jFrame1;
private javax.swing.JFrame jFrame2;
private javax.swing.JLabel jLabel1;
private javax.swing.JLabel jLabel10;
private javax.swing.JLabel jLabel2;
private javax.swing.JLabel jLabel3;
private javax.swing.JLabel jLabel4;
private javax.swing.JLabel jLabel5;
private javax.swing.JLabel jLabel6;
private javax.swing.JLabel jLabel7;
private javax.swing.JLabel jLabel8;
private javax.swing.JLabel jLabel9;
private javax.swing.JLabel jLabelBearing;
private javax.swing.JLabel jLabelBearing2;
private javax.swing.JLabel jLabelBearing3;
private javax.swing.JLabel jLabelBending;
private javax.swing.JLabel jLabelNumPlies;
private javax.swing.JPanel jPanel1;
private javax.swing.JPanel jPanel2;
private javax.swing.JPanel jPanel3;
private javax.swing.JLabel plug1;
private javax.swing.JLabel plug2;
private javax.swing.JLabel plug3;
private javax.swing.JLabel plug4;
private javax.swing.JComboBox plyCount;
private javax.swing.JLabel sleeve1;
private javax.swing.JLabel sleeve2;
private javax.swing.JLabel sleeve3;
private javax.swing.JLabel sleeve4;
// End of variables declaration
}
```